THE UNIVERSITY OF MICHIGAN

INDUSTRY PROGRAM OF THE COLLEGE OF ENGINEERING

THRESHOLD PRESSURE PHENOMENA IN POROUS MEDIA

Leonard K. Thomas

A dissertation submitted in partial fulfillment
of the requirements for the degree of
Doctor of Philosophy in the
University of Michigan
Department of Chemical and Metallurgical Engineering
1967

March, 1967

IP-772

Doctoral Committee:

Professor Donald L. Katz, Chairman
Professor Louis I. Briggs
Professor John E. Powers
Professor M. Rasin Tek
Associate Professor James O. Wilkes

ACKNOWLEDGMENTS

The author wishes to express his appreciation to the many people who have contributed to this research work. Special acknowlegments to the following people and organizations are appropriate:

Professor Donald L. Katz, chairman of the doctoral committee, for his advice and guidance in formulating and pursuing this research work. His professional, but cordial manner has made this work worthwhile.

Professor M. Rasin Tek for his donation of both time and moral support toward this dissertation.

Professor John E. Powers, and Associate Professor James O. Wilkes for their interest and helpful suggestions.

Professor Louis I. Briggs for his assistance in classifying the core samples used in this work.

The Michigan Gas Association for their financial support in the form of a fellowship during the author's graduate study.

Continental Oil Company, Northern Illinois Gas Company, and Phillips Petroleum Company for providing core samples for the experimental research.

Personnel at Core Laboratories and Pan American Research for their time in discussing various experimental techniques pertinent to this research.

Mr. Rusins Albertins, Mr. Ronald W. Bowman, Mr. Leo F. Carter, Dr. Max W. Legatski, and Mr. Alfred J. Martin for their valued advice and moral support.

My parents, Mr. and Mrs. Leonard R. Thomas, for providing financially for my earlier education and for their invaluable moral support.

My wife, Kayleen, whose patience, encouragement, and moral support have made this dissertation possible and worthwhile. Also, for her time and effort in typing the draft of this dissertation.

The Industry Program of the College of Engineering for the excellent job of producing this manuscript in its final form.

TABLE OF CONTENTS

TABLE OF CONTENTS (CONT'D)

LIST OF TABLES

LIST OF FIGURES

LIST OF FIGURES (CONT'D)

LIST OF FIGURES (CONT'D)

NOMENCLATURE

Symbol	Definition
A	Cross-sectional area, (L^2)
A'	Surface area per bulk volume, L^{-1}
A'_p	Surface area per unit volume of pore space, L^{-1}
d	Diameter of a tube, (L)
D_{AB}	Mass diffusivity in a binary system, (L^2/T)
F	Formation Resistivity Factor of a porous medium
F_a	Apparent formation factor
$\sum F$	Summation of forces acting, (F)
g	Acceleration of gravity, (L/T^2)
h	Height of capillary rise, (L)
$j(S_w)$	Leverett J-Function
K	Permeability, (darcys or L^{-2})
k_o	Shape factor in Kozeny equation
k_{rg}	Relative permeability to gas, (L^{-2})
k_{rw}	Relative permeability to water, (L^{-2})
k_z	Kozeny constant
L	Length, (L)
L_a	Average, effective length of a pore through porous media ($L_a > L$), (L)
m	Hydraulic radius, (L)
M	Molecular weight
N_{Az}	Molar flux of A relative to stationery coordinates, (M/L^2T)
p	Vapor pressure over a flat surface, (F/L^2)

Symbol	Definition
P	Pressure, (F/L^2)
p_o	Vapor pressure over a curved vapor-liquid surface, (F/L^2)
P_a	Atmospheric pressure, (F/L^2)
P_c	Capillary pressure, (F/L^2)
P_G	Gauge pressure, (F/L^2)
P_{nw}	Pressure in the nonwetting phase, (F/L^2)
P_T	Threshold pressure ,(F/L^2)
P_w	Pressure in the wetting phase, (F/L^2)
q	Volumetric flow rate, cm^3/sec, (L^3/T)
Q	Cummulative flow, (L^3)
r	Capillary radius, (L), Resistance across a porous medium saturated with an electrolyte, (ohm)
R	Gas constant, Resistivity, (ohm -cm)
R_a	Resistivity of a porous medium containing clay, (ohm -cm)
R_c	Resistivity of clay materials in a porous medium, (ohm -cm)
R_o	Resistivity of a porous medium saturated with an electrolyte of resistivity R_w, (ohm -cm)
R_w	Resistivity of an electrolyte, (ohm -cm)
R_1&R_2	Principal radii of curvature of a capillary interface, (L)
S	Saturation, percent
S_w	Water Saturation, percent
t	Time, (T)
T	Temperature, (°F or °R)
v	Superficial velocity, (L/T)
v_a	Average fluid velocity for laminar flow inside a tube (L/T)

Symbol	Definition
v_g	Superficial gas velocity, (L/T)
v_w	Superficial water velocity, (L/T)
$\underline{V}$	Specific volume, (L^3/M)
W	Mass flow rate, (M/T)
x	Dependent variable, (L)
y	Independent variable, (L)
z	Compressibility factor, Independent variable, (L)

Greek Letters

β	Turbulence factor, (L^{-1})
θ	Contact angle between wetting fluid and solid surface, Dimensionless Time
μ	Fluid Viscosity, (M/LT)
ρ	Density of water, (M/LT)
σ	Surface tension between two immiscible fluids (F/L)
τ	Tortuosity of a porous medium
ϕ	Porosity

ABSTRACT

The purpose of this research was to study the phenomenom of a nonwetting phase, gas, displacing a wetting phase, water, from low permeability porous media such as caprocks overlying natural gas storage reservoirs. Particular attention has been given to the study of threshold displacement pressures, the minimum pressure needed to initiate the displacement of a wetting phase by a nonwetting phase.

A method for measuring the threshold pressures of low permeability porous media is presented. Threshold pressures for eight samples of low permeability porous media were measured. Other measurements of the physical properties of the porous media were made, and correlations between these properties and the measured threshold pressure were obtained.

Mercury injection capillary pressure curves were measured by injecting mercury into portions of the samples of porous media used in this research. These curves were extrapolated to zero mercury saturation to obtain a value for the mercury entry pressure. These values were then related to the air-water threshold pressures through the capillary pressure equation. Thus, a correlation between mercury and air-water threshold pressures was obtained.

The effect of time on the threshold pressure of a porous medium was studied. It was concluded that the threshold pressure of a porous medium is not a function of time.

The movement of the gas-water interface at the base of a sample of porous medium subjected to gas pressures less than the threshold pressure was studied. A qualitative description as well as a mathematical analysis of this movement is presented.

The nature of the gas flow through a core after the threshold pressure is reached was observed. An areal photograph is presented of the gas phase emerging from the outlet end of a core after its threshold pressure has been exceeded.

A study of whether or not a caprock can be resealed after its threshold pressure has been exceeded is presented. This study includes a discussion of the substantial but somewhat lower threshold pressures required to displace water from porous media containing small saturations of gas.

I. INTRODUCTION

The primary purpose of this research work has been to study the phenomenon of a nonwetting phase, gas, displacing a wetting phase, water, from low permeability porous media. This research topic was fostered by the natural gas industry's interest in storing gas underground at pressures above the discovery pressures of their gas storage reservoirs.

The development of natural gas storage fields has stemmed from the increasing need of highly populated industrial centers for natural gas. Many of these areas are located in the Northeast and Northcentral United States where there are little proven gas reserves. The supply for these areas must consequently be piped in from other areas such as the Southwestern United States and Western Canada.

In order to furnish natural gas to Northern areas as economically as coal or some other fuel, pipeline transportation costs must be minimized. To do this the pipelines must be operated as close to their design capacity as possible. This means that during summer months when fuel consumption is low, part of the transported gas must be stored underground near the terminal end of the pipeline. Then during peak fuel loads in the winter the gas which was stored during the summer can be withdrawn to supplement the normal gas supply of the pipeline.

Overpressure is the term used to designate a pressure above the discovery or the initial pressure in a reservoir. It has been established that gas storage can be carried out at pressures above discovery, or during overpressure conditions. This is of economic importance since the storage capacity of a gas reservoir is proportional to its pressure. In

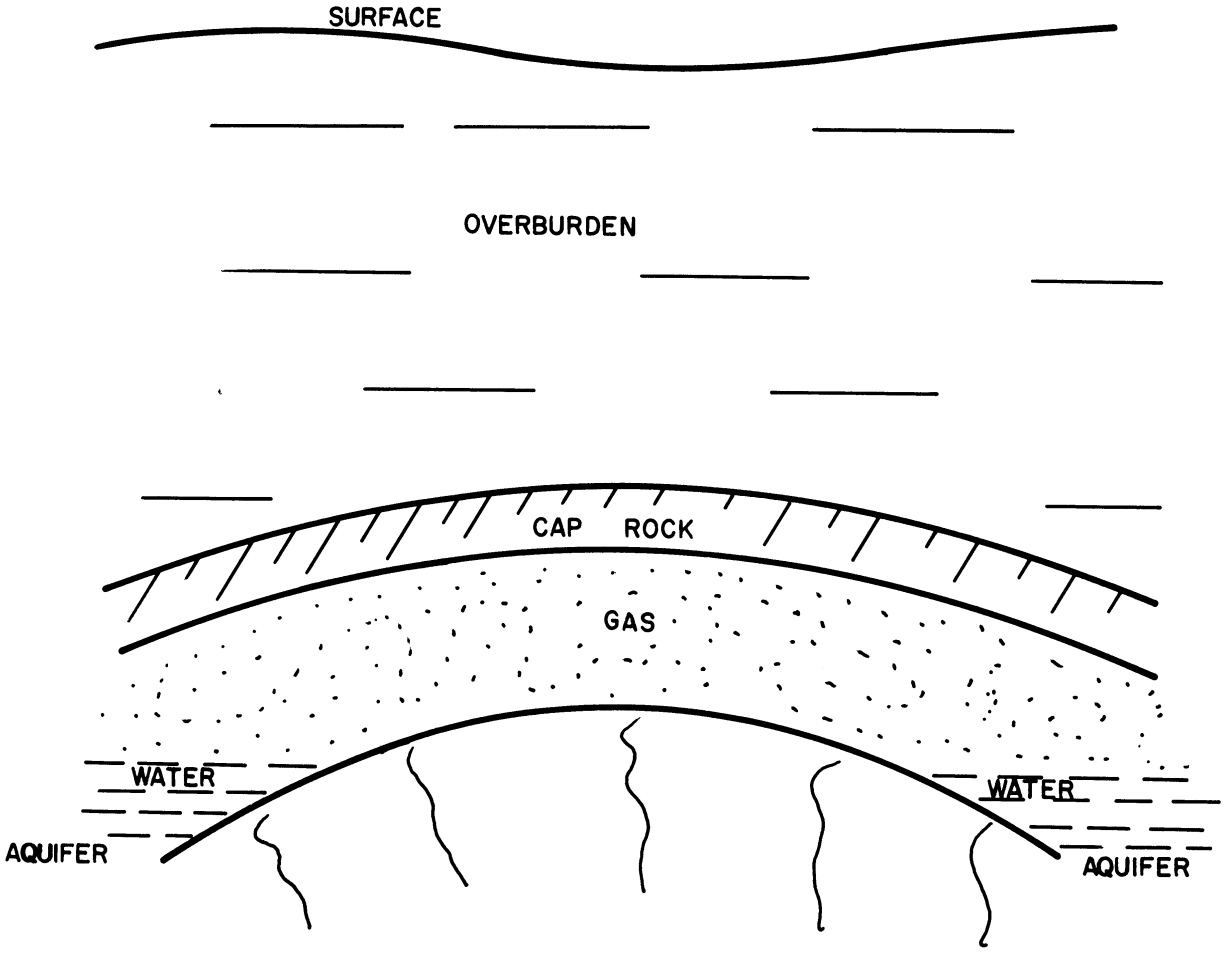

Figure 1: Typical Gas Storage Reservoir (usually at depths of 1,000' or more).

aquifer storage overpressure must be used to displace the contained water, while growing the reservoir.

The specific problem of interest to the gas industry is being able to predict how much "overpressure" a gas reservoir can withstand before leakage occurs by gas displacing water from the caprock overlying the reservoir.

The original underground storage fields were depleted oil and gas reservoirs. These formations made ideal storage reservoirs because they already possessed a proven ability for containing hydrocarbons under pressure.

Many oil and gas wells are in contact with aquifers which outcrop at the surface of the earth. The discovery pressure of these reservoirs usually is determined by the hydraulic gradient relative to the outcrop location.(30) Even the discovery pressures of reservoirs which are not known to be in contact with ground water often conform to this gradient.

Any variations in the discovery pressure of a reservoir from the hydrostatic pressure are usually attributed to varying brine saturations in the water or to the compaction of an isolated shale formation by the overburden.(11,19) Thus, the discovery pressures for most reservoirs are found somewhere between the upper and lower limits shown in Figure 2. The lower limit of .433 psi/ft corresponds to the hydraulic gradient of pure water. The upper limit, 1.psi/ft, corresponds to the weight of the overburden (the gradient of the rock itself). Somewhere between these two limits lies a safe operating pressure for a particular gas storage reservoir.

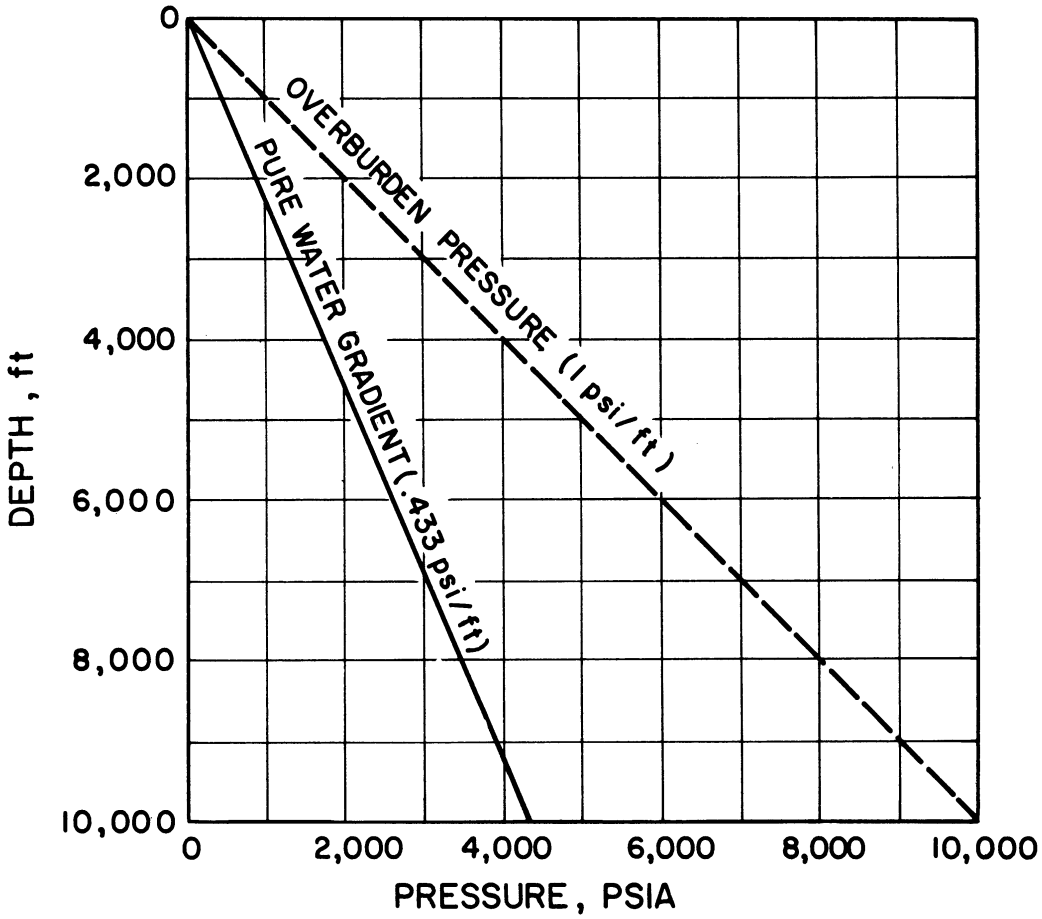

Figure 2. Hydraulic and Overburden Pressure Gradients in the Earth.

Previous interest in immiscible fluid displacement in high permeability porous media has stemmed from the chemical and petroleum industries. Examples of immiscible fluid displacement through porous media in these industries include: (1) primary, secondary, and even tertiary recover schemes in petroleum production, (2) immiscible movement of two phases in a packed absorption or distillation column, (3) dewatering of filter cakes, (4) gas flow through a wetted membrane.

An area of interest to the gas storage industry which has not been studied extensively to date is the nature of the fluid behavior in a caprock while operating a storage reservoir at pressures above its discovery pressure. This subject constitutes the purpose of this research work and is discussed in the following paragraphs.

Scope of this Research

This research work is primarily concerned with studying the phenomenom of gas displacing water from a low permeability porous medium such as a caprock overlying a natural gas reservoir. Emphasis in this work has been divided in two main parts: first, the development of an experimental technique for measuring the threshold displacement pressure of low permeability porous media; and second, the prediction of threshold displacement pressures from other measurements which can be made on porous media. Throughout this work, unless otherwise stated, threshold displacement pressure refers to that pressure difference between the wetting and nonwetting phase, which will iniate displacement of the wetting phase from a portion of a porous system 100% saturated with the wetting phase. For sake of brevity this pressure may also be referred to as the threshold pressure.

In developing the experimental technique for measuring threshold pressures, the effect of time as a variable has been studied. The manner in which the gas phase penetrates a porous medium has also been examined.

In addition to measuring and predicting threshold pressure a study has been made of the flow which occurs after the threshold pressure is reached. This area of research is important in determining whether or not a caprock can be resealed after its threshold pressure has been exceeded.

II. CONCEPT OF CAPILLARY PRESSURE

The capillary pressure which occurs in multiphase systems is a result of the molecular forces acting at the interface when two immiscible fluids are in contact. If the interface between these two immiscible fluids is located in very small spaces such as the pores in a porous medium, large capillary pressures may arise.

By definition, capillary pressure is that pressure difference which exists as a result of surface forces between a nonwetting phase and a wetting phase.

$$P_c = P_{nw} - P_w \tag{1}$$

where

P_c = capillary pressure

P_{nw} = pressure in the nonwetting phase

P_w = pressure in the wetting phase

The terminology wetting and nonwetting phase refers to the ability of a phase to wet the solid surface involved such as the pore walls of a porous medium.

A general expression for capillary pressure can be written in terms of the surface tension between the wetting and nonwetting phases and the principal radii of curvature of the interface.(1,30)

$$P_c = \sigma\left(\frac{1}{R_1} + \frac{1}{R_2}\right) \tag{2}$$

where

P_c = capillary pressure

σ = surface tension between two immiscible fluids

R_1 & R_2 = principal radii of curvature of the interface

It should be pointed out that the principal radii of curvature, R_1 and R_2, in Equation (2) are functions of the relative amounts of wetting and nonwetting phases present in a porous medium. Unfortunately R_1 and R_2 can not be measured directly when working with a porous medium.

A. Capillary Rise in a Tube

Consider the capillary tube immersed in water shown in Figure 3. Water will rise in the capillary tube to a height h, which is the position of the interface where the gravity forces due to the weight of the liquid are equal to the surface forces. Thus, the capillary rise is given by

$$2\pi r\sigma \cos\theta = \pi r^2 hg\rho \qquad (3)$$

or

$$h = \frac{2\sigma \cos\theta}{rg\rho} \qquad (4)$$

where

h = height of capillary rise

g = gravitational constant

r = capillary radius

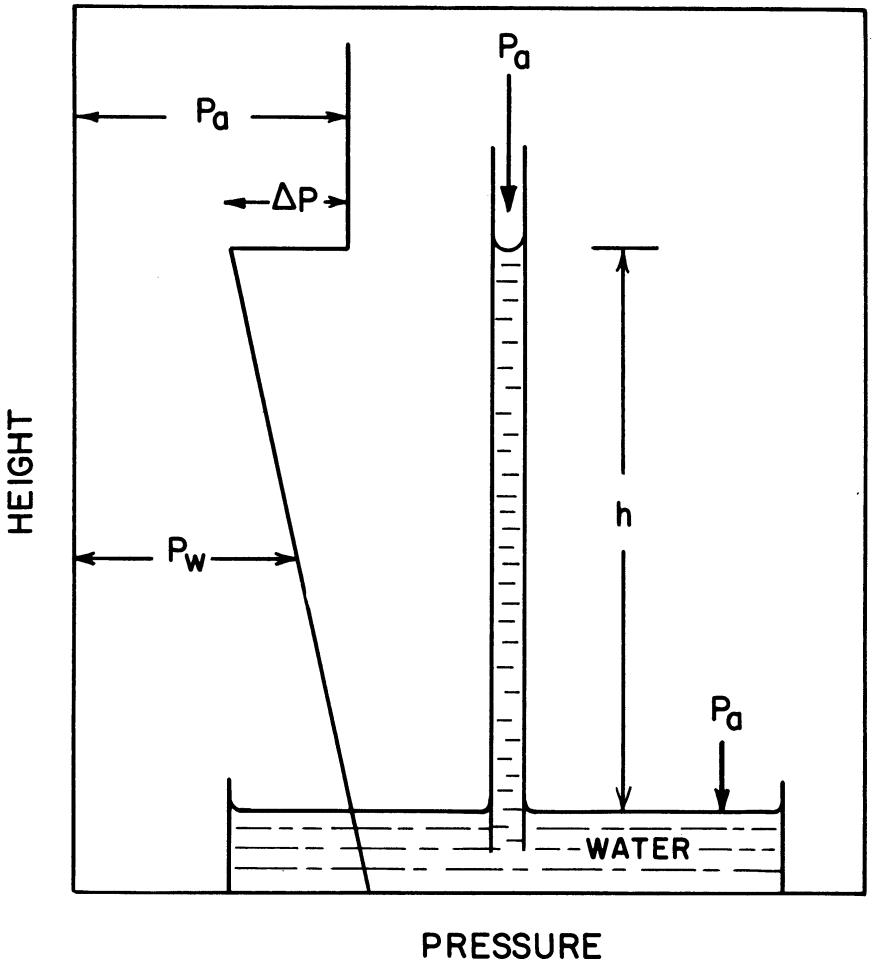

Figure 3. Capillary Rise in a Small Tube.

ρ = density of water

σ = surface tension between gas and water

Θ = contact angle between the water and the capillary tube

Equation (4) can now be written in terms of capillary pressure, P_c .

$$P_c = \rho gh = \frac{2\sigma \cos \Theta}{r} \qquad (5)$$

Equation (5) is the customary way of expressing the capillary rise in a tube. This equation states that the pressure difference resulting from surface tension which occurs across the gas-water interface in a capillary tube is equivalent to the pressure caused by a column of water having a height h . In other words, the pressure in the water just a few molecular layers below the interface is less than the gas pressure by an amount ρgh .

If the pressure of the gas phase in the stem of the capillary tube is increased and the pressure over the free water surface remains the same, the level of the water in the capillary tube will drop until a new equilibrium position is reached. If this pressure is increased by an amount ρgh over P_a the value of h will be reduced to zero.

B. Threshold Displacement Pressure of a Capillary Tube

The ability of a capillary tube filled with a wetting fluid such as water to resist the flow of a nonwetting fluid such as gas is a result of the adhesion forces between water and the capillary tube. No gas flow will occur through the capillary unless sufficient pressure is supplied in the gas phase to overcome these adhesive forces.

Now, consider that the capillary tube shown in Figure 3 is lying in a horozontal position. Assume that one end of the tube is joined to a container filled with water such that there are no capillary effects at this end of the tube.

The pressure in the gas phase overlying the stem of the capillary tube must be increased by an amount slightly exceeding $P_c = 2\sigma \cos \theta / r$ before any movement of the gas-water interface will occur. If the increased gas pressure is held at a constant value, steady flow will result in the tube until it has been emptied.

If the same capillary tube is connected to the bottom of a reservoir filled with water, Figure 4, water will completely fill the tube unless the length of the tube, L , is such that

$$L > h = \frac{2\sigma \cos \theta}{rg\rho} \qquad (6)$$

If this were the case the adhesion forces would not be as strong as the gravity forces and water would drain out of the end of the capillary tube.

The gas pressure needed to start an upward movement of the gas-water interface must exceed the capillary pressure plus the weight of the column of water, i.e.

$$P_b > P_c + \rho g L$$

or

$$P_b > \frac{2\sigma \cos \theta}{r} + \rho g L$$

If P_b satisfies the above inequality a continuous, increasing, upwards movement of the gas-water interface will occur. The increasing rate of movement is due to the diminishing weight of the column of water in the

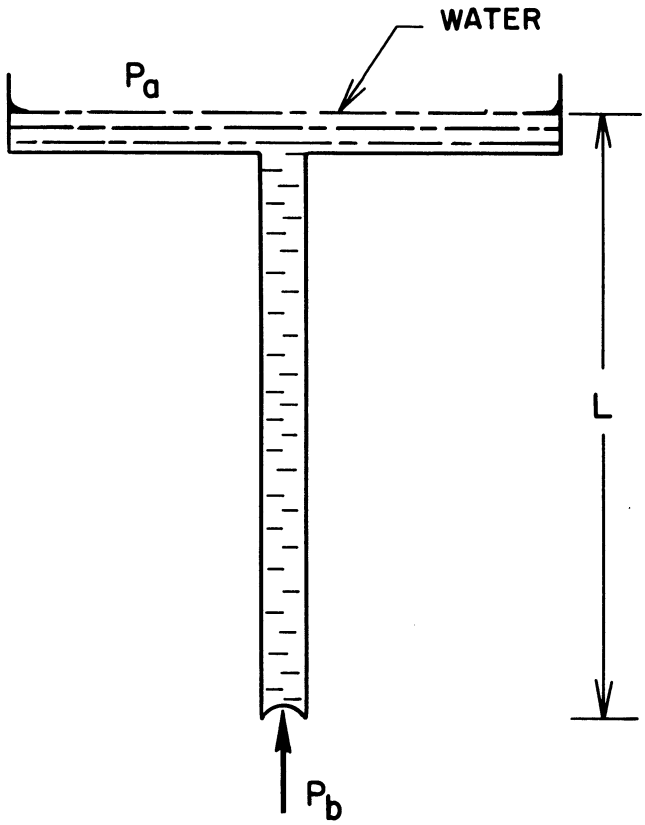

Figure 4. Inverted Capillary Rise Apparatus.

capillary tube. If, however

$$P_b < P_c + \rho g L$$

no movement of the gas-water interface will occur.

The inverted capillary rise apparatus in Figure 4 is a simplified example of the physical situation which exists across a caprock in a gas storage field. The capillary tube corresponds to the caprock, the region below the capillary tube containing gas at a pressure P_b corresponds to the gas reservoir, and the water above the capillary tube corresponds to the part of the water table which occupies the stratum overlying the caprock.

The threshold pressure for the capillary tube in Figure 4 is that pressure which will just start and maintain movement of the gas-water interface and is given by

$$P_T = \frac{2\sigma \cos \Theta}{r} + \rho g L \qquad (7)$$

where P_T is equal to the P_T threshold displacement pressure.

C. Capillary Pressure in Porous Media

Capillary pressure in a porous medium is a function of the relative amounts of wetting and nonwetting phases present. It is also a function of the history of the saturation process.

A typical plot of capillary pressure versus saturation is shown in Figure 5, and for convenience of discussion it will be referred to as a gas-water system. Figure 5 indicates that two separate distinct curves are obtained: one for drainage; and one for imbibition. The drainage capillary pressure curve is usually obtained by a downward displacement of

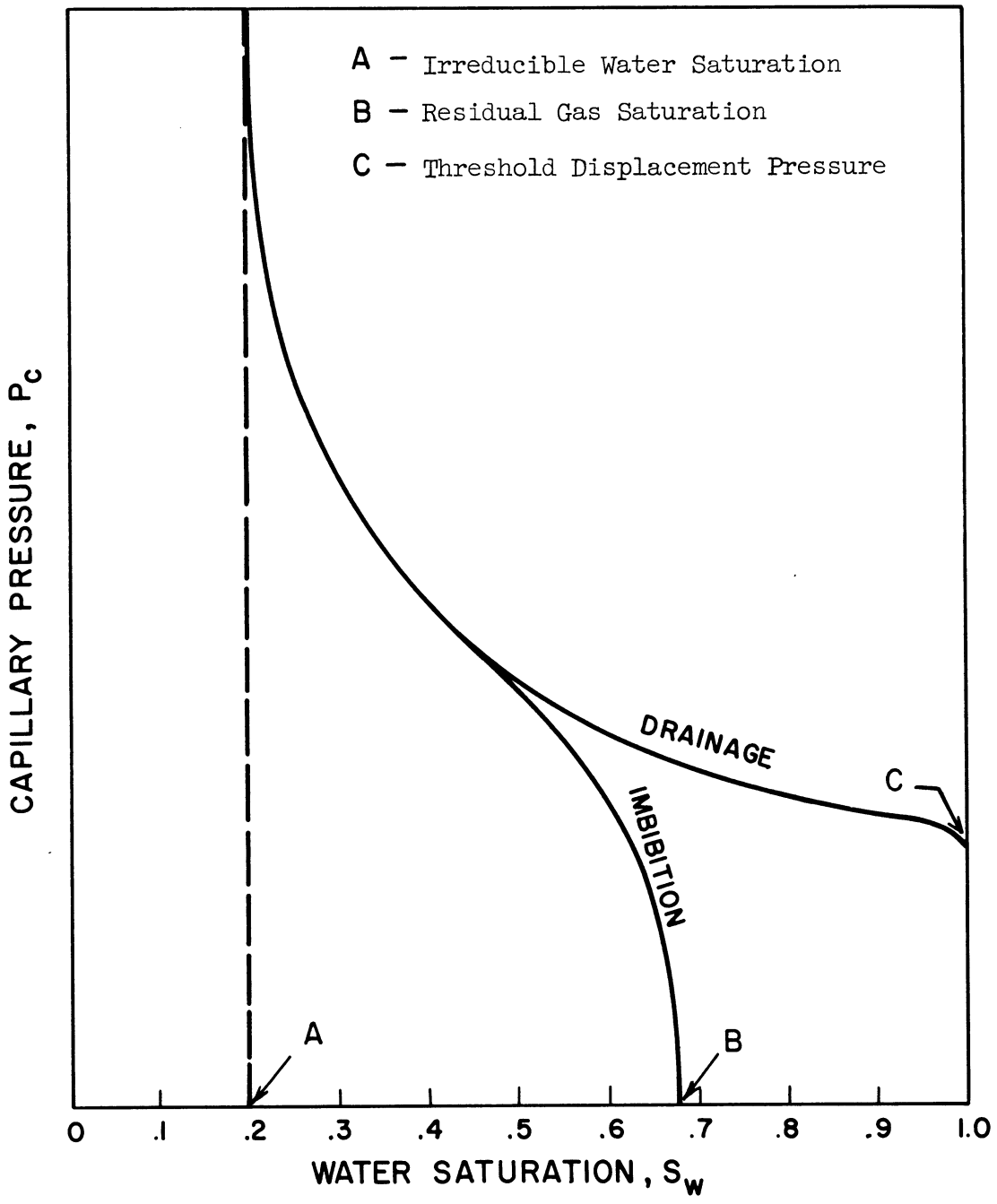

Figure 5. Typical Gas-Water Capillary Pressure Curve.

a wetting phase, water, by a nonwetting phase, gas, while the imbibition curve is usually obtained by the upward displacement of the nonwetting phase, gas, by the wetting phase, water.

The saturation corresponding to point A is common to both the drainage and imbibition curves. This saturation is known as the irreducible water saturation. At water saturations higher than the irreducible water saturation, water completely wets the solid surface and is therefore continuous. This type of saturation in the wetting phase is referred to as funicular, Figure 6.

As the water saturation is decreased a state of pendular saturation, Figure 6, is reached when gas is in contact with some of the solid surface. The irreducible water saturation, therefore, is that saturation where the wetting phase becomes discontinuous.

Point B at the base of the imbibition capillary pressure curve is referred to as the residual equilibrium gas saturation. This saturation corresponds to the largest gas saturation which can be left behind an advancing water fromt during imbibition. Lower gas saturations arising say from gas coming out of solution will result in an insular saturation distribution of gas. The gas phase in this region of saturation is discontinuous and consists of discrete bubbles of gas completely surrounded by water.

The hysterisis between the drainage and imbibition capillary pressure curves in Figure 5 is attributed to the varying pore sizes and shapes which occur in a porous medium. Amyx, Bass and Whiting[1] have attempted to explain this phenomenom by considering the capillary rise (imbibition) and the drainage from a capillary tube of varying diameter. The capillary rise of water into the tube is halted at the first opening

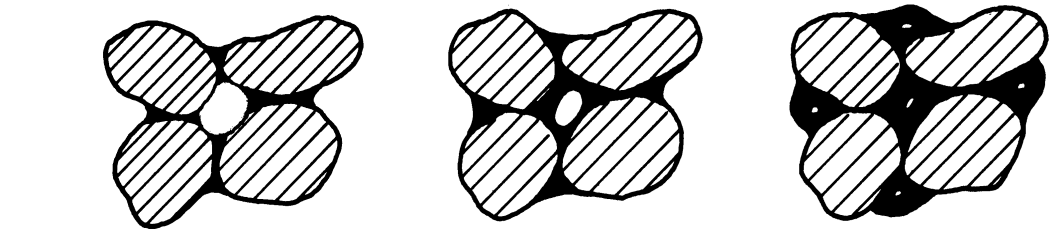

Pendular Saturation to Water
Funicular Saturation to Gas

Funicular Saturation
to both Water & Gas

Insular Saturation to Gas
Funicular Saturation to Water

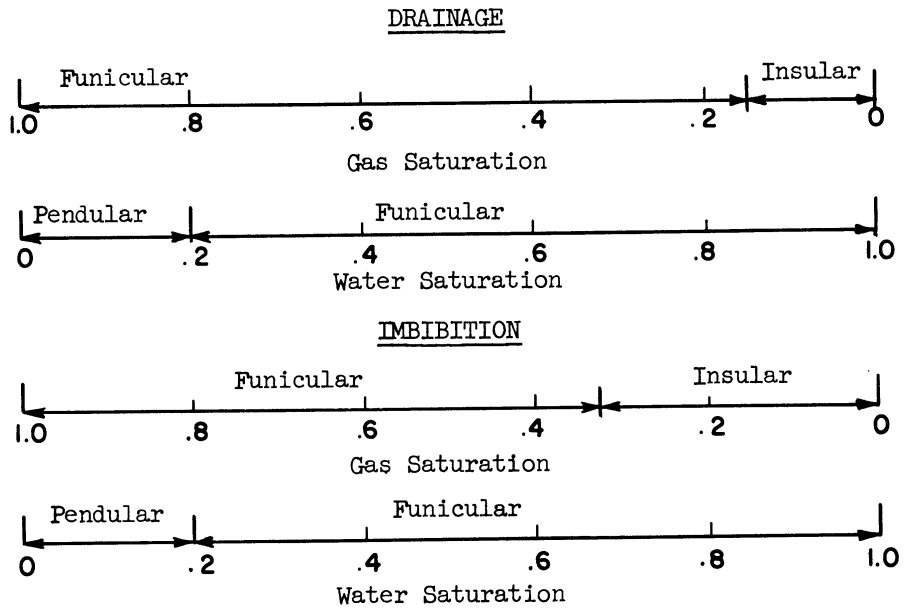

Figure 6. Types of Saturation Occuring in Porous Media.

large enough so that capillary equilibrium is obtained. The drainage of water by gravity, however, results when the tube narrows to a point where capillary equilibrium is reached. The capillary pressure in both cases is the same, but in the case of drainage the tube is still almost fully saturated with water, whereas in the case of imbibition the tube is barely filled with water.

The occurance of an equilibrium residual gas saturation during imbibition has been studied and satisfactorily explained by Gorring.(23) This saturation is attributed to the possibility that any given pore can be surrounded by smaller pores. When this is the case the wetting phase will rise around the pore in question due to the higher capillary suction in the smaller pores, and will ultimately pinch off the larger pore. Capillary jumps of this nature result in trapped globules of gas.

The end point of the drainage capillary pressure curve, point C, indicates the smallest pressure which is needed to start desaturation. This pressure is called the threshold displacement pressure and is the topic of the next section.

D. Threshold Displacement Pressures of Porous Media

The retention of gas in a reservoir by a caprock saturated with water is a result of the capillary forces acting at the gas-water interface (position of the interface where 100% water saturation occurs). Without the presence of water in the caprock, gas would leak out of the reservoir at a rate determined by the permeability of the caprock to gas.

The ability of a caprock to contain gas is expressed in terms of its threshold pressure which is defined as that pressure which is large enough to just cause continuous motion of the gas-water interface through

the caprock. This pressure essentially corresponds to the end point of the drainage capillary pressure curve, Figure 5. There is some doubt experimentally, however, just where this point occurs.

Let us now consider what happens to the gas-water interface in a reservoir as the gas pressure is increased. At low reservoir pressures, this interface will lie somewhere in a transition zone which lies between the porous reservoir rock and the caprock. This is illustrated by the end point of the dotted curve (100% water saturation) in Figure 7. As the pressure of the gas reservoir is increased, the interface will move upward to some level corresponding to a position which we shall designate as the bottom of the caprock (end point of the solid curve in Figure 7). This position is reached long before the gas pressure equals the threshold pressure and corresponds to the position where a uniform porous medium is reached in the caprock.

The application of larger pressures to the reservoir results in very little movement of the gas-water interface until the threshold pressure is reached. At this time a continuous motion of the gas-water interface will occur in the caprock.

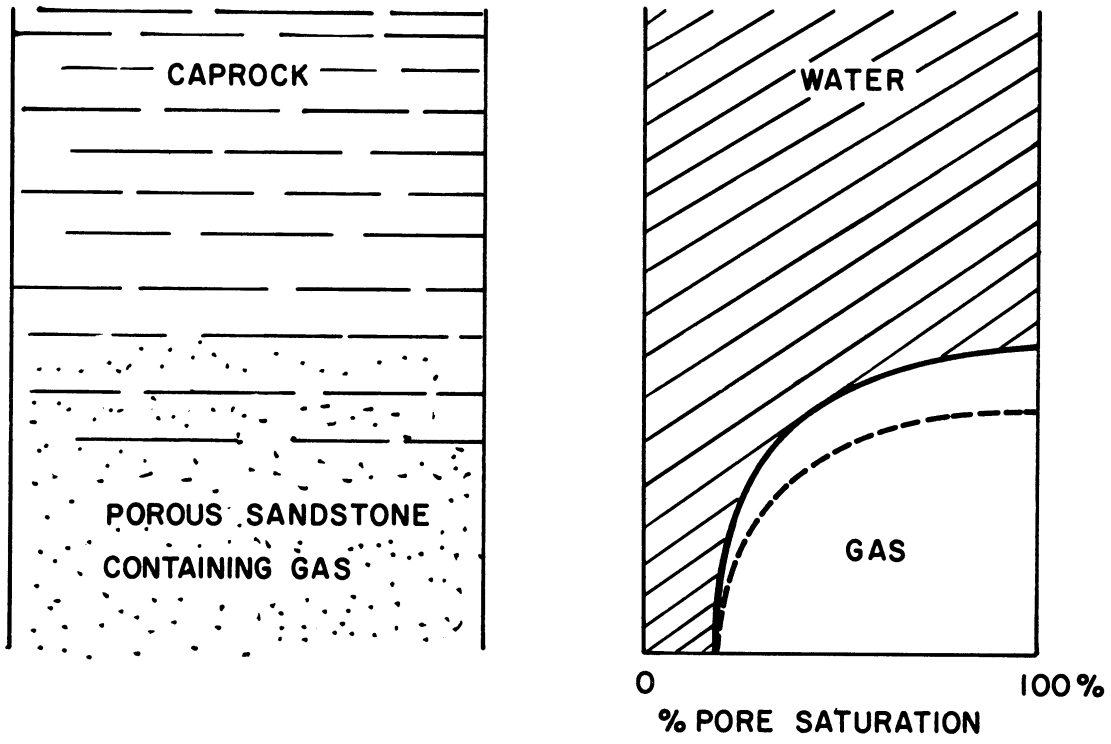

Figure 7. The Gas-Water Contact at the Bottom of a Caprock.

III. LITERATURE SURVEY AND THEORETICAL DEVELOPMENTS

In searching through the literature for theoretical developments involving the threshold pressures of porous media a rather broad subject list was reviewed. This undertaking was necessary since this research work, to my knowledge, is the first attempt to study and correlate threshold pressures for very low permeability porous media such as caprocks overlying gas storage reservoirs.

The theoretical developments pertaining to capillary pressure in porous media which have been reported in the literature are of necessity semi-empirical. This is due to the complex nature of the interstices of porous materials.

A. Leverett J-Function

One of the earliest attempts to correlate capillary pressure curves was presented by Leverett[33,34] in 1941. Leverett developed the semi-empirical relation

$$j(S_w) = \frac{\Delta\rho g h}{\sigma}\sqrt{\frac{K}{\phi}} = \frac{P_c}{\sigma}\sqrt{\frac{K}{\phi}} \qquad (8)$$

where

g = gravitational constant

h = height of capillary interface above free wetting phase surface.

K = permeability of the porous medium

P_c = capillary pressure of the porous medium

S_w = wetting phase saturation

ϕ = porosity of the medium

σ = surface tension between the two fluid phases

$\Delta\rho$ = density difference between the two fluid phases

by dimensional analysis and this relation has been supported to some extent by experimental data. Equation (8) is usually referred to as the Leverett "J-Function" or the "capillary pressure function."

The term $j(S_w)$ was assumed by Leverett to be a dimensionless function only of the wetting phase saturation, but it has also been shown to be a function of the type of the rock formation.

The capillary pressure, P_c, as expressed by Equation (8) is shown to be proportional to $j(S_w)$ and to the interfacial tension, σ, and inversely proportional to the square root of the permeability-porosity ratio $(K/\phi)^{1/2}$, which has units of length. Thus, there is theoretical justification for Equation (8) since it has the same basic form as the general capillary pressure equation for porous media

$$P_c = \sigma\left(\frac{1}{R_1} + \frac{1}{R_2}\right) \qquad (2)$$

or as the capillary pressure equation for a tube

$$P_c = \frac{2\sigma \cos\theta}{r} \qquad (5)$$

Leverett's experimental work showed that a plot of $j(S_w)$ versus wetting phase saturation for clean unconsolidated materials fall satisfactorily near two curves, one for imbibition, and the other for drainage. Rose and Bruce[47] have presented data (drainage capillary pressures curves) for consolidated systems along with a replot of Leverett's data, Figure 8. Their data show that consolidated systems are not all

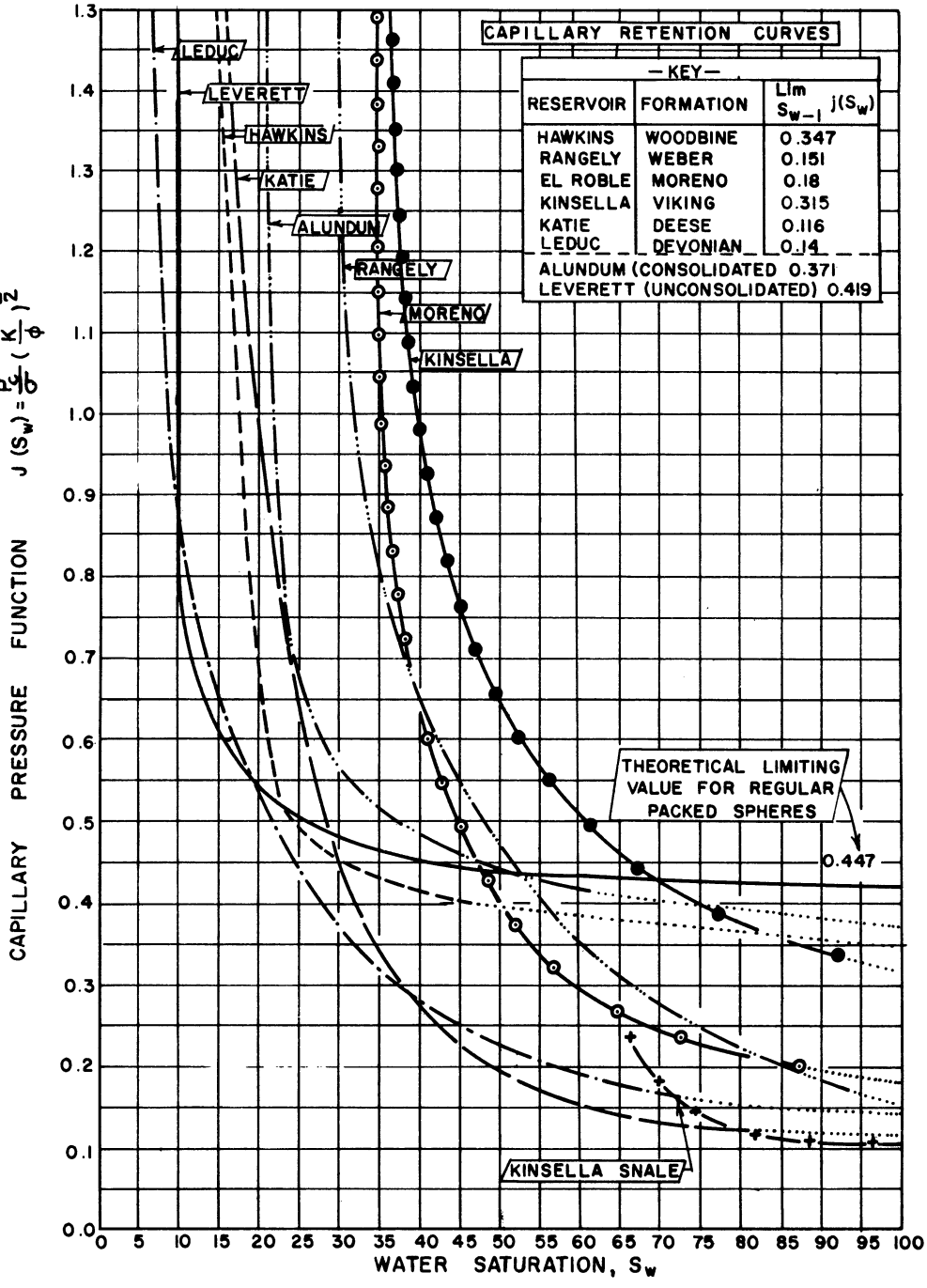

Figure 8. Capillary Retention Curves. (Rose and Bruce[47]).

uniquely represented by a single J-Function curve. Their data does indicate, however, that samples taken from individual reservoirs may be texturely enough alike so that a single J-Function curve may be obtained for a particular reservoir.

B. Kozeny-Carman Equation

Carman[12] who also studied clean unconsolidated sand systems derived the following equation for capillary pressure

$$P_c = \frac{\sigma A'}{\phi} , \tag{9}$$

where A' is the surface area in units of bulk volume. This equation was derived from the concept of hydraulic radius and Carman seemed to obtain experimental data confirming his theoretical argument.

The work of Leverett[33,34] and Carman[12] is closely connected if one considers the Kozeny equation which describes streamline flow through porous systems, Equation (10). This equation will be derived in detail in this section.

$$K = \frac{\phi}{k_z (A'_p)^2} \tag{10}$$

The term, k_z , is a "fudge factor", dependent on the particular porous system involved, which makes the Kozeny equation describe streamline flow through porous systems. The term, A'_p , is the surface area per unit volume of pore space and is related to A' by the following equation:

$$A' = \phi A'_p \tag{11}$$

By combining Equations(9), (10), and (11) an expression similar to Equation (8) is obtained. Thus when S_w (wetting phase saturation)

is unity

$$\frac{P_T}{\sigma}\left(\frac{K}{\phi}\right)^{\frac{1}{2}} = \left(\frac{1}{k_z}\right)^{\frac{1}{2}}_{\text{minimum}} \tag{12}$$

where P_T is the threshold pressure defined as

$$P_T = \lim_{S_w \to 1} P_c \tag{13}$$

A comparison of Equations (8) and (12) suggests a possible minimum value for $j(S_w)$.

$$\lim_{S_w \to 1} j(S_w) = \left(\frac{1}{k_z}\right)^{\frac{1}{2}}_{\text{minimum}} \tag{14}$$

Although Equations (8) and (12) are of fundamental importance in the study of capillary pressure in porous systems, they both include terms which can not be directly measured.

C. Model for Correlating Threshold Pressures

In the following paragraphs a theoretical development is presented which should prove useful in correlating threshold pressures with other measurable quantities of porous media.

Consider a model for porous media composed of a bundle of identical capillary conduits of total cross-sectional area ϕA and average effective length L_a .

Four basic equations must be written for this model before the threshold pressure can be related to other properties of porous media. These four equations are listed below and are either stated or derived in the development which follows.

(1) Poiseuille's law

(2) Darcy's law

(3) Capillary pressure equation

(4) Equation for the effective length of a porous medium

Poiseuille's law for laminar flow through a tube of circular cross-section is given by

$$v_a = \frac{d^2 \Delta P}{32 \mu L} \tag{15}$$

where

v_a = average velocity inside the tube

d = diameter of tube

L = length of tube

μ = fluid viscosity

ΔP = pressure drop

For conduits with non-circular cross-sections it has been experimentally shown that a mean hydraulic radius, m, should replace the diameter term in Equation (15).

$$m = \frac{\text{volume of tube}}{\text{area of wetted surface}} \tag{16}$$

For a tube, $m = d/4$. Equation(15), therefore, may be generally written as

$$v_a = \frac{m^2 \Delta P}{2 \mu L} \tag{17}$$

In this form, Poiseuille's equation approximates flow in non-circular conduits quite well. The constant, 2.0, in the denominator of Equation (17) should, however, be replaced by a shape factor, k_o, which has been shown to fall between 2.0 - 3.0 for the majority of non-circular conduits.

In applying Poiseuille's law to the flow which takes place inside a pore of a particular porous medium, a further correction for the length of the tortuous path the fluid takes must be made, since the average distance traversed by the fluid is greater than the length, L, of the porous medium. Let L_a be this average effective distance. Then

$$v_a = \frac{m^2 \Delta P}{k_o L_a} \tag{18}$$

Expressing v_a in terms of the superficial velocity, v, we have

$$v_a = \frac{v L_a}{\phi L} \tag{19}$$

Now writing Equation (18) in terms of the superficial velocity yields

$$v = \frac{\phi m^2 \Delta P}{k_o \mu L} \left(\frac{L}{L_a} \right)^2 \tag{20}$$

For porous media, m is equal to the ratio of the pore space per unit volume, ϕ, to the surface area per unit volume, A'. Then

$$m = \frac{\phi}{A'} = \frac{1}{A'_p} \tag{21}$$

where A'_p is the surface area per unit volume of pore space.

Introducing Darcy's law[30] for flow through porous media

$$v = \frac{K \Delta P}{\mu L} \tag{22}$$

it is possible to express Equation (20) in terms of the permeability, K, of a porous system. Making this substitution we have

$$K = \frac{\phi m^2}{k_o} \left(\frac{L}{L_a} \right)^2 \tag{23}$$

Equation (23) is known as the Kozeny-Carman equation, but it is usually written in terms of surface area per unit volume, A', rather than in terms of the hydraulic radius, m.

Before continuing the derivation relating threshold pressures with other rock properties it should be pointed out that Equation (23) can can be reduced to the Kozeny equation. Equation (23) can be written in the same form as the Kozeny equation by combining it with Equation (21) and the following definition*:

$$(L/L_a)^2 = \tau = \text{tortuosity of the porous medium}$$

$$k_z = k_o\tau = \text{Kozeny constant}$$

After making these substitutions we see that Equation (23) becomes

$$K = \frac{\phi}{k_z(A'_p)^2} \tag{10}$$

Returning now to the derivation relating threshold pressures with other rock properties, it is time to introduce the third equation, the capillary pressure equation.

The equation for the threshold pressure of a tube assuming a zero contact angle for gas and water is

$$P_T = \frac{2\sigma}{r} \tag{24}$$

Written in terms of hydraulic radius Equation (24) becomes

$$P_T = \frac{\sigma}{m} \tag{25}$$

Now, combining Equations (23) and (25) the following expression for threshold pressure is obtained.

* Carman[12] was responsible for writing the Kozeny constant, k_z, as the product of two parameters: one, a shape factor, k_o, and the other term, $(L_a/L)^2$, which Rose and Bruce[47] called tortuosity, τ.

$$P_T = \frac{\sigma}{\sqrt{k_o}} \frac{L}{L_a} \sqrt{\frac{\phi}{K}} \tag{26}$$

The above expression still contains one term, L/L_a , which needs to be expressed in terms of measureable quantities. Wyllie and Rose's[62] paper presents a method for determining L/L_a from the resistivity of the core which will now be discussed. Actually, the purpose of their paper was to obtain an expression for resistivity measurements on cores in terms of measureable properties of rocks rather than vise-versa.

The formation resistivity factor of a core is defined by Archie[2] is

$$R = \frac{R_o}{R_w} \tag{27}$$

where R_o is the resistivity of the rock when saturated with an electroyte having a resistivity, R_w . Resistivity is given by

$$R = \frac{rA}{L} \tag{28}$$

where

R = resistivity

A = cross-sectional area of the conductor

r = resistance across the core

L = length of the conductor

Now, let us determine the formation factor for a unit cube of length L and area A of the proposed model. The resistance across a unit cube of electrolyte having resistivity, R_w , is

$$r_1 = \frac{R_w L}{A} \tag{29}$$

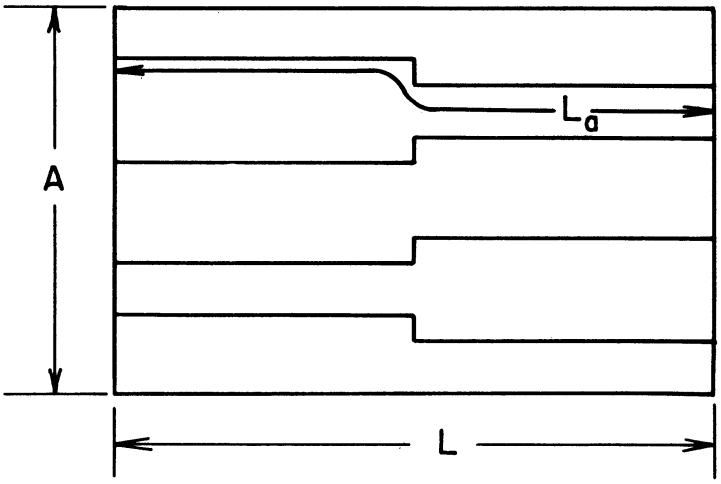

Figure 9. Straight Capillary Tube Model of Porous Media (Presented by Amyx Bass, & Whiting[1] to illustrate the model proposed by Wyllie et al[63,64]).

The resistance across a unit cube of the proposed model saturated with the same electrolyte is

$$r_2 = \frac{R_w L_a}{\phi A} \tag{30}$$

By definition, Equation (28),

$$R_o = \frac{r_2 A}{L} \tag{31}$$

Combining Equations (30) and (31) we have

$$R_o = \frac{R_w L_a}{L\phi} \tag{32}$$

Therefore

$$F = \frac{R_o}{R_w} = \frac{L_a}{L}\frac{1}{\phi} \tag{33}$$

Combining Equations (26) and (33) we arrive at the desired result, an expression for threshold pressure in terms of measureable properties* of porous media.

$$P_T = \frac{\sigma}{\sqrt{k_o}\,\phi F}\sqrt{\frac{\phi}{k}} \tag{34}$$

or

$$P_T = \frac{\sigma}{\sqrt{k_o}\,F}\sqrt{\frac{1}{\phi K}} \tag{35}$$

---

* All of the variables in Equations (34) and (35) are measureable except k_o . This variable is a shape factor which varies between 2.0 and 3.0 depending upon whether a pore's cross-section is circular, elliptical, square, etc. Since the term appears to the one half power little error is introduced by using a value for k_o between 2.0 and 3.0 .

The model used in deriving Equation (35) was first described and formally presented in an article by Wyllie and Spangler.[64] Previous theoretical investigations by authors such as Rose and Bruce,[47] and Wyllie and Rose[63] have also implied this model.

It is appropriate now to summarize the assumptions which were made in deriving Equation(35):

(1) The porous medium consists of a bundle of straight identical capillaries of complex shape oriented in a direction parallel to the macroscopic flow.

(2) The porous medium is uniform and isotropic with a flow area normal to the macroscopic flow of ϕA .

(3) To account for the complex shape of the capillary conduits Poiseuille's law may be written in terms of a mean hydraulic radius, m , and a shape factor, k_o , which lies in the range 2.0 - 3.0 .

(4) The path length of flow through the porous medium is not L but is some distance, L_a , greater than L due to the tortuous path which the fluid takes. It is also assumed that this average effective length is the same in fluid flow as in electrical conduction.

(5) The threshold pressure for the conduits of this model can be written in terms of their hydraulic radius.

(6) The contact angle between water and the rock surface in the porous medium is zero.

Many of the assumptions listed above have been implied in the work done by Wyllie and Spangler[64] and have been listed by Wyllie and Gardner[62] in their review of the generalized Kozeny-Carman equation.

Wyllie and Spangler[64] in an attempt to account for pore size distributions which occur in porous media have arrived at the following equation.

$$K = \frac{\phi_\sigma^2}{k_o(F\phi)^2}\int_o^1 \frac{dS_w}{P_c^2} \qquad (36)$$

This equation was derived by summing the individual flows for all of the infinitesimal portions of the pore space. Each of the individual flow rates were calculated from the Kozeny-Carman equation.

Although Equation (36) is more sophisticated than Equation (35), it can not be written explicitly in terms of the threshold pressure, P_T. The threshold pressure appears inside the integral as the end point of the capillary pressure curve. Thus, Equation (36) does not appear to be suitable for correlating threshold pressures since it requires the measurement of the entire capillary pressure curve.

Equation (35), on the other hand, should at least give a qualitative and hopefully a quantitative description for the threshold pressure of a porous medium in terms of other properties of the medium.

In addition to the development presented in this section, another development for correlating air-water threshold pressures with threshold pressures obtained by mercury injection is presented in Chapter VI.

Also a purely empirical correlation of the form

$$P_T = A\left(\frac{\phi}{K}\right)^B$$

is presented in Appendix D. This correlation was developed by the author[56] during his first year of graduate work, 1962. Data to test this correlatipm were supplied by the Northern Illinois Gas Co. and were taken by Core Laboratories in Dallas, Texas. This correlation was later used by Tek, et al.[53] with additional data, mostly for low threshold pressures, included.

IV. EXPERIMENTAL PROGRAM

In the following pages a description of the experimental apparatus and of the various measurements needed to characterize a core sample is presented. The measurements described in this section include porosity, air permeability, turbulence factor, water permeability, formation factor, mercury injection data, and threshold displacement pressure. All of the experimental techniques with the exception of the procedure for measuring threshold displacement pressure are fairly standard to the industry. The procedure for making some of these measurements, though, may differ somewhat from conventional methods found in the literature due to the complexities arising from the "tightness" of the cores being measured.

A. Experimental Apparatus

1. Apparatus for Saturating Core Samples

The apparatus which was used for saturating core samples with either water or sodium chloride solutions is illustrated in Figure 10.

The apparatus consists of two main parts: a vacuum chamber (bell jar sitting on a glass plate), and a water reservoir. The water reservoir is connected to the vacuum chamber by ground glass fittings. A vacuum stopcock is located between the water reservoir and the vacuum chamber so that water can be introduced into the beaker after evacuating the vacuum chamber.

The pressure in the vacuum chamber is obtained by reading a McLeod gauge.

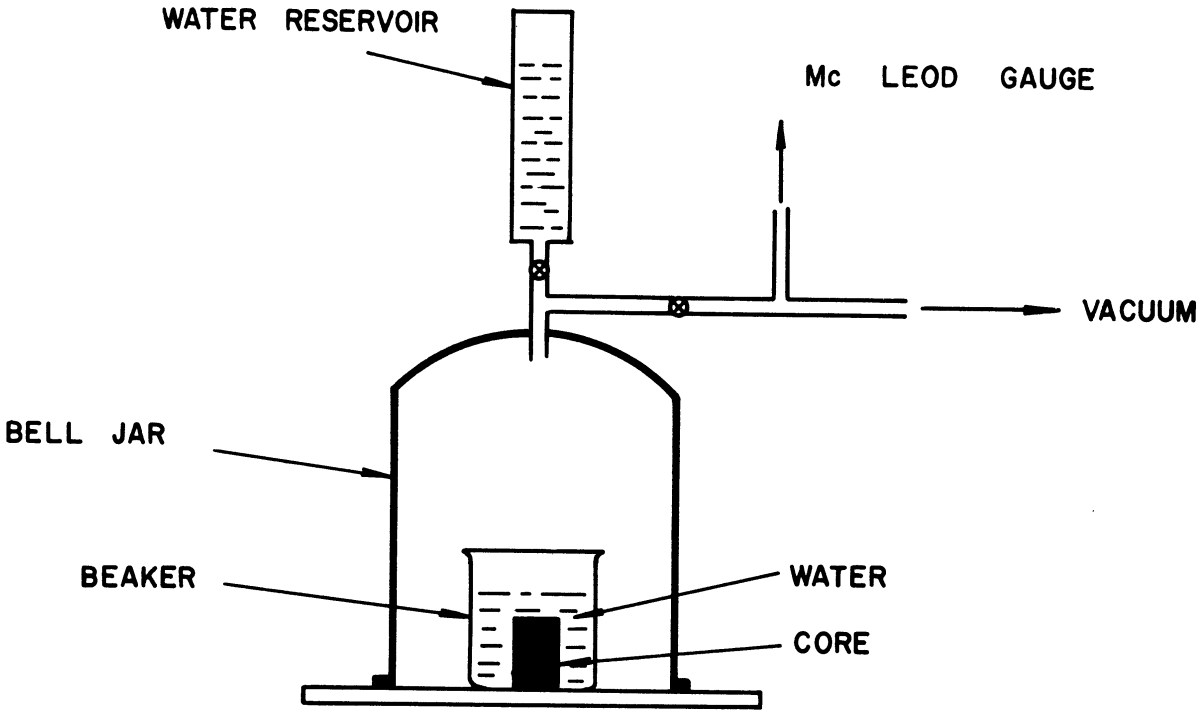

Figure 10. Apparatus for Saturating Core Samples.

2. Ruska Pump

The Ruska pump shown in Figure 11 was used to supply constant water flow rates. The pump consists essentially of a cylinder fitted with a piston which is driven by a screw and gear drive. Flow rates of 1 to 224 cc/hr (448 cc/hr for both cylinders) can be obtained by setting the gear box on the Ruska Pump. Accurate displacement volumes for each cylinder are indicated on a scale whose smallest division is .02 cc.

3. High Pressure Core Holder

An overall view of the high pressure core holder and its auxiliary equipment which was used in this research work is shown in Figure 12. A schematic drawing of the core holder drawn to scale is presented in Figure 13. The design for this core holder was developed by Core Laboratories in Dallas, Texas.

The core holder was constructed from 304 stainless steel and was designed for an operating pressure of 1500 psi. The end plates of the holder are fitted with 2" x 2-3/8" x 3/16" O-rings which serve as a seal for the sleeve pressure. These plates are held in position by threaded end caps either of which can be removed to allow access to the inside of the holder. The top end plate is also fitted with a second O-ring (1/4" x 3/8" x 1/16") which seals the core holder at the point where the stem of the holder protrudes through the end plate. The bottom end plate for the core holder was drilled and threaded for 1/8" pipe.

Both end plates for the core sample are scored with lines radiating from the center of the plates and also with concentric circles about the center of the plates. These lines allow even fluid and pressure distributions across the ends of a core. The top core end plate is attached

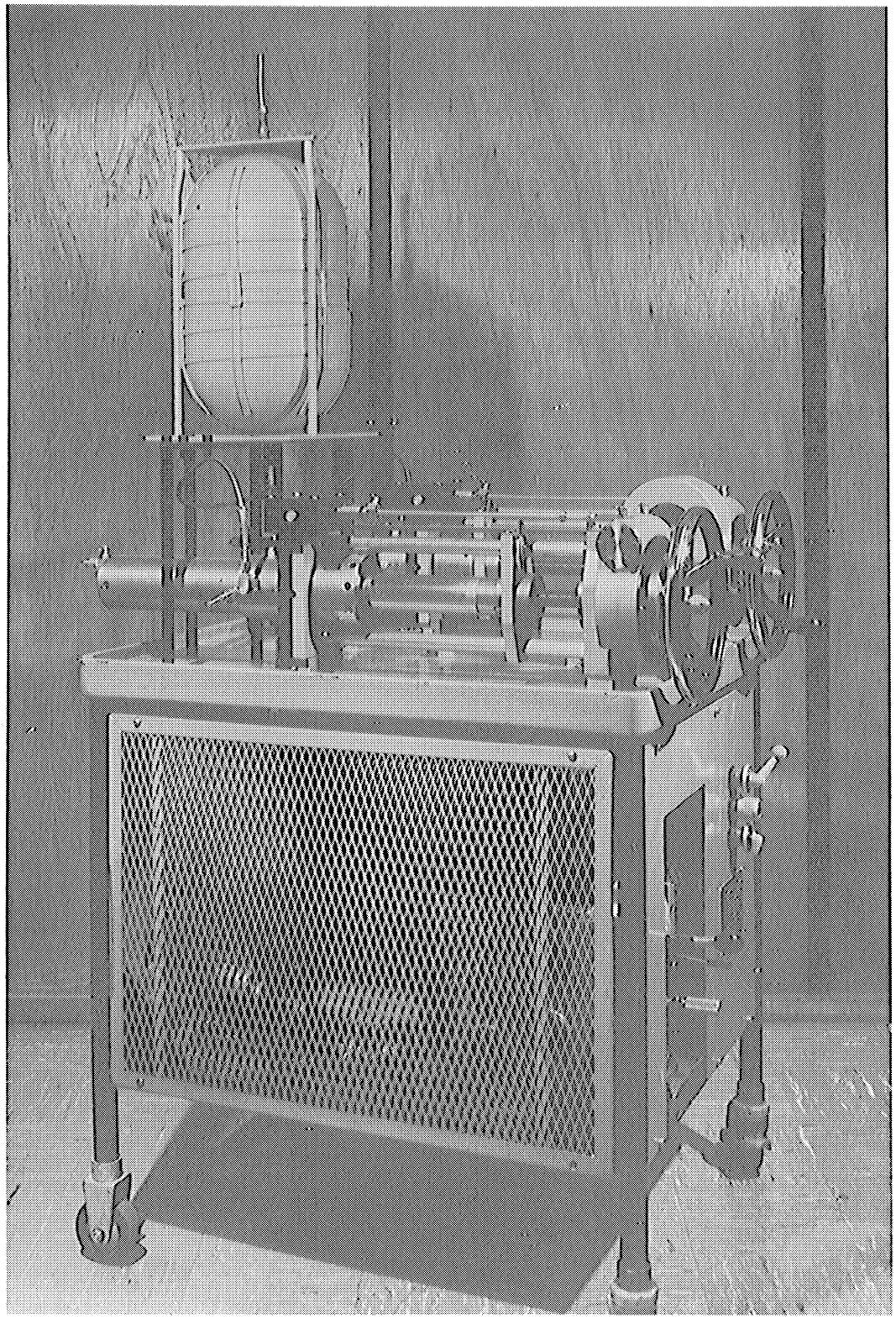

Figure 11. Ruska Pump.

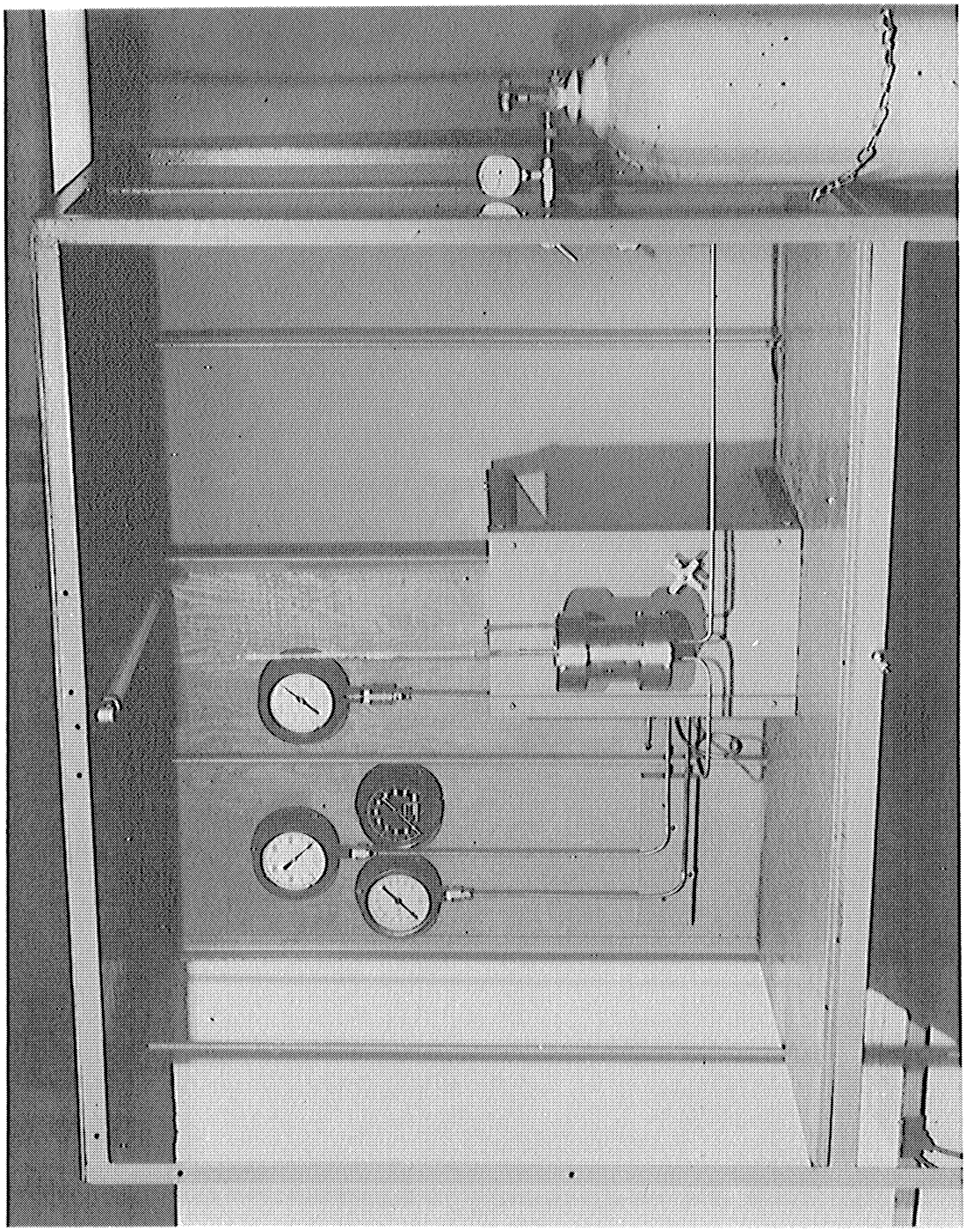

Figure 12. High Pressure Core Holder Apparatus.

to the stem of the core holder. The bottom core end plate also serves as the bottom core holder end plate.

The rubber sleeve used in the high pressure core holder was fabricated from buna rubber. The sleeve was purchased through Maeder Instrument Co. in Dallas, Texas and was made by wrapping a continuous thin layer of rubber around a 1-1/2 inch cylinder until the desired thickness of sleeve was obtained. The sleeve was then vulcanized to laminate the layers together.

In addition to the components of the core holder discussed here and illustrated in Figure 13 two additional solid end plates similar in overall dimensions to the top core holder end plate were constructed. These end plates allow the use of the core holder as a pressure vessel during the core saturation procedure.

A flow diagram of the entire high pressure core holder apparatus is shown in Figure 14. The inlet side of the core holder can be attached to either the Ruska pump for water permeability tests or to a nitrogen cylinder for air permeability or threshold pressure tests.

The core holder is equipped with three pressure gauges (0-60 psi, 0-500 psi, 0-1000 psi) on the core side of the core holder in order to yield accurate readings over the entire operating pressure range of the apparatus.

Nitrogen over water was used to supply the sleeve pressure for the core holder. The nitrogen-water interface was located in the pressure surge tank and water extended from this tank thru 1/4" stainless steel tubing to the outside of the rubber sleeve. The pressure surge

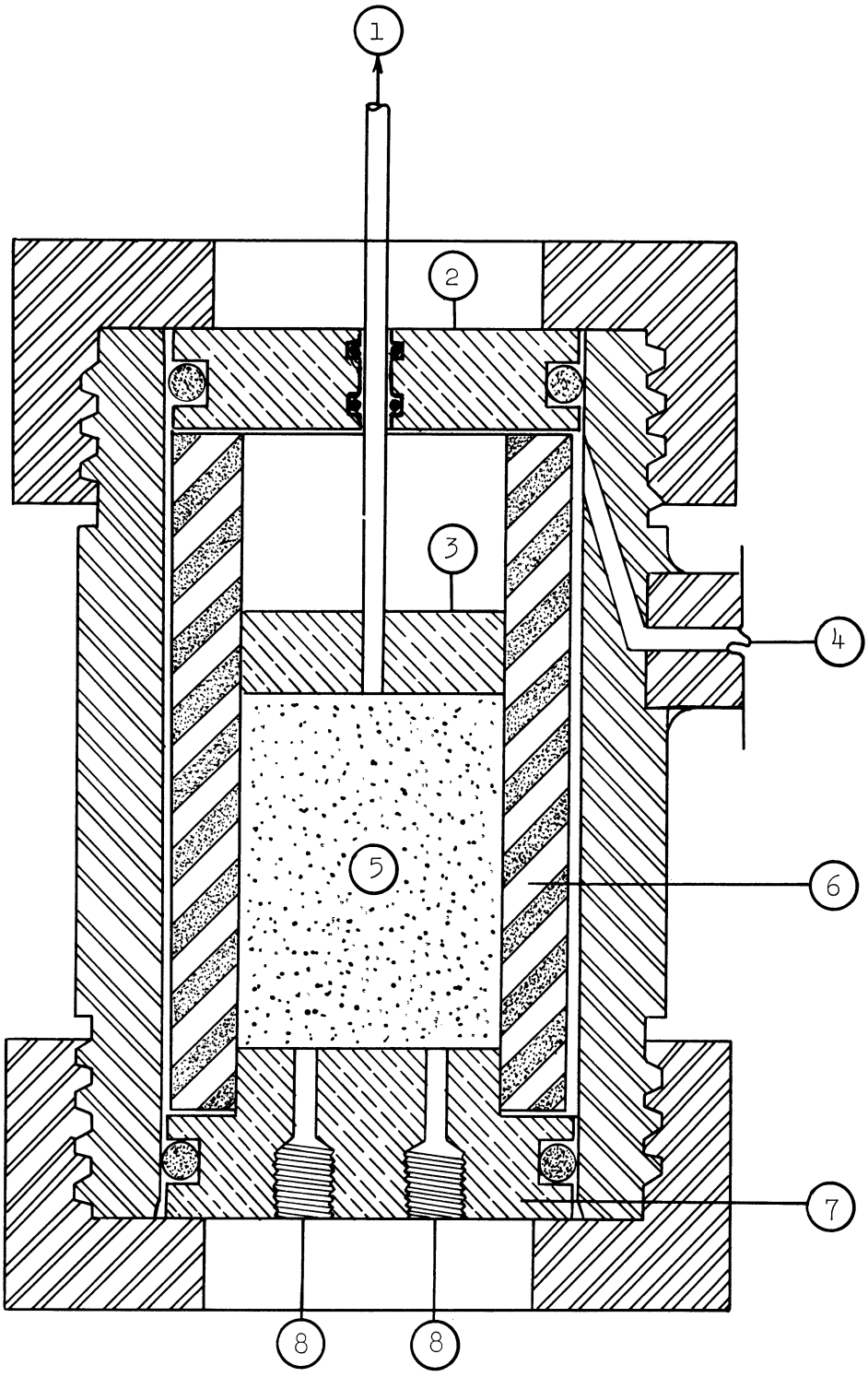

Legend:

1. Outlet stem
2. Top coreholder endplate
3. Top core sample endplate
4. Pressure inlet for rubber sleeve
5. Core sample
6. Rubber sleeve
7. Bottom core holder and sample end plate
8. Gas or water inlets

Figure 13. Longitudinal Section of High Pressure Core Holder

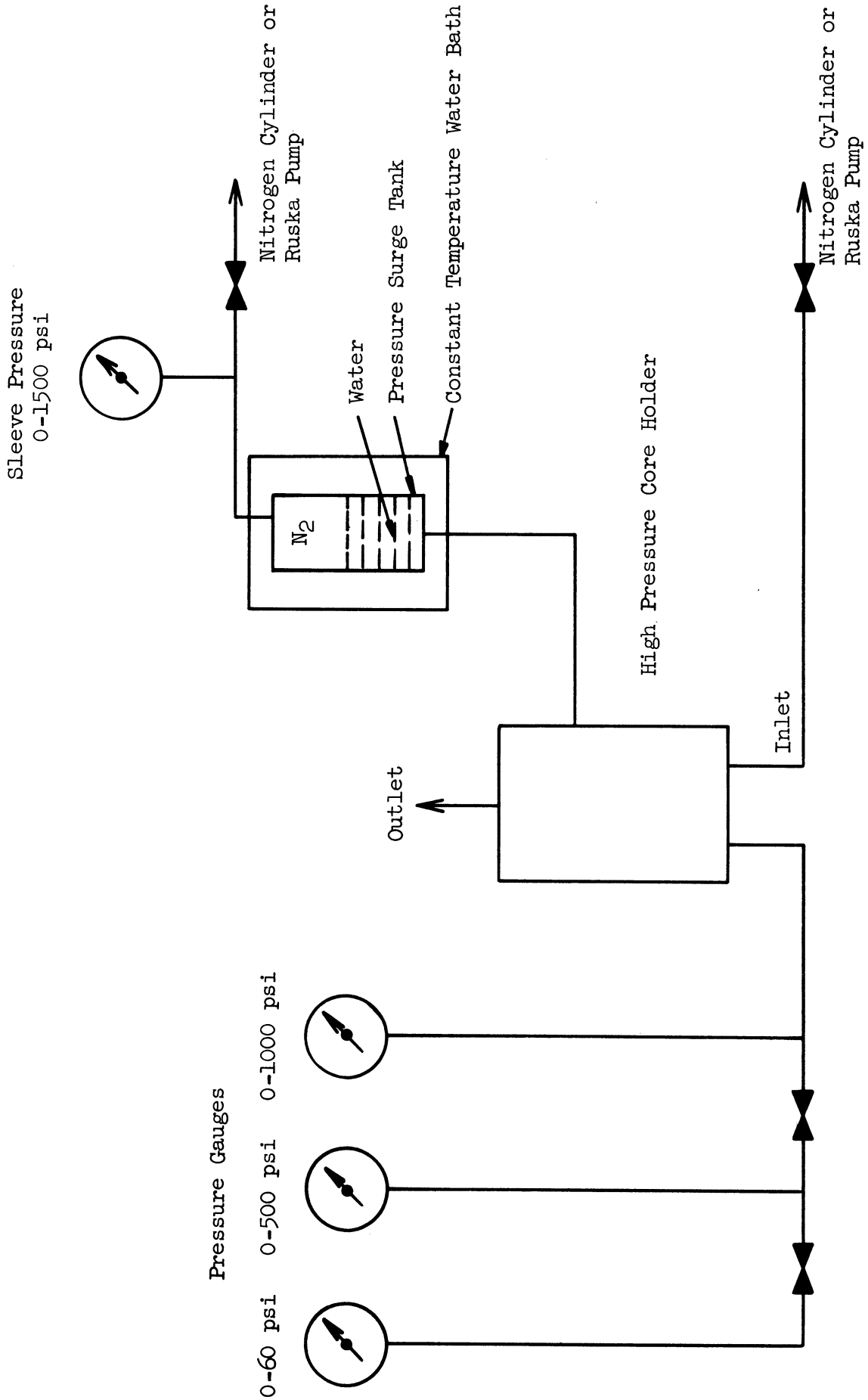

Figure 14. Schematic Flow Diagram of the High Pressure Core Holder Apparatus.

tank was placed in a constant temperature water bath to eliminate changes in sleeve pressure caused by room temperature fluctuations. Early experiments were made using an exclusive water sleeve pressure system, without a constant temperature bath, but this was soon abandoned since small changes in room temperature result in large pressure variations for confined incompressible liquids.

When the core holder was used as a pressure chamber for saturating core samples the entire volume of the pressure surge tank was filled with liquid. The Ruska pump was then operated manually to supply fluid pressure to the pressure chamber.

Figure 15 shows a Hassler core holder which was used in a limited capacity in this research work for flow experiments on a few of the higher permeability samples.

4. Resistivity Apparatus

The apparatus used for measuring the resistivity of a core sample is shown in Figure 16. The apparatus was constructed from 3/8" lucite and is capable of holding a core sample 6 inches long.

The electrodes for this apparatus were made from platinum foil and are backed by felt to assure a good electrical contact.

The leads in the foreground of Figure 16 are connected to a 60 cycle per second A.C. bridge which was used to obtain the resistance across the platinum electrodes.

5. Mercury Injection Apparatus

The mercury injection apparatus used in this research work was an Aminco-Winslow Porosimeter. A schematic piping diagram of this porosimeter is shown in Figure 17. A cross-sectional view of the penetrometer

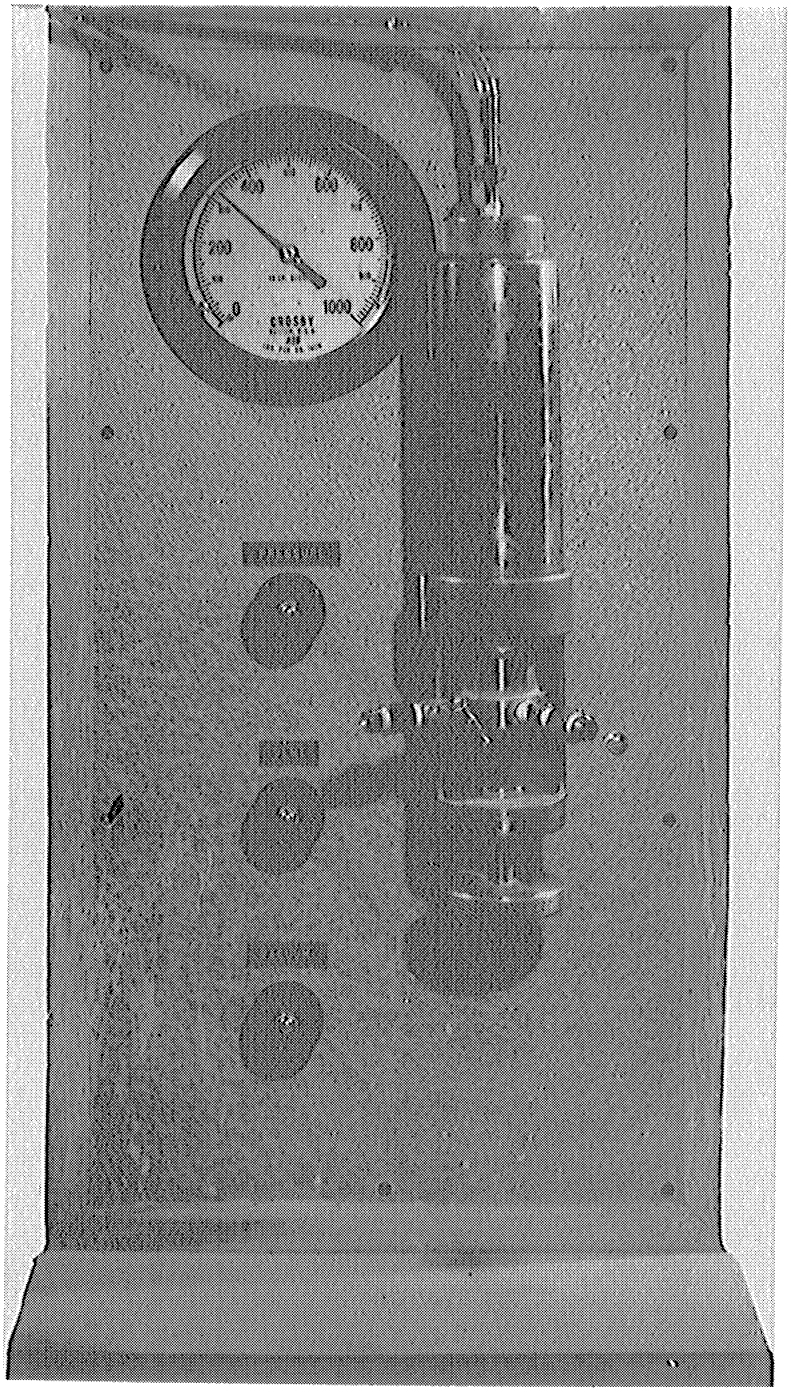

Figure 15. Hassler Core Holder.

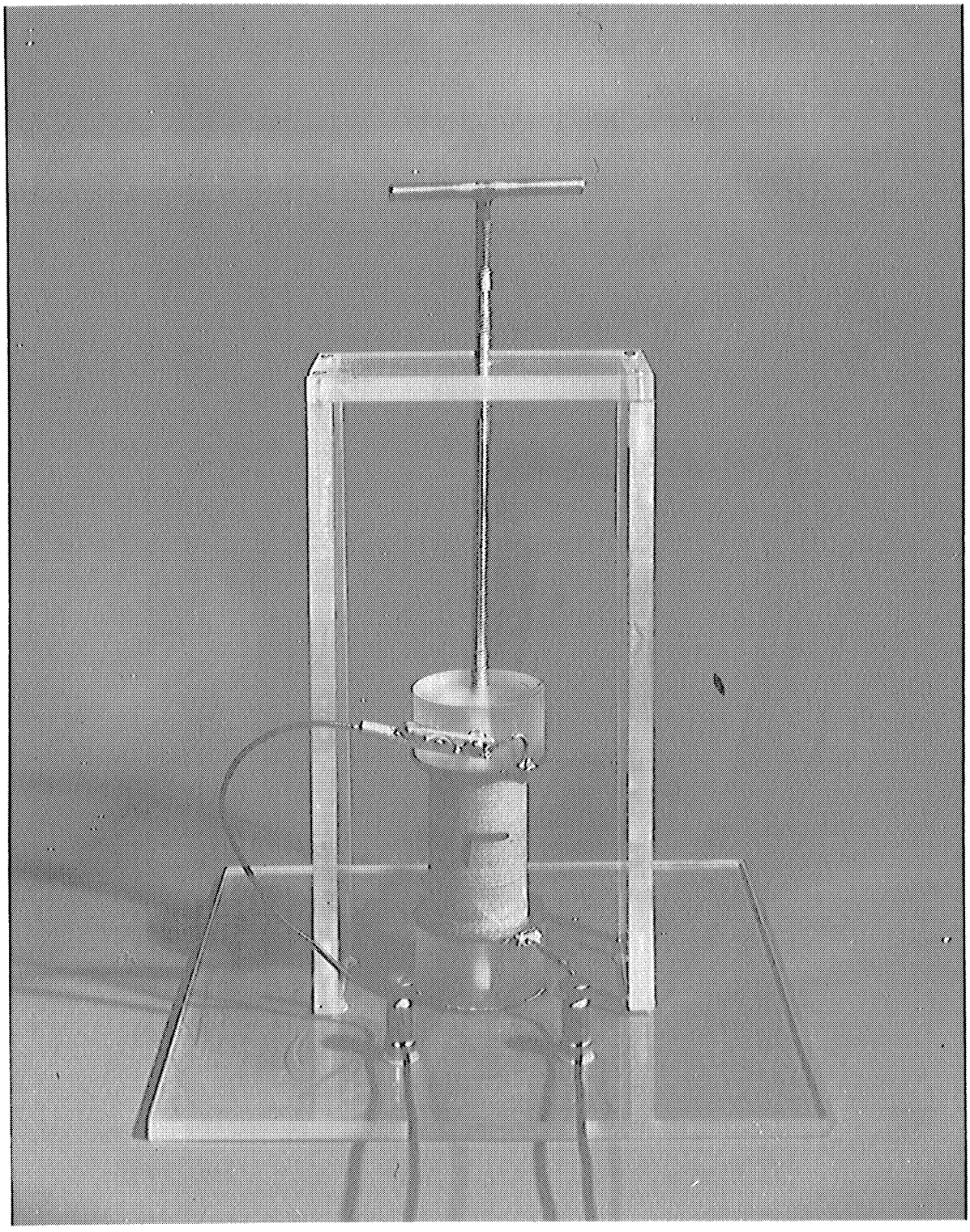

Figure 16. Resistivity Apparatus.

which holds the core sample is shown in Figure 18. The smallest division on the stem of the penetrometer was .002 cm^3.

The apparatus consists of two main parts: a mercury filling device; and a hydraulic pressure chamber. The hydraulic system is equipped with blead valves to eliminate air from the system. The pressure for the system is supplied by a hand operated piston-cylinder pump. Isopropyl alcohol is used for the hydraulic fluid in this apparatus.

B. Experimental Procedure

1. Core Preparation

The core samples used in this work were 1-1/2 inches in diameter. These samples were received from various companies in industry and the majority of them were already cut to a 1-1/2 inch diameter. The rest of the cores were obtained by coring with a 1-1/2 inch diamond drill bit.

Each core was cut to length (1-2 inches) with a diamond saw. The ends were then faced off perpendicular to the sides by placing each sample in a lathe and grinding the ends with a high speed grinding stone driven by air.

2. Drying Procedure

Core samples can be thoroughly dried by heating them in an oven for 24 hours at a temperature of 220°F. Longer drying times resulted in no substantial change in weight of the samples.

After drying, the cores were kept in a dessicant bed to prevent capillary condensation from occuring.

3. Air Permeability

The method of Cornell and Katz[17] was used for obtaining air permeabilities. To account for turbulent flow a quadratic modification

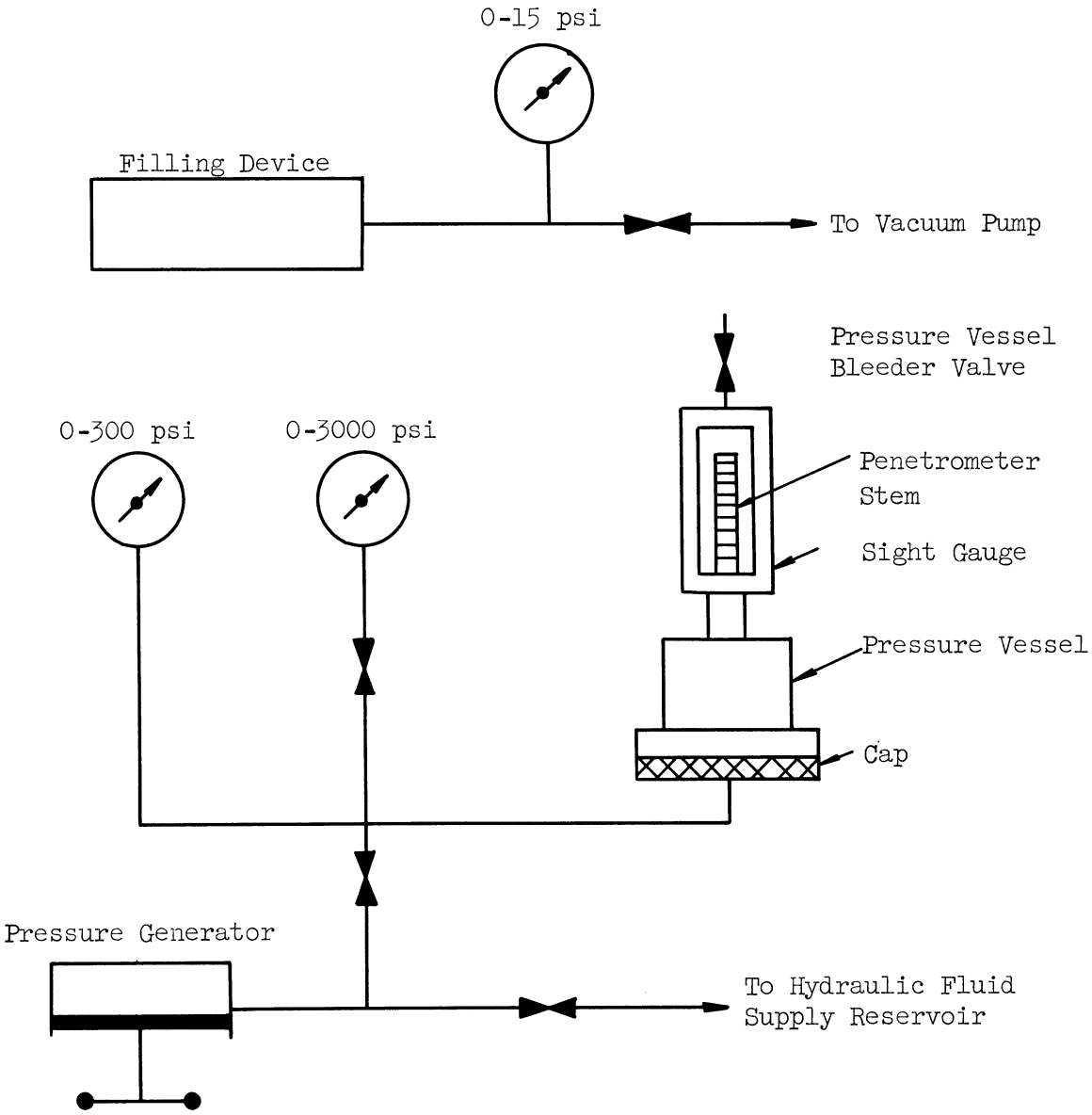

Figure 17. Schematic Piping Diagram of Aminco Winslow Porosimeter.

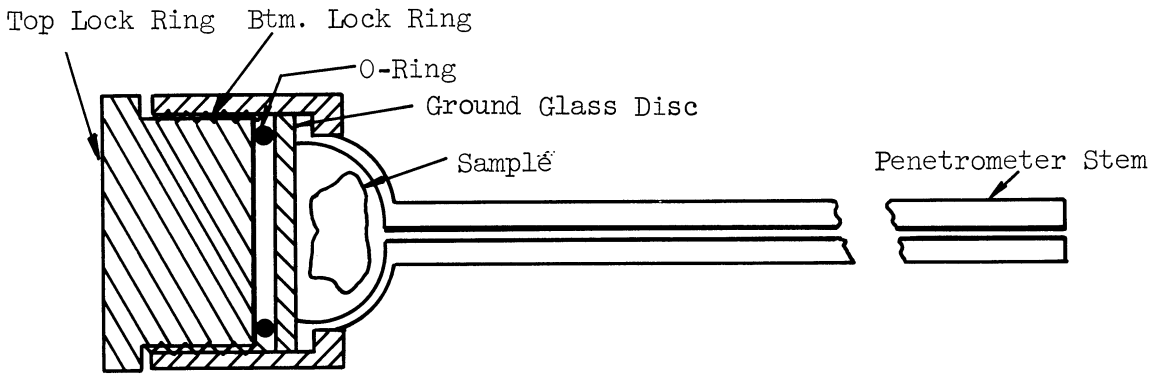

Figure 18. Penetration Assembly for Aminco Winslow Porosimeter.

of Darcy's Law is used.

$$-\frac{dP}{dL} = \frac{\mu v}{K} + \beta \rho v^2 \qquad (37)$$

where

P = pressure, atm

L = length, cm

μ = viscosity, cps

K = permeability, darcys

ρ = density, gm/cm^3

β = turbulence factor, atm sec^2/gm [commonly expressed in units of ft^{-1} by multiplying by a conversion factor of $3.10(10^7)$]

For gases it is convenient to express Equation (37) in terms of mass velocity, $W/A = \rho v$, which remains constant. Then Equation (37) can be integrated from point 1 to 2 to yield

$$\frac{MA(P_1^2 - P_2^2)}{2zRT\mu LW} = \frac{W}{A\mu}\beta + \frac{1}{K} \qquad (38)$$

where

W = mass flow rate, gm/sec

A = cross sectional area, cm^2

μ = molecular weight

z = compressibility factor (evaluated at an average pressure

M = Molecular Weight

R = gas constant

T = absolute temperature

Now if one plots the parameter $(MA(P_1^2 - P_2^2))/(2zRT\mu LW)$ versus $W/(A\mu)$ the resulting graph is a straight line with a slope equal to the turbulence factor, β , and an intercept equal to the reciprocal of the permeability, $1/K$.

Both the high pressure core holder and the Hassler core holder were used for taking air permeability measurements. The high pressure core holder was used on the lower permeability samples. The gas used for the air permeability measurement was nitrogen. The flow of gas for a set pressure drop across the core was measured at the outlet end by collecting the gas over water.

4. Saturation Procedure

The procedure for saturating a core is somewhat involved, but each of the required steps are necessary especially for low permeability core samples.

First, a dry core sample was saturated with carbon dioxide by passing several pore volumes of carbon dioxide through the core. The purpose of this step is to replace the air in a core, which is practically insoluble in water at standard conditions, with a gas which is soluble in water, carbon dioxide.

Next, the core was placed in a beaker and set inside a vacuum chamber where a pressure of less than 10 microns of mercury was achieved. The core was left overnight in the vacuum chamber prior to flooding it with water to insure pressure equalization inside the core. The system pressure was 2 microns or less at the end of this interval of time.

Each core was saturated with de-aerated distilled water containing 25 ppm mercuric chloride by flooding it in its evacuated state.

The mercuric chloride was added as a bactericide.

The last step in saturating a core was to place it in a water pressure chamber at a pressure of at least 1000 psi for a period of a time. This step speeds up the imbibition of water into the core and during this time any carbon dioxide still remaining inside the core will go into solution. Total saturation is reached when the chamber pressure no longer decreases with time.

5. Porosity Determinations

The porosity of the core samples was measured by weight difference. Each core sample was weighed dry and was again weighed after the saturation step. Percent porosities were calculated from the following equation.

$$\phi = \frac{(\text{wet weight of core sample-dry weight})100}{(\text{density of water})\ AL} \qquad (39)$$

The porosities of three of the core samples used in this research work were checked by an independent method. The porosities of these samples were obtained using a Boyles law apparatus by Pan American Research personnel during a visit by the author to that company. The results checked very closely with the weight difference method Chapter V, and it was concluded that the weight difference method was sufficient for this research.

6. Single Phase Permeability to Water

The water permeability of a core is obtained by measuring the pressure drop across the core resulting from a constant flow of water through it. The permeability is then given by Darcy's[39] equation

$$q = \frac{-KA}{\mu}\frac{dP}{dL} \qquad (40)$$

where

q = volumetric flow rate, $cm^3/sec.$

μ = viscosity of the flowing fluid, cps

K = permeability, darcys

A = cross sectional area, cm^2

P = pressure, atm

L = length,

In this work de-aerated distilled water was used in the water permeability experiments. The constant flow rate was supplied by a Ruska pump and the flow was checked at the outlet end of the core by a 0.1 cm^3 micropipette whose smallest division was 0.001 cm^3.

a. Effect of Different Fluids on Single Phase Permeability of Porous Media

Single phase permeability according to Darcy's law should be independent of the fluid flowing through the porous media. This is only true, however, for consolidated porous media, whenever the fluid in the pores of the porous media does not alter the size and shape of the pores.

The presence of clay in porous media results in a lowering in permeability to fresh water as compared to permeability to air. The phenomena involved has been invertigated by several people[28] and has been found to be caused by the hydration and consequent swelling of clay material which may line the walls of pores or which are part of the cementing material between the solid grains of the porous media. The swelling of these clays causes a reduction in the size of the pores and thus a reduction in the permeability of this porous media to water.

The degree of swelling due to hydration of clays is a function of the salinity of water and is a reversible process. The permeability increases at first with increasing water salinity and then approaches some constant value with further increases in water salinity, Figure 19.

7. Threshold Displacement Pressure Measurement

The threshold pressure measurements were performed in the high pressure core holder. While mounting a given core sample in the holder a layer of water was placed on top of the core sample and extended into the stem of the holder, Figure 13. Care was taken during this step to eliminate air bubbles from this water. A micropipette was attached to the stem of the core holder with a short section of tygon tubing. Again, care was taken to eliminate air bubbles from the tygon tubing and pipette.

A pressure between 1,000-1,500 psi was applied to the sleeve of the core holder. Some flow of water from the core and its holder took place as a result of the sleeve pressure. Due to the low permeabilities of caprock samples this flow sometimes took as long as a day to stop. Each core sample was allowed to set an extra day after this flow had ceased to be sure that none of the flow during the threshold pressure measurement was a result of the sleeve pressure. After this amount of time the threshold pressure measurements were started.

Gas pressure was applied to the bottom of the core sample. The size of the pressure increment was determined by the "tightness" of the core. The lower the permeability of the core the larger the pressure increment. The largest pressure increment used for any sample was 100 psi.

After each increment of pressure the average rate of water flow from the core was measured with time until the flow ceased. When the

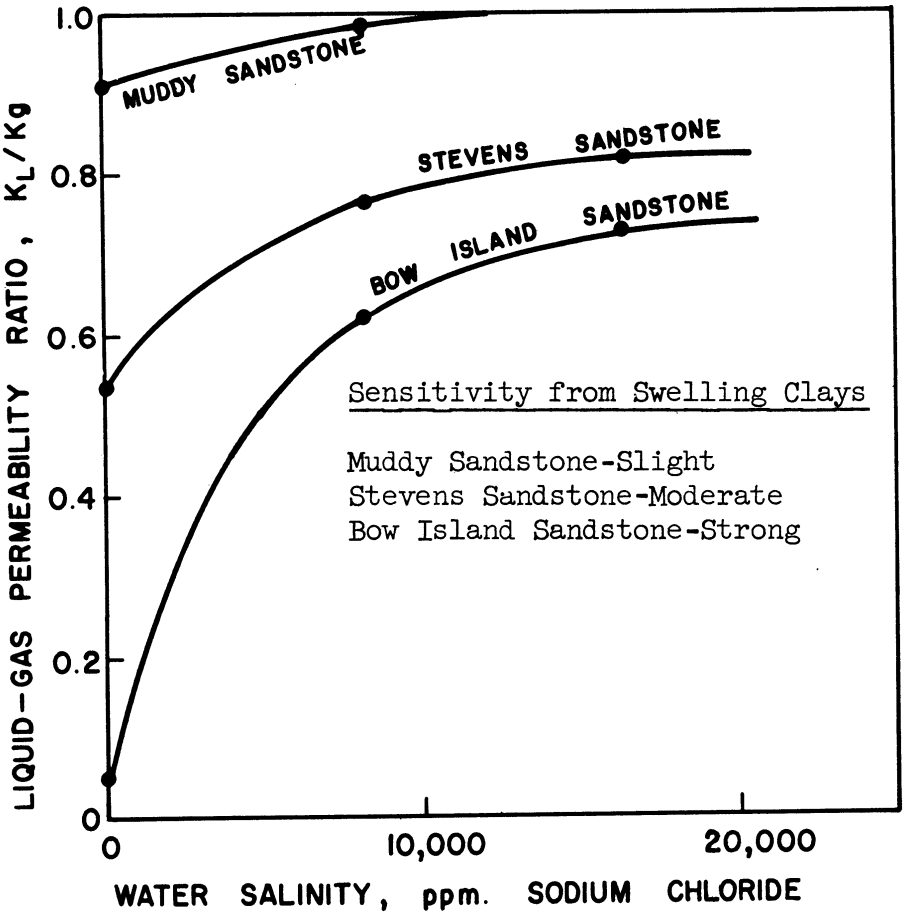

Figure 19. Effect of Water Salinity on the Permeability of Porous Media Containing Clay (from Hewitt[28]).

threshold pressure was reached, a continuous flow of water resulted and if enough time was allowed gas finally appeared from the outlet end of the core.

8. Resistivity Measurement

The first step in measuring the resistivity of a core was to saturate it with an electrolyte of known resistivity. The technique of saturating the core with the electrolyte is the same as was previously outlined for saturating a core with distilled water. Each core, however, was allowed to "age" in a covered beaker containing electrolyte for at least one week before the resistivity measurement was made.

To measure the resistance of the saturated core it was placed between two platinum electrodes (backed by felt) as is illustrated in Figure 16. The resistance across the bridge was then obtained by balancing a 60 cycle per second A.C. bridge.

a. Effect of Conductive Solids on Formation Resistivity Factor

The derivation of formation factor for porous media assumed that the porous matrix is not a conductor. This may or may not be true depending on whether or not clay materials are present. Pathnode and Wyllie(42) and others have shown that clays contribute substantially to the conductivity of a rock when the rock is saturated with dilute electrolytes. Wyllie suggested that this is due to having two electrical circuits in parallel: the conducting clay materials and the pores filled with electrolyte. The total resistivity of a sample containing clay would then be given by

$$\frac{1}{R_a} = \frac{1}{R_c} + \frac{1}{R_o} \qquad (41)$$

where

R_a = total resistivity of sample saturated with an electrolyte of resistivity R_w

R_c = resistivity of the clay materials

R_o = resistivity of the rock (assuming no clay present) saturated with electrolyte of resistivity R_w

Multiplying both sides of Equation (41) by R_w and assuming that $1/R_c$ is a constant for a given sample yields

$$\frac{1}{F_a} = cR_w + \frac{1}{F} \tag{42}$$

where

F_a = apparant formation resistivity factor

F = true formation resistivity factor

Equation (42) or an equivalent form of this equation was first presented by Patnode and Wyllie[42] and deWitte[18] and was later discussed and tested by Hill and Milburn.[29] For values of low water resistivity, data are approximated by Equation (42) and yield a straight line when reciprocal apparent formation factor in plotted versus water resistivity, Figure 20.

The problem of clay materials influencing measurements for true formation factor (non-conducting porous system) can be almost eliminated if electrolytes of high conductivity are used. This is illustrated by both Figure 20 and Figure 21.

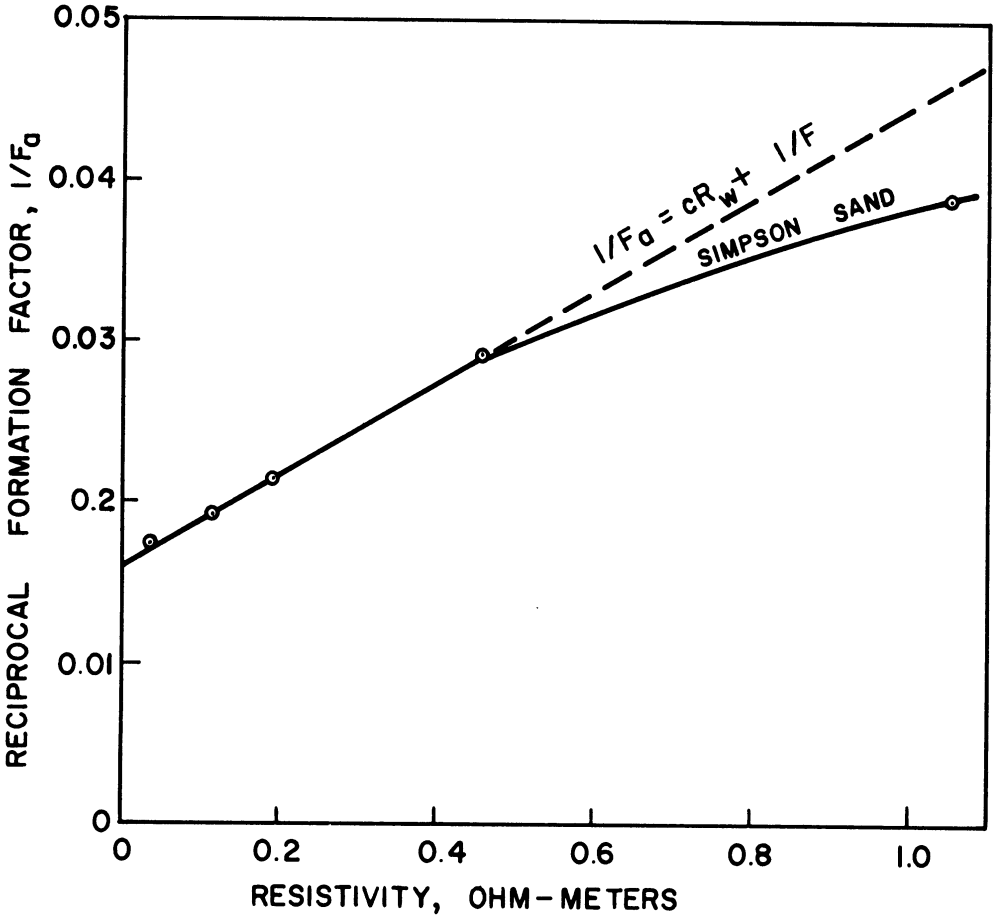

Figure 20. Reciprocal Formation Factor versus Water Resistivity (from Hill & Milburn[29]).

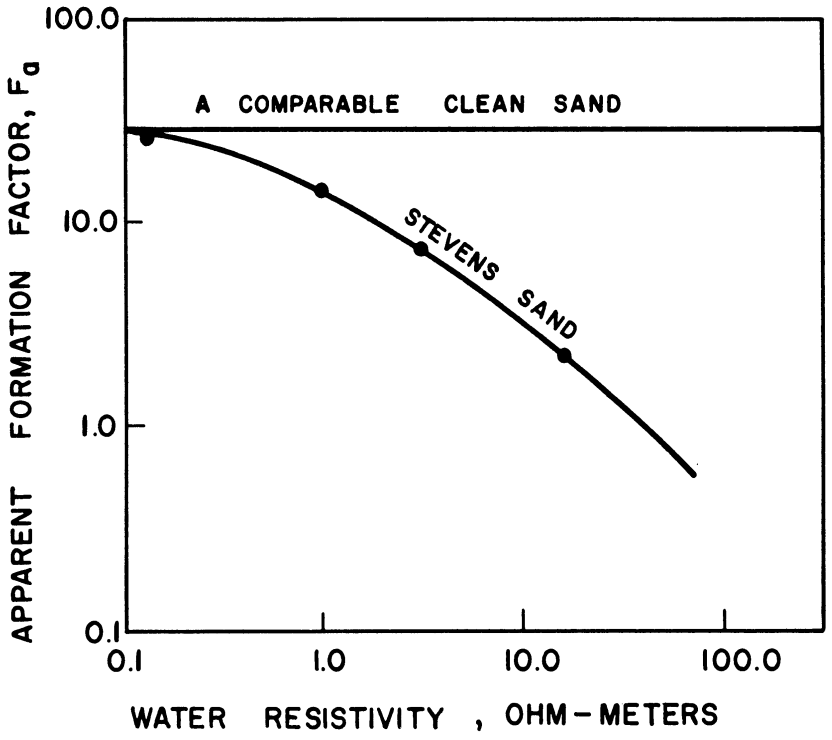

Figure 21. Apparent Formation Factor versus Water Resistivity for Stevens Sand of Paloma Field, California (from Winn[61]).

In this research work formation factors were measured for each sample using 5 and 10 weight percent solutions of sodium chloride except for the extremely low permeability samples.

For the higher permeability samples each core was first saturated with the 5 weight percent sodium chloride solution and then the resistivity of the sample was measured following the procedure previously outlined. The 5 weight percent sodium chloride solution was then displaced by the 10 weight percent sodium chloride solution by flowing several pore volumes of the latter solution through the core sample.

For the low permeability samples ($K < 10^{-4}$ md.) the 10 weight percent solution of sodium chloride (lower resistivity) was used since the time needed to displace one electrolyte solution by another would have been prohibitive.

9. Mercury Injection Data

The mercury porosimeter previously described was used for obtaining mercury penetration of a core sample versus the applied mercury pressure.

The first step in this procedure was to place a dried sample of porous medium into the penetrometer, Figure 18. The penetrometer was then placed in the filling device and evacuated. After the penetrometer was thoroughly evacuated, mercury was introduced into the bottom of the penetrometer by first covering the bottom of the penetrometer with mercury and then venting the filling device to the atmosphere. In this manner mercury extended through the stem of the penetrometer and was forced completely around the sample of porous medium. Intermediate

pressures between zero and 15 psi showed no penetration of mercury into the "tight" porous samples used in this research work.

After the penetrometer was filled with mercury it was placed inside the pressure chamber. The chamber was then filled with isopropyl alcohol and air bubbles were bled from the hydraulic system. Increasing pressure increments were then applied to the pressure chamber and mercury penetration into the porous sample was measured by taking readings on the penetrometer stem.

V. EXPERIMENTAL RESULTS

Experimental measurements on eight samples of porous medium have been made. The source, type, and overall dimensions of these samples are listed in Table I. A lithological description of each core sample is presented in Table II.

Values of air permeability and turbulence factors were obtained by plotting $MA(P_1^2 - P_2^2)/(2zRT\mu LW)$ versus $W/A\mu$. These plots are shown in Figures 22-29. The intercept for each of these plots at zero mass flow rate indicates the reciprocal permeability to air, $1/K$, and the slope of these plots indicates the value of the turbulence factor, β .

Experimental values of threshold pressure obtained for these samples are listed in Table III. In addition to threshold pressure measurements, the porosity, air permeability, turbulence factor, water permeability, formation factor, and pore size distributions were measured for each sample. This data with the exception of the pore size distribution is listed in Table IV.

The formation factors for samples having a permeability greater than 10^{-4} were corrected for conductive solids using Equation (42).

$$\frac{1}{F_a} = cR_w + \frac{1}{F} \qquad (42)$$

The intercept of Equation (42) gives the reciprocal of the true formation factor. For samples having a permeability less than 10^{-4}, a low resistivity electrolyte, 10 wt.% NaCl, was used.

The pore size distribution data for these samples is shown in Figures 30-37. The pore size distribution data presented here was

obtained from mercury injection data by plotting the percent of pore volume occuring between two sizes of pores. Pore size was calculated by substituting the mercury injection pressures into the capillary pressure equation,

$$r = 2\sigma \cos \theta / P_c \, . \qquad (43)$$

This data is also presented in Chapter VI of this work in the form of mercury capillary pressure curves.

Duplicate measurements of porosity, Table V, for four of the eight samples used resulted in a precision of less than 1%. Checks of porosity measurements by independent means, Table V, resulted in an average reproducibility of 2.4%.

Water permeability measurements showed an average reproducibility of 2.8% with a maximum deviation of 5.5%. Duplicate measurements, Table VI, for five samples were made.

Repeated measurements of resistivity showed a precision of less than 2%.

The reproducibility of threshold pressure measurements was checked for a "fairly high" and a "low" permeability sample. Samples L and K were used. The threshold pressure measurement for sample L was completely reproducible, Table III. The threshold pressure measurement for the low permeability sample, sample K, was reproducible to within 7%, Table III. Part of the deviation for sample K is a result of the size of pressure increment used in measuring the threshold pressure.

TABLE I

TYPE AND SOURCE OF CORE SAMPLES

Core Label	Length, Inches	Type	Source
Sample G	2.84	Paradox Limestone	Continental Oil Company
Sample I	1.85	Dean Sandstone	Continental Oil Company
Sample K	2.05	Paradox Limestone	Continental Oil Company
Sample L	2.47	Eau Claire Sandstone	Northern Illinois Gas Company
Sample P	2.02	Sprayberry Sandstone	Continental Oil Company
Sample Q	2.04	Sandstone	Continental Oil Company
Sample R	.665	Mount Simon Sandstone	Northern Illinois Gas Company
Sample S	1.95	Dolomite	Northern Illinois Gas Company

All diameters = 1.5 inches

TABLE II

LITHOLOGICAL DESCRIPTION OF CORE SAMPLES

Core Label	Description
Sample G	Fine grained, fossiliferous, calcarenite limestone
Sample I	Fine grained, calcite cemented sandstone
Sample K	Fine grained, crystalline limestone
Sample L	Fine grained, slightly dolomitic, glaucomitic sandstone. Quartz cement as secondary overgrowth.
Sample P	Fine grained sandstone with argillaceous calcite cement. Thinly laminated and cross-bedded.
Sample Q	Fine grained sandstone with argillaceous calcite cement. Thinly laminated and cross-bedded.
Sample R	Fine grained sandstone with argillaceous dolomitic cement.
Sample S	Fine grained, calcarenite dolomite.

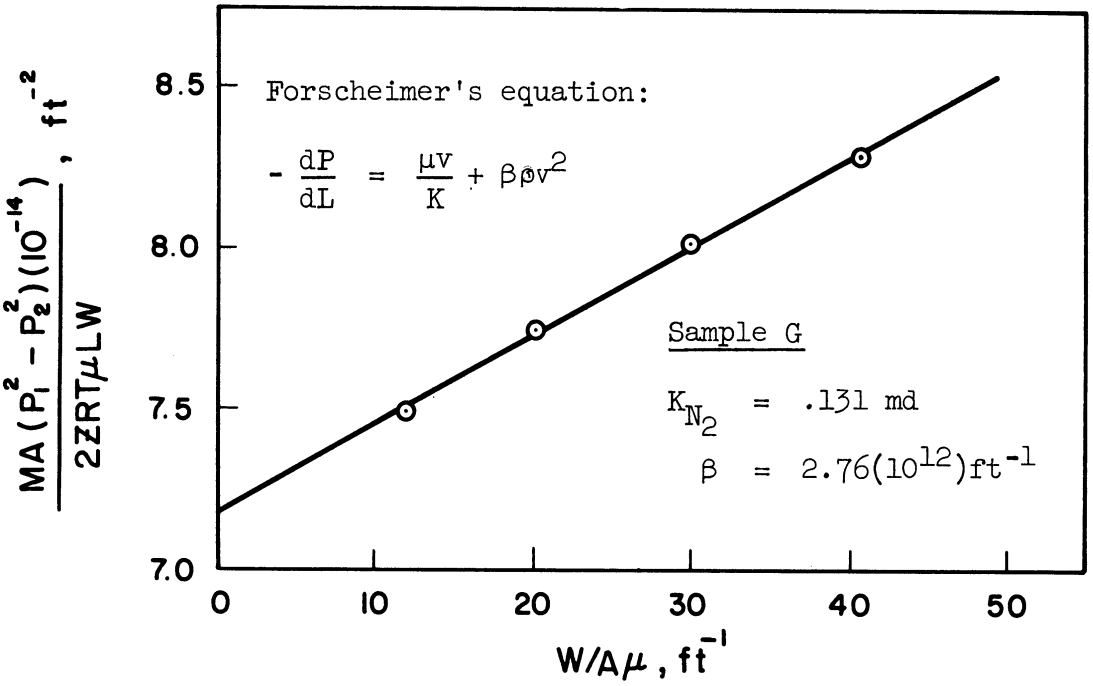

Figure 22. Determination of Air Permeability for Sample G.

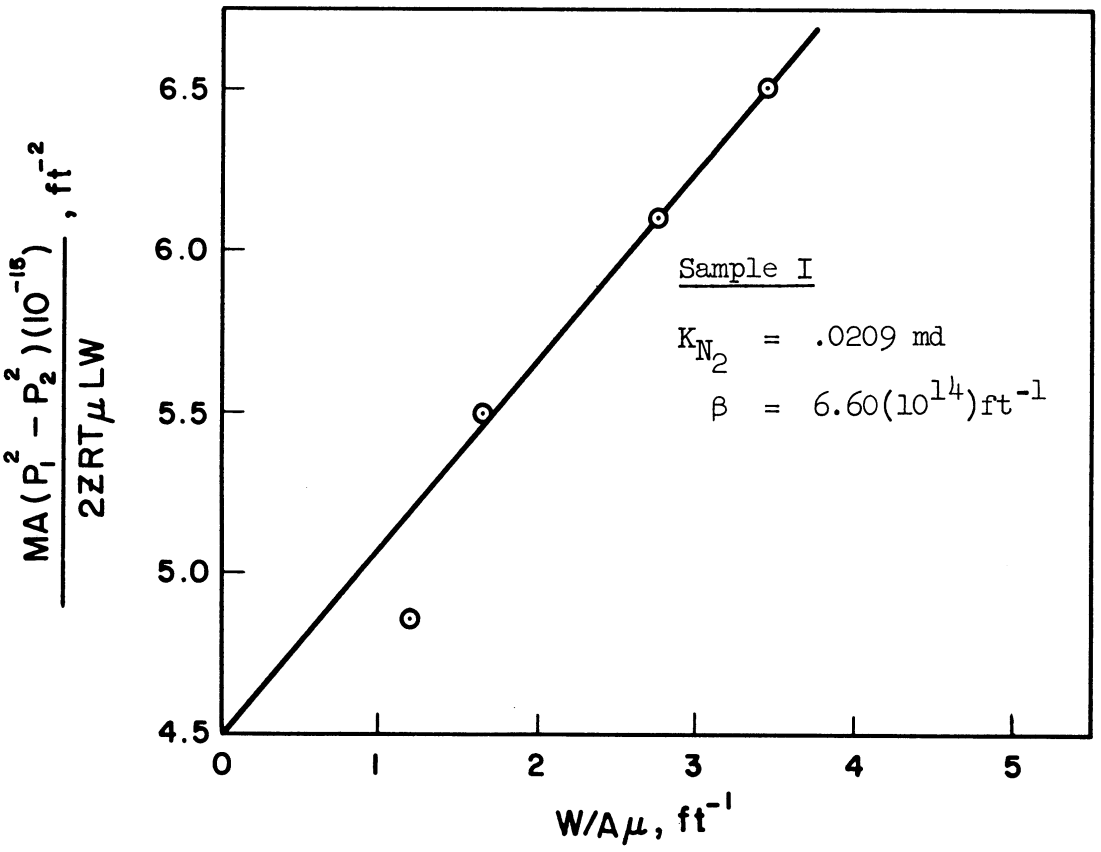

Figure 23. Determination of Air Permeability for Sample I.

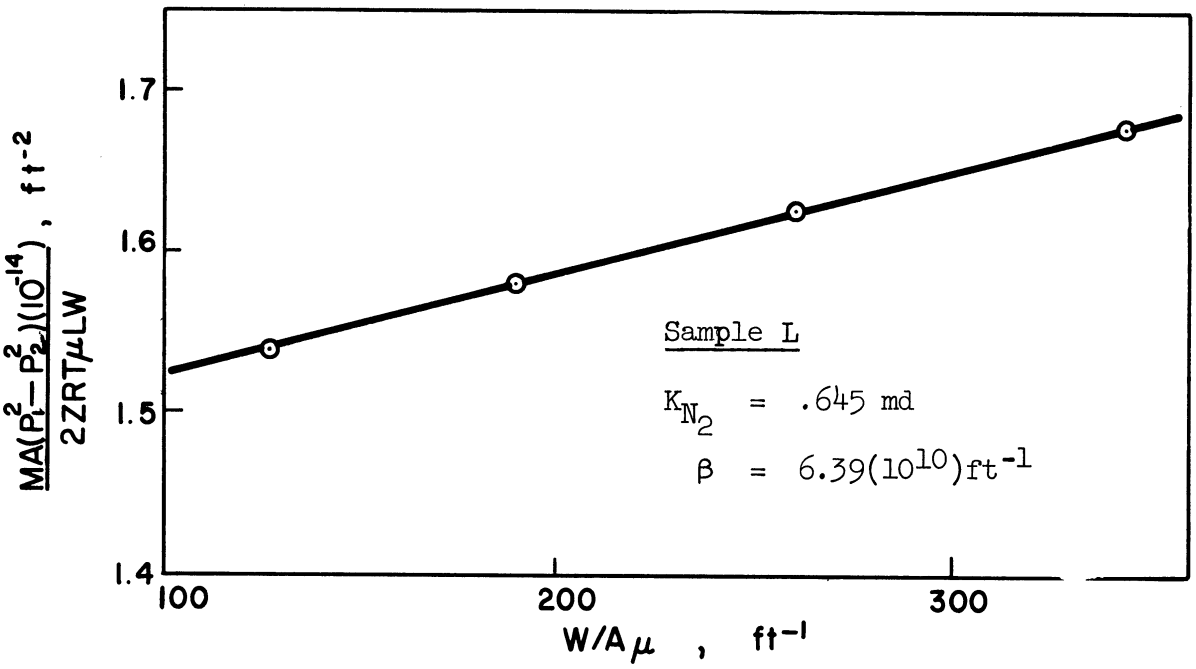

Figure 24. Determination of Air Permeability for Sample L.

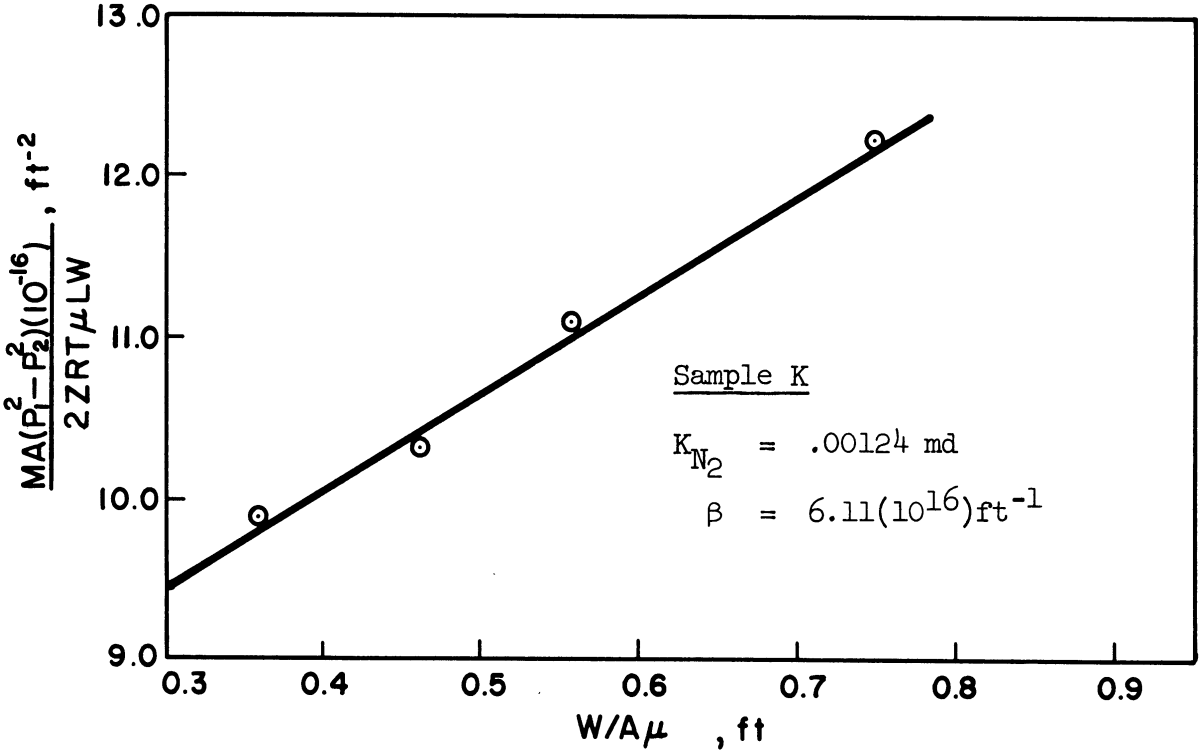

Figure 25. Determination of Air Permeability for Sample K.

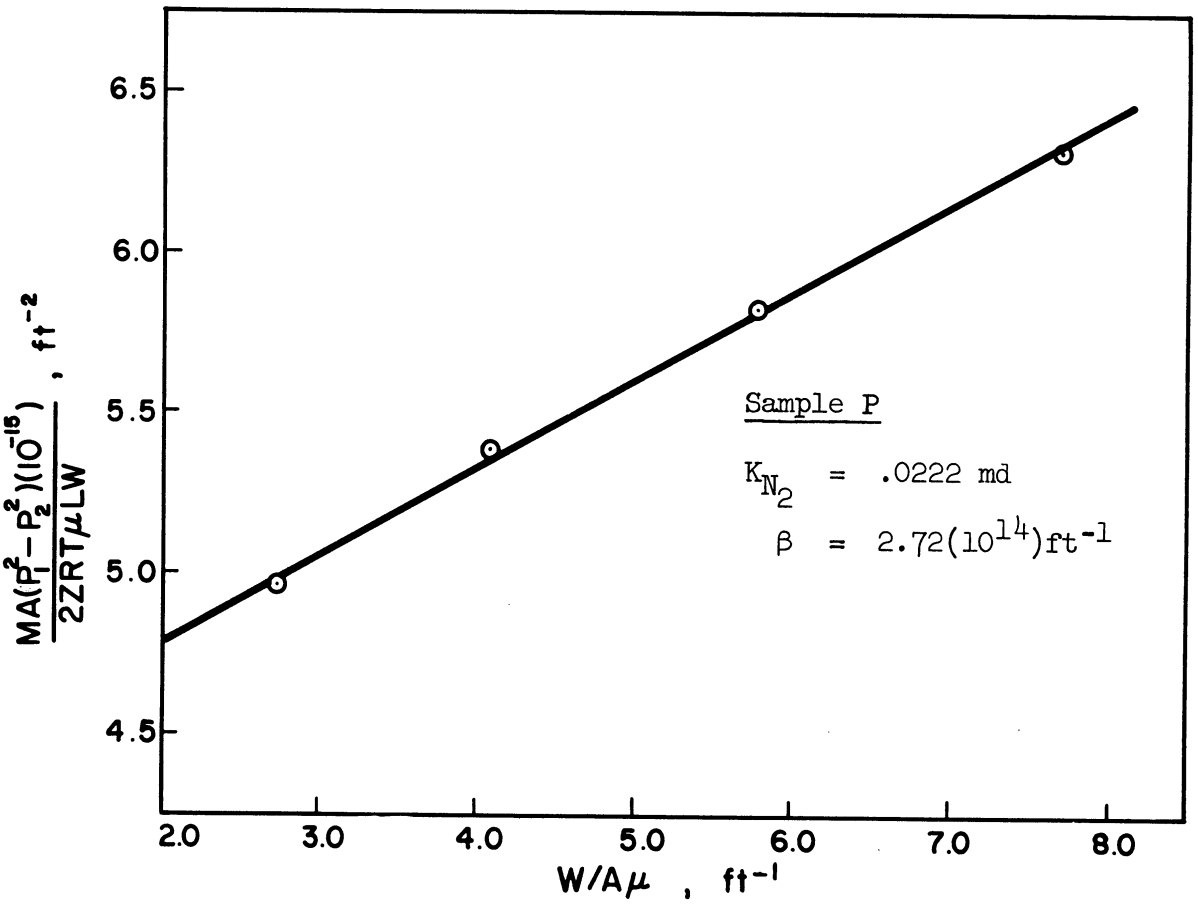

Figure 26. Determination of Air Permeability for Sample P.

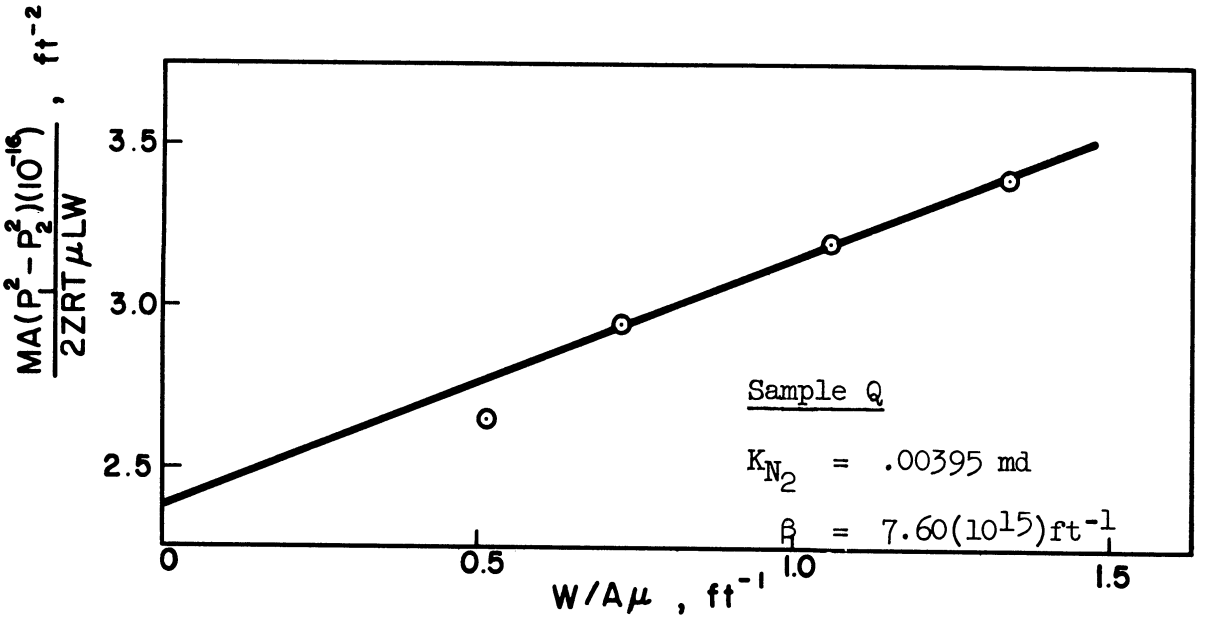

Figure 27. Determination of Air Permeability for Sample Q.

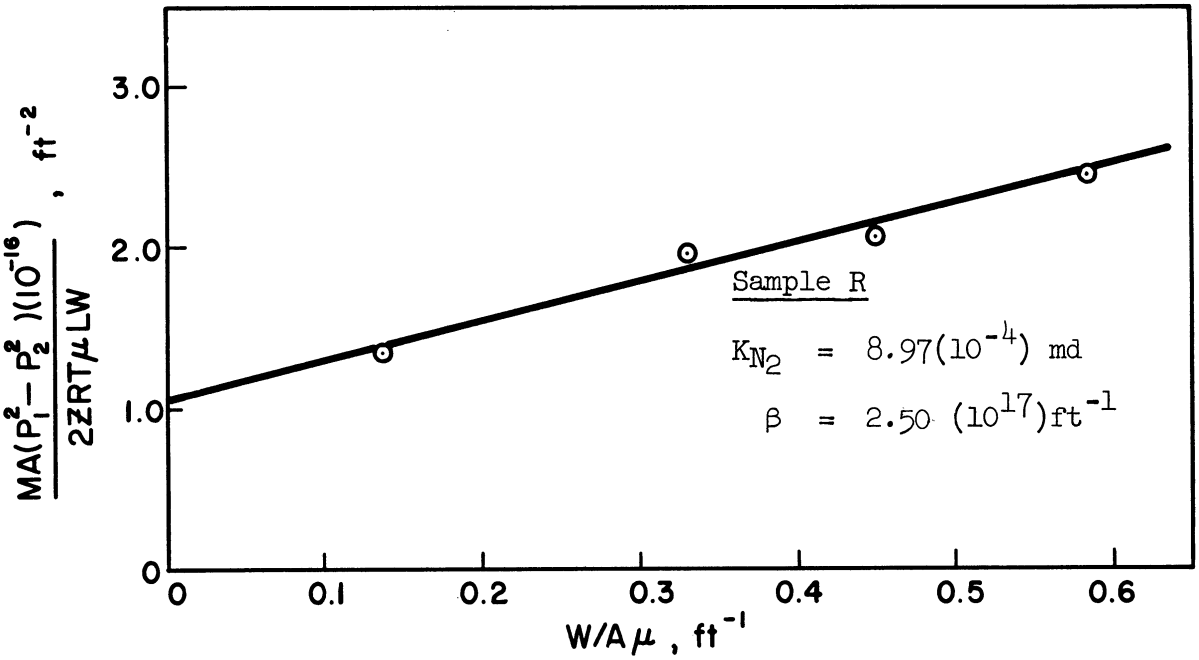

Figure 28. Determination of Air Permeability for Sample R.

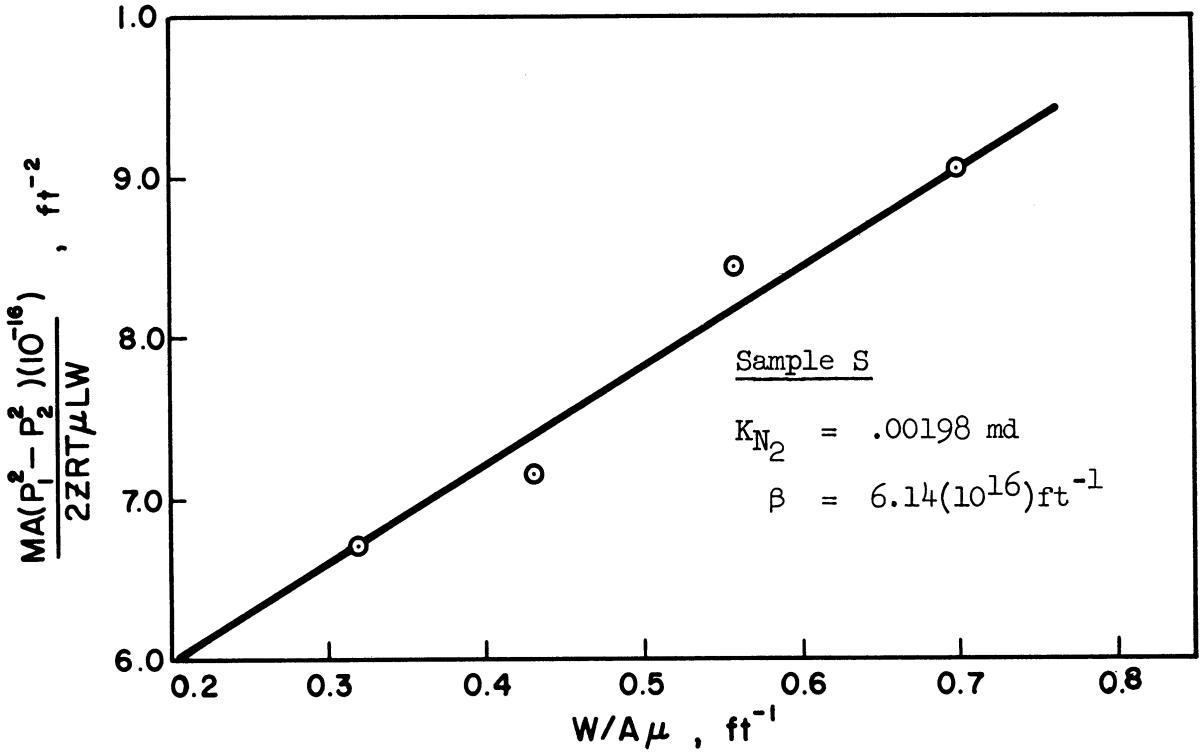

Figure 29. Determination of Air Permeability for Sample S.

TABLE III

THRESHOLD PRESSURES MEASURED BY GAS DISPLACING WATER

Core Label	Surface Tension*, dyne/cm	Threshold Pressure, psi
Sample G	72.	> 20 < 25
Sample I	72.	> 100 < 150
Sample K	72.	> 200 < 225
Sample K	75.**	> 225 < 250
Sample L (first run)	72.	> 15 < 16
Sample L (Second run)	72.	> 15 < 16
Sample P	72.	> 150 < 175
Sample Q	72.	> 500 < 550
Sample R	72.	> 350 < 450
Sample S	72.	> 600 < 700

* Room Temperature
** Fluid was 10 wt% NaCl

TABLE IV

CORE SAMPLE PROPERTIES

Core Label	Porosity, Percent	Air Permeability, Millidarcys	Turbulence Factor, ft^{-1}	Water Permeability, Millidarcys	Formation Resistivity Factor
Sample G	10.0	.131	$2.76(10^{12})$	.0742	77.0
Sample I	9.48	.0209	$6.60(10^{14})$	$1.0(10^{-3})$	67.6
Sample K	3.26	$1.24(10^{-3})$	$6.11(10^{16})$	$2.62(10^{-4})$	317.
Sample K	3.26	$1.24(10^{-3})$	$6.11(10^{16})$	$2.97(10^{-4})$*	317.
Sample L	15.9	.645	$6.39(10^{10})$	.178	59.3
Sample P	11.9	.0222	$2.72(10^{14})$	$1.52(10^{-3})$	60.5
Sample Q	9.64	$3.95(10^{-3})$	$7.60(10^{16})$	$4.61(10^{-5})$	115.
Sample R	1.31	$8.97(10^{-4})$	$2.50(10^{17})$	$9.15(10^{-5})$	656.
Sample S	2.89	$1.98(10^{-3})$	$6.14(10^{16})$	$4.07(10^{-5})$	359.

* Flowing fluid was 10wt.% NaCl.

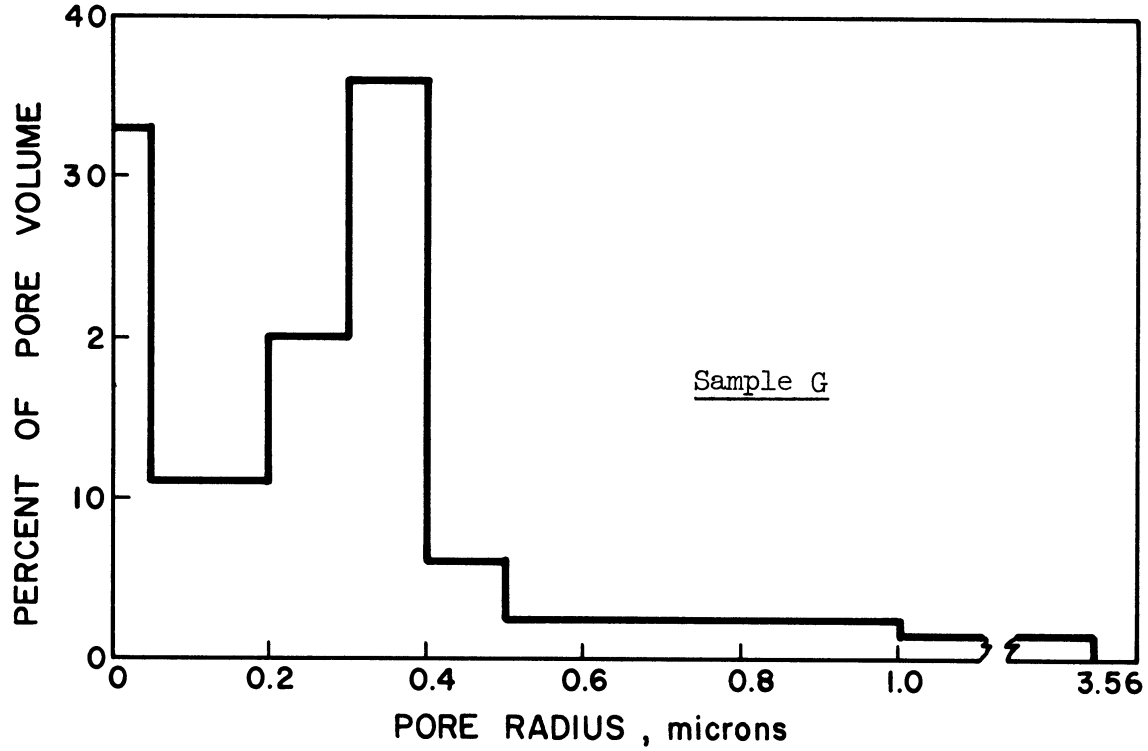

Figure 30. Pore Size Distribution for Sample G.

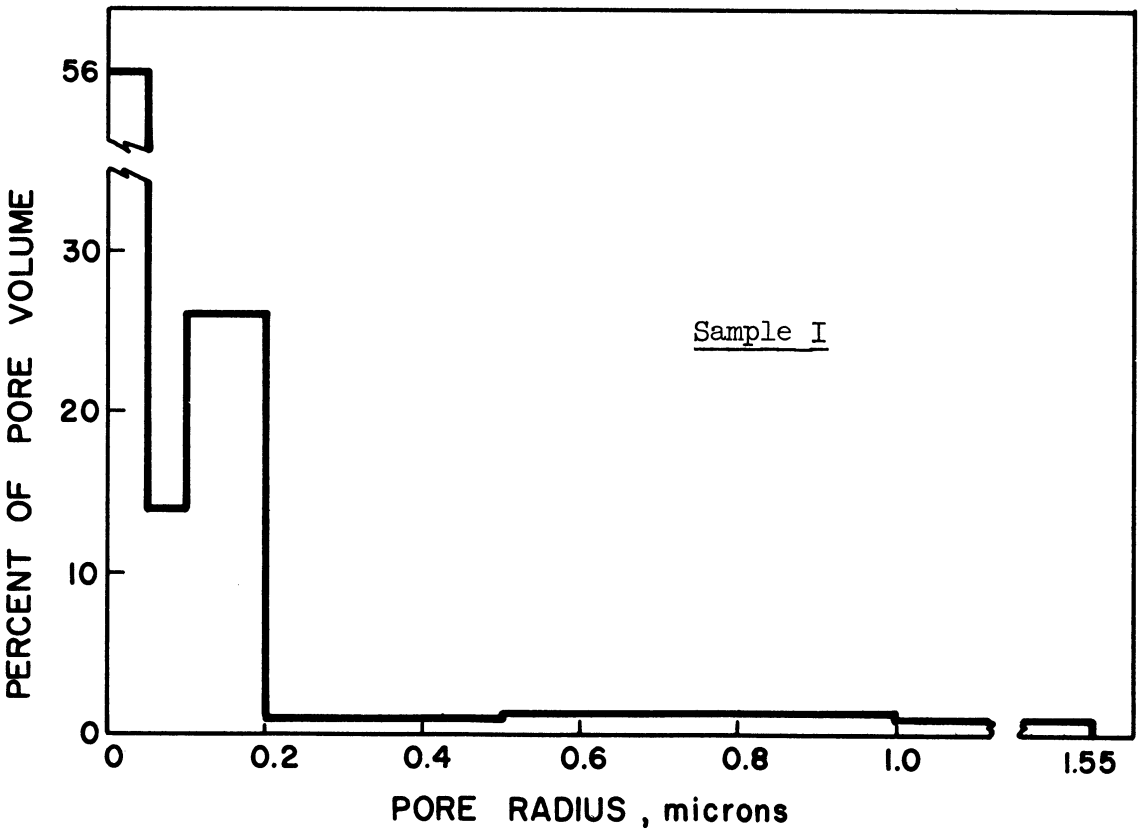

Figure 31. Pore Size Distribution for Sample I.

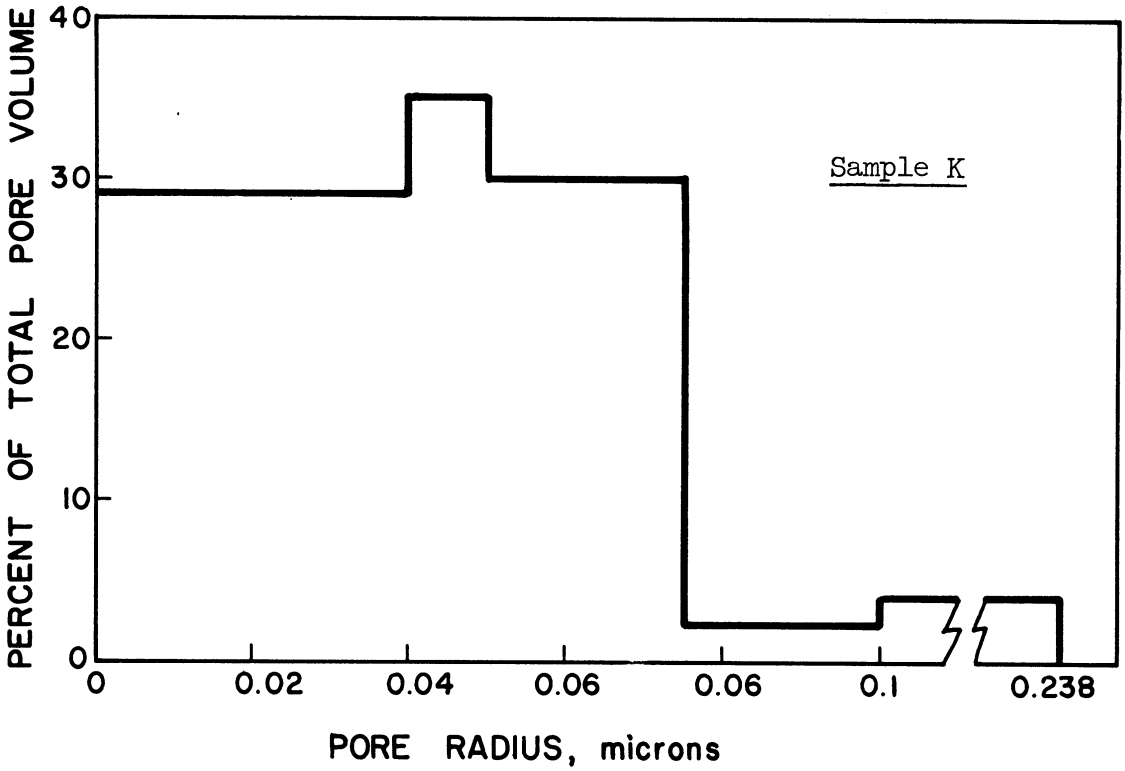

Figure 32. Pore Size Distribution for Sample K.

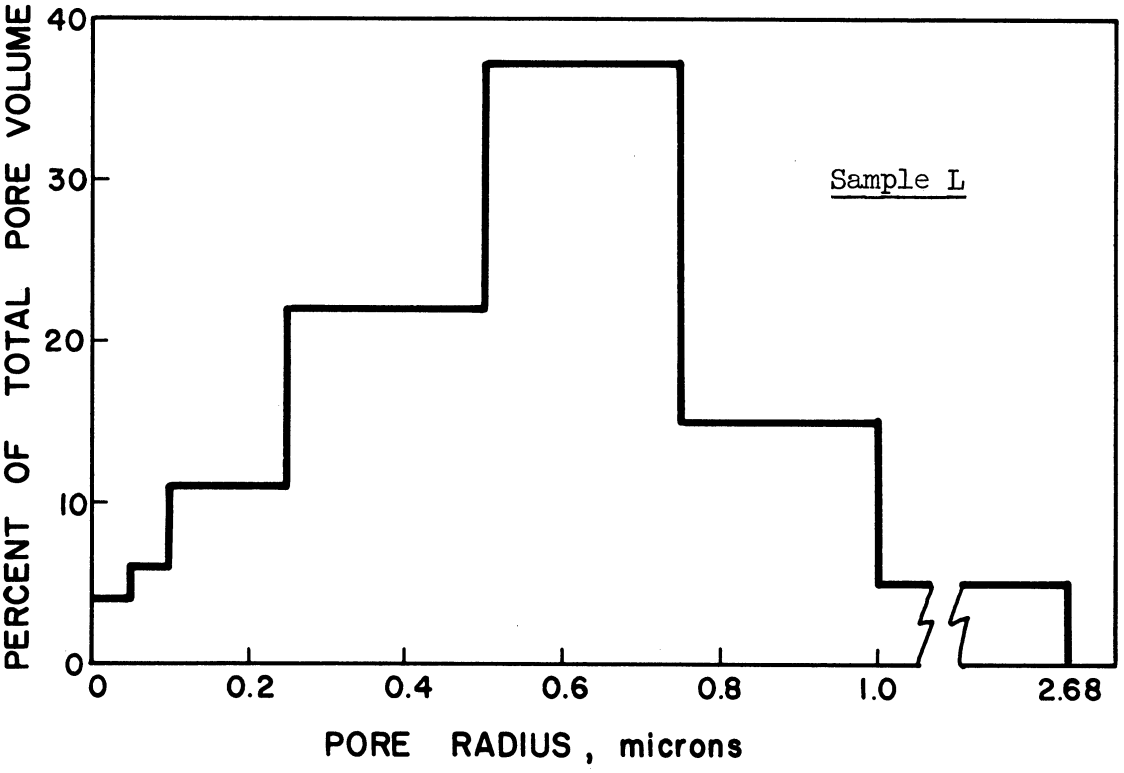

Figure 33. Pore Size Distribution for Sample L.

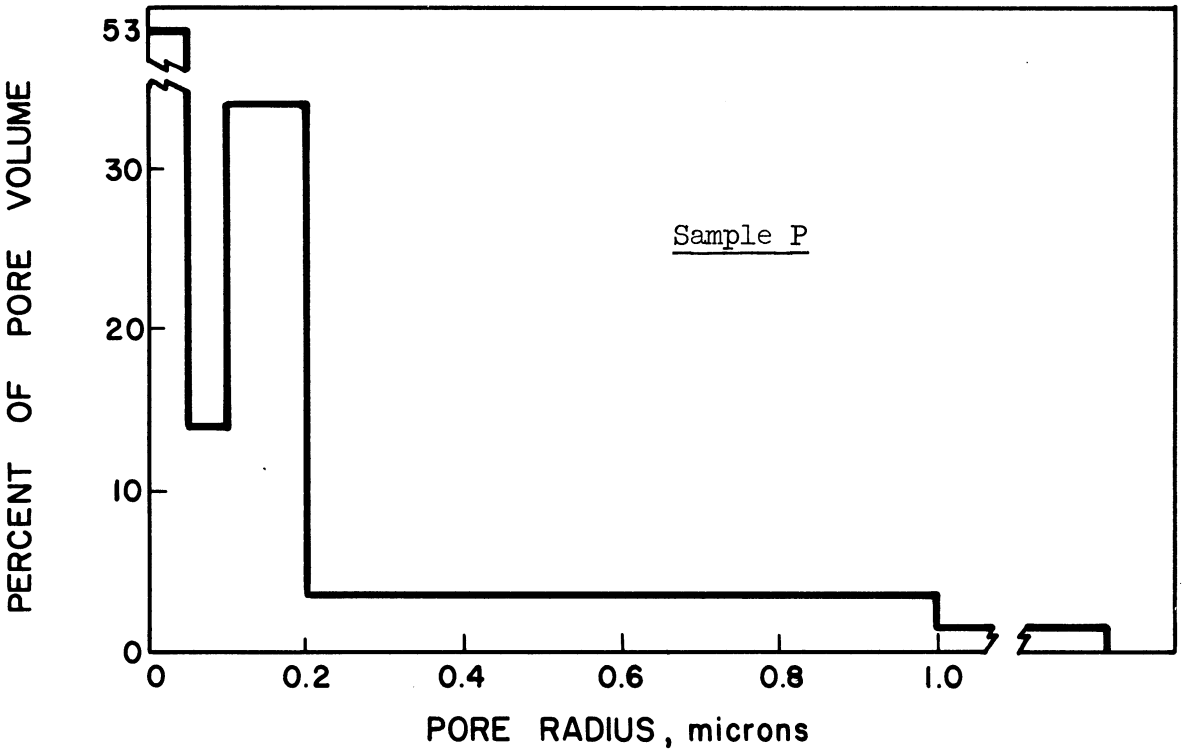

Figure 34. Pore Size Distribution for Sample P.

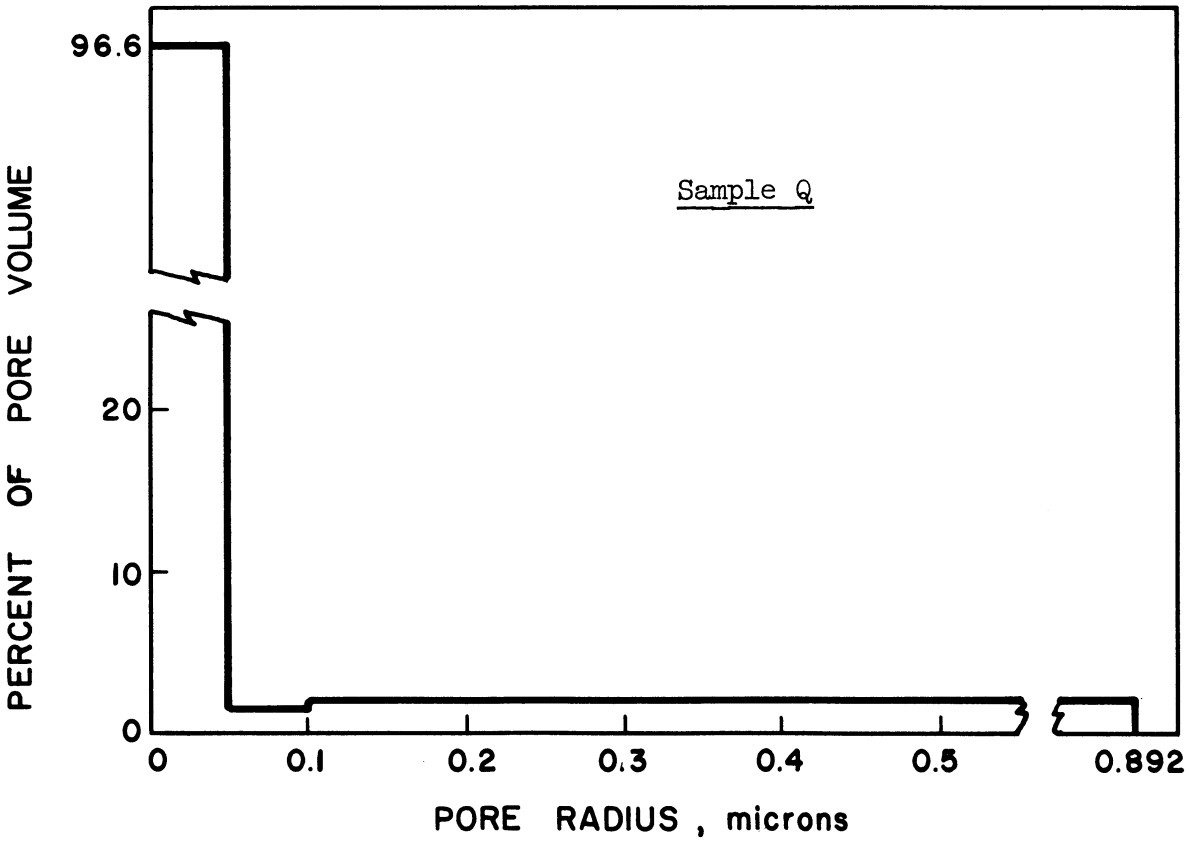

Figure 35. Pore Size Distribution for Sample Q.

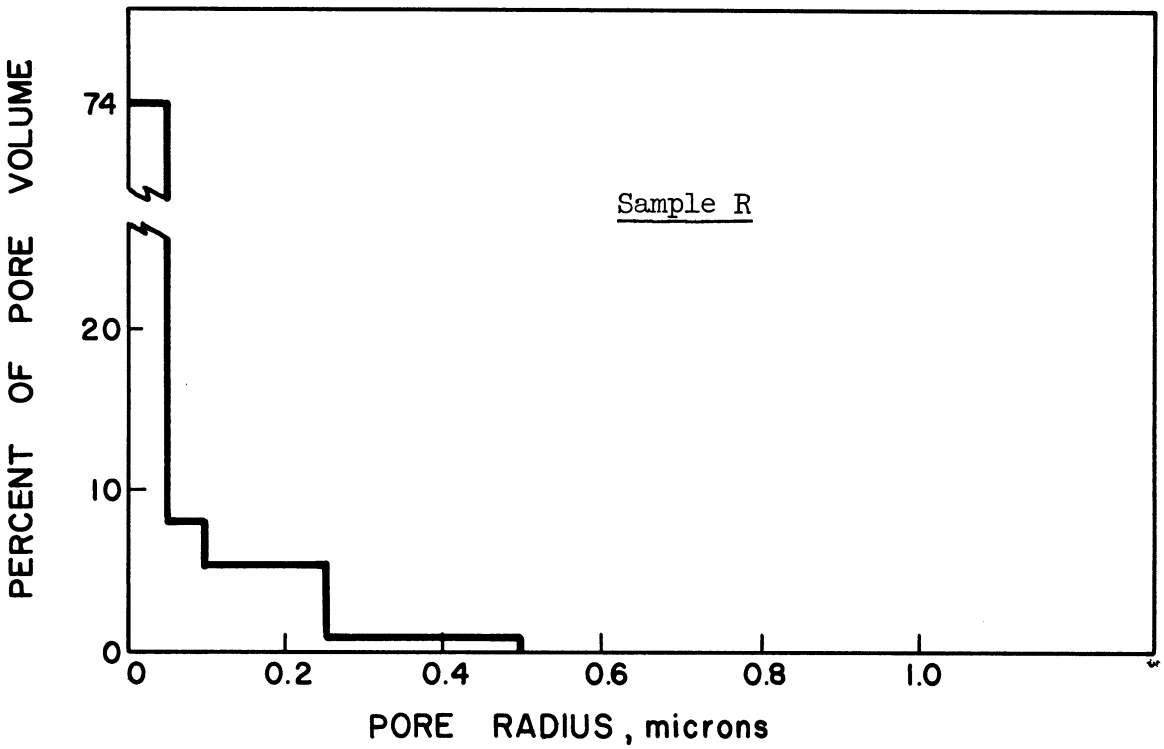

Figure 36. Pore Size Distribution for Sample R.

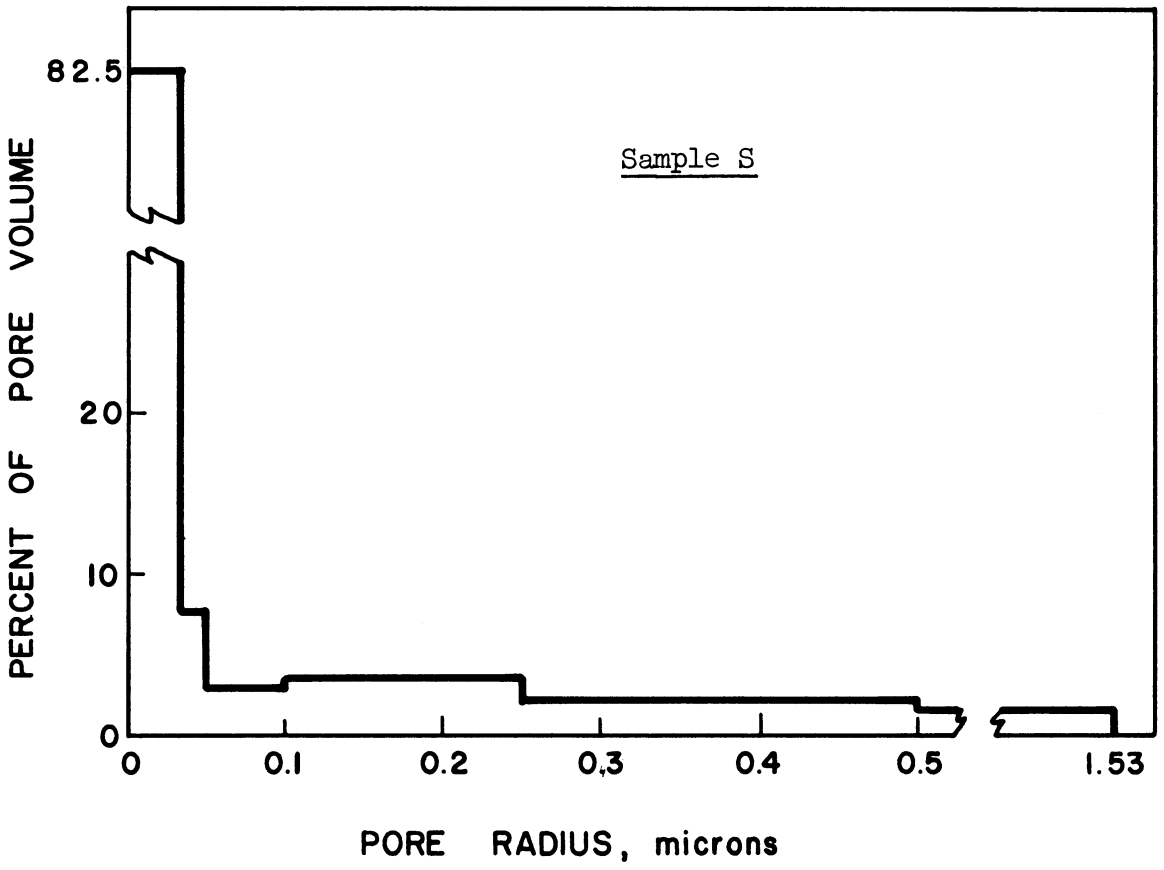

Figure 37. Pore Size Distribution for Sample S.

TABLE V

REPRODUCIBILITY OF POROSITY MEASUREMENTS

	Porosity, Percent		
Core Label	First Run	Second Run	Independent Measurements
G	10.0	10.1	9.84*
I	9.48	9.47	-----
K	3.27	3.25	-----
L	15.95	15.9	-----
P	11.9	----	11.9**
Q	9.64	----	8.9**
S	2.89	----	2.9***

* Data taken by Pan American Research, Tulsa, Oklahoma

** Data taken by Continental Oil Co., Ponca City, Oklahoma

*** Data taken by Tek et al (53)

TABLE VI

REPRODUCIBILITY OF PERMEABILITY MEASUREMENTS

	Permeability, md.	
Core Label	First Run	Second Run
G	$7.22(10^{-2})$	$7.63(10^{-2})$
I	$9.95(10^{-4})$	$1.01(10^{-5})$
K	$2.62(10^{-4})$	$2.61(10^{-4})$
L	.181	.175
P	$1.50(10^{-3})$	$1.54(10^{-3})$

VI. ANALYSIS OF THRESHOLD PRESSURE PHENOMENA

A complete analysis of the data taken in this work as well as any data available from the literature is made in this section. Several correlations for threshold pressure are presented as well as an analysis of various phenomena associated with threshold pressures and the displacement of a wetting phase, water, by a nonwetting phase, gas.

A. Correlation of Threshold Pressure with other Properties of Porous Media

Sufficient data have been taken for each sample used in this work to check the validity of the theoretical equation developed in Chapter III for predicting threshold pressures, Equation (35).

$$P_T = \frac{.146|\sigma}{\sqrt{k_o F}} \sqrt{\frac{1}{\phi F}} \qquad (35)$$

where

P_T - psi

σ - dynes/cm

ϕ - fraction porosity

K - darcys

Data for each of the variables appearing in Equation (35) were previously presented in Tables III and IV. A comparison of the measured threshold pressure with the threshold pressure predicted by Equation (35) appears in Table VII. Additional data pertaining to Equation (35) for higher permeability samples was obtained by Wyllie and Rose.[63] This data is presented in tabular for in Table VIII.

Data also have been reported in the literature for Equation (44).

TABLE VII

TABULATED COMPARISON OF MEASURED AND PREDICTED THRESHOLD PRESSURES

Core Description	Threshold Pressure, P_T, psi.	$\frac{.1461\sigma}{\sqrt{k_o}\ F}\sqrt{\frac{1}{\phi K}}$, psi
Sample G	20 - 25	34.
Sample I	100 - 150	337.
Sample K	200 - 225	240.
Sample K*	225 - 250	234.
Sample L	15 - 16	22.
Sample P	150 - 175	272.
Sample Q	500 - 550	916.
Sample R	350 - 450	309.
Sample S	600 - 700	568.

* Fluid used was 10 wt.% NaCl.

σ = Surface tension

ϕ = Porosity

K = Permeability

F = True formation factor

k_o = 2.25

TABLE VIII

THRESHOLD PRESSURE DATA PRESENTED BY WYLLIE & ROSE[63]

Core Description	P_T (psi.)	σ (dynes/cm)	ϕ (frac.)	K (md.)	F	$\frac{.1461\sigma}{\sqrt{k_o}\ F}\sqrt{\frac{1}{\phi K}}$ (psi.)
Alundum	.75	43.	.258	693.	13.7	.723
"	1.05	43.	.254	667.	11.3	.901
"	.994	43.	.265	688.	11.9	.825
"	1.05	43.	.262	657.	13.0	.776
Pyrex	.653	43.	.344	2300.	7.2	.654
Nicholls Buff	1.73	43.	.200	232.	12.5	1.55
" "	2.10	43.	.198	205.	12.4	1.68
Berea	.874	43.	.225	907.	11.7	.792
"	.880	54.2	.226	695.	12.7	.832
Alundum	4.24	54.2	.236	64.	11.5	3.74
"	1.23	54.2	.294	1305.	8.0	1.063
Pyrex	2.13	54.2	.298	322.	7.7	2.21
"	2.82	54.2	.303	353.	5.7	2.83
"	2.13	54.2	.304	342.	7.1	2.3
"	2.55	54.2	.268	149.	8.4	3.15
"	3.86	54.2	.366	129.	4.04	6.01
"	5.21	54.2	.325	105.	6.4	4.47
"	18.0	54.2	.374	8.2	4.4	21.6
"	.82	54.2	.286	3900.	6.2	.808
Alundum	4.71	54.2	.232	60.8	10.9	4.08

P_T = Threshold pressure
σ = Surface tension
ϕ = Porosity
K = Permeability
F = True formation factor
k_o = 2.25

$$P_T = .1461 j(S_w)\sigma\sqrt{\frac{\phi}{K}} \qquad (44)$$

This data was presented by Rose and Bruce[47] and is listed in Table IX of this section. The values of Leverett's limiting J-Function, $\lim_{S_w \to 1} j(S_w)$, were obtained by measuring the entire capillary pressure curve for each sample and extrapolating this data to 100% water saturation.

All of the data which is presented in Tables VII, VIII, and IX has been presented on a single plot of measured versus predicted threshold pressures, Figure 38. Figure 38 shows that Equations (35) - (44) are fairly well represented by the data over the entire range of data presented.

Some of the measured values of threshold pressure for the lower permeability samples presented in Figure 38 fall below the line representing the predicted values of threshold pressure. This is to be expected since Equation (35) was derived on the basis of an average hydraulic radius. One would expect that this radius would be somewhat smaller than the radius of the largest pores. Any average radius obtained from permeability measurements, however, is greatly influenced by the largest pores in a porous medium. This is because the flow through a conduit is a function of its radius to the fourth power, while its area is only a function of radius squared. Thus, most of the flow through a porous medium having a broad pore size distribution occurs through its largest pores.

The good quantitative agreement for most of the data presented in Figure 38, and the excellent qualitative agreement of all of the data suggest that this correlation should prove quite useful.

TABLE IX

THRESHOLD PRESSURE DATA PRESENTED BY ROSE & BRUCE[47]

Core Description	P_T (psi.)	σ (dynes/cm)	ϕ (frac.)	K (md.)	lim $j(S_w)$ $S_w \rightarrow 1.0$	$.1461 j(S_w)\sigma\sqrt{\frac{\phi}{K}}$ (psi.)
Weber Sandstone	16.7	70	.118	2.1	.20	15.4
" "	12.3	70	.119	2.4	.22	15.8
" "	8.1	70	.124	4.4	.17	9.22
" "	8.5	70	.125	5.9	.18	8.46
" "	6.5	70	.112	3.4	.17	9.98
" "	11.3	70	.122	2.9	.15	9.96
" "	7.4	70	.132	5.9	.17	8.22
" "	10.5	70	.136	11.1	.27	9.7
" "	7.0	70	.121	2.2	.07	5.31
" "	8.5	70	.111	1.3	.10	9.45
Viking Sandstone	3.7	70	.17	10.0	.10	4.21
" "	1.5	70	.22	650.	.31	1.84
Unconsolidated Sand (after Leverett)	.6	70	.39	17500.	.42	.64
Alundum	2.0	70	.24	208.	.38	4.17
"	.8	70	.24	208.	.38	1.19
Deese Sandstone	1.0	70	.15	253.	.16	1.26

P_T = Threshold pressure
σ = Surface tension
ϕ = Porosity
K = Permeability
$j(S_w)$ = Leverett's J-Function

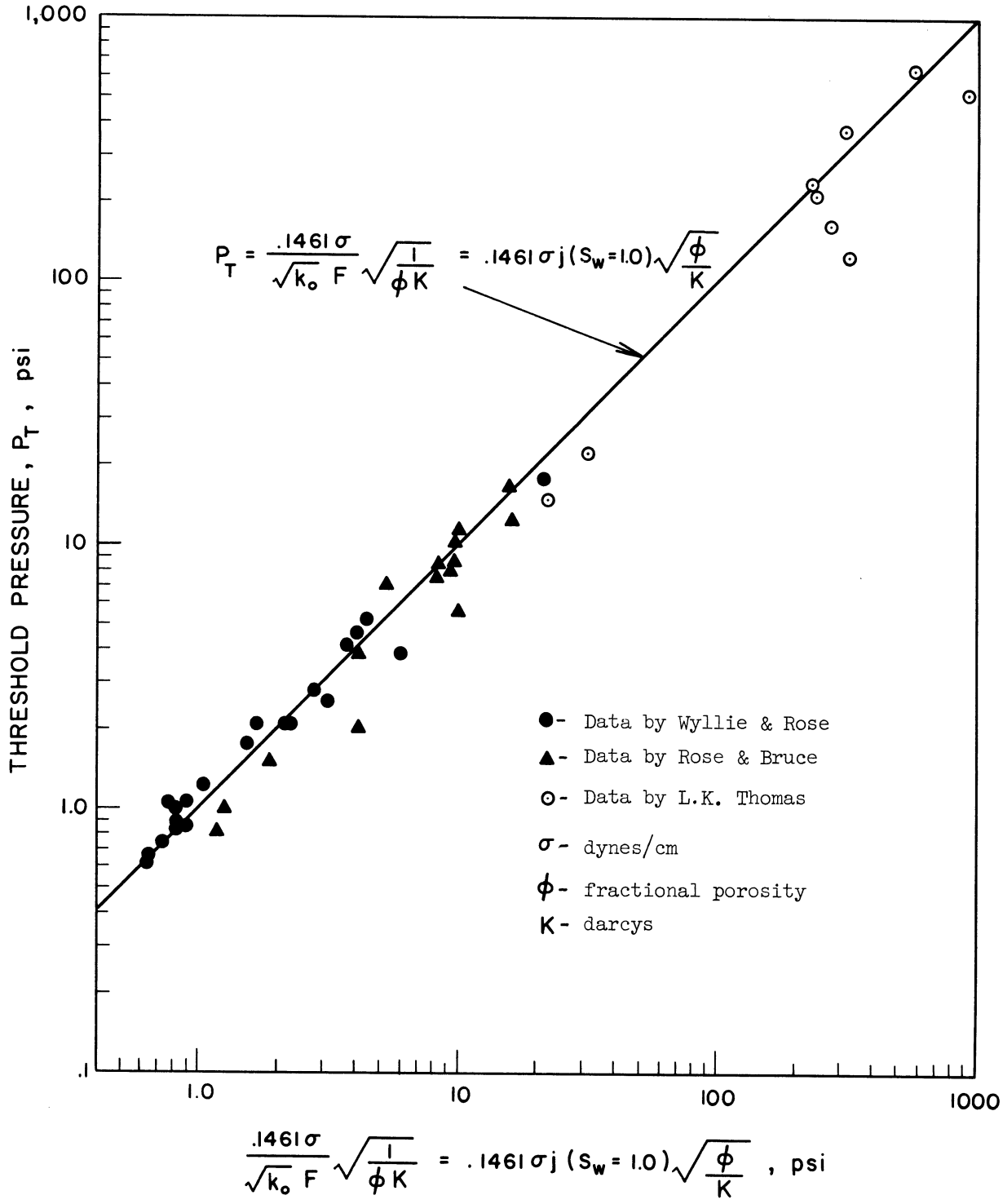

Figure 38. Correlation of Threshold Pressure with other Properties of Porous Media.

Plots of threshold pressure versus reciprocal permeability, porosity divided by permeability, and reciprocal porosity times permeability appear in Figures 39, 40, and 41, respectively. According to Equations (8) and (35),

$$P_T = j(S_w = 1.0)\sigma\left(\frac{\phi}{K}\right)^{\frac{1}{2}} \tag{8}$$

$$P_T = \frac{\sigma}{\sqrt{k_o}\ F}\left(\frac{1}{\phi K}\right)^{\frac{1}{2}} \tag{35}$$

these plots should have a slope equal to 0.5.

A least squares fit of the data appearing in Figures 39-41 was obtained by minimizing the sum of the squares of the deviations along the ordinate. The following correlations were obtained:

$$P_T = 7.37\left(\frac{1}{K}\right)^{.43} \tag{45}$$

$$P_T = 19.1\left(\frac{\phi}{K}\right)^{.497} \tag{46}$$

and

$$P_T = 4.74\left(\frac{1}{\phi K}\right)^{.351} \tag{47}$$

The standard deviation of the points about the regression line,

$$S = \frac{\sum_{M=1}^{M=M}(y_i - a - bx)^2}{M - N - 1} \tag{48}$$

where

S = standard deviation

M = number of data points

N = order of polynomial = 1

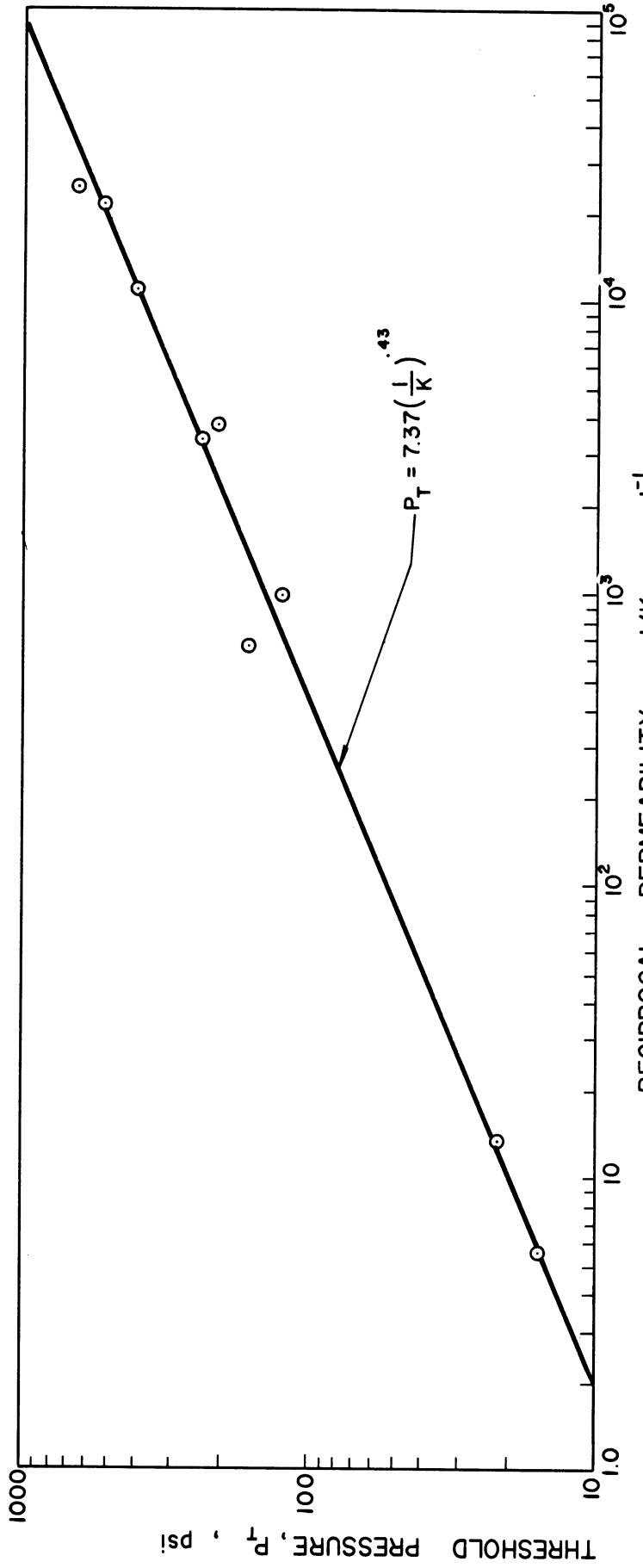

Figure 39. Threshold Pressure versus 1/Permeability.

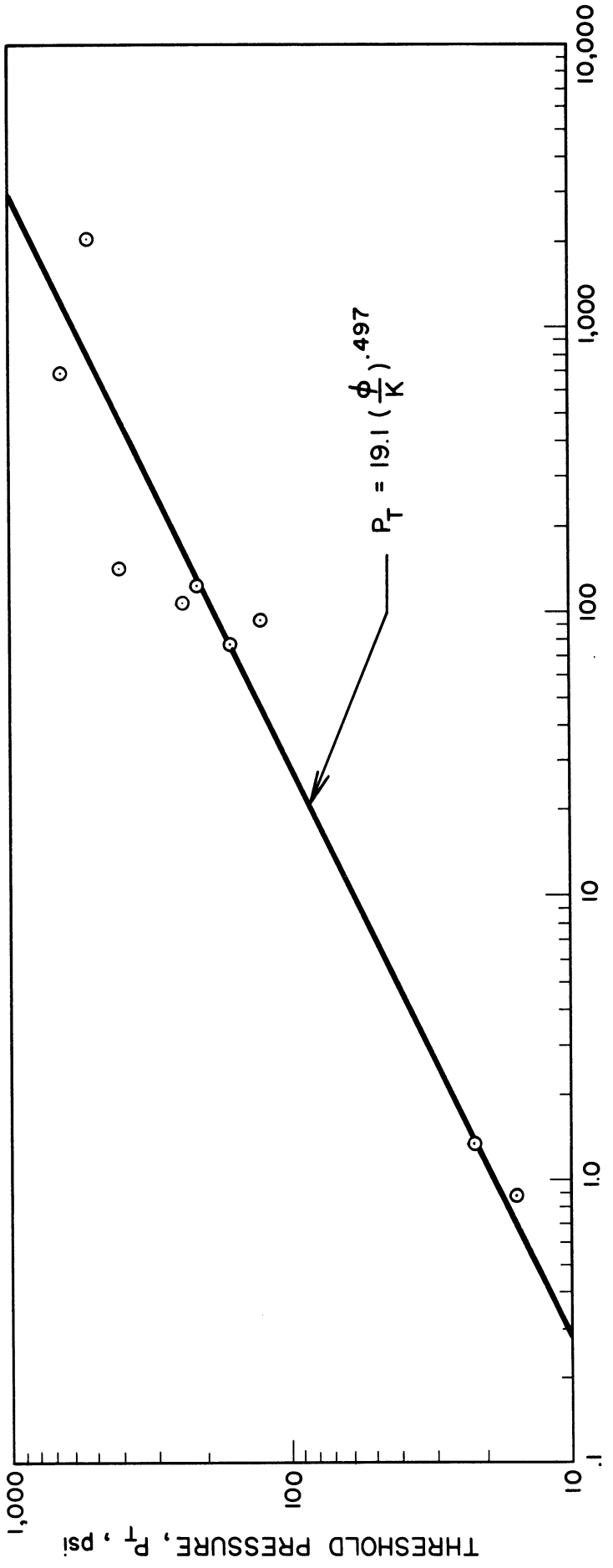

Figure 40. Threshold Pressure versus Porosity/Permeability.

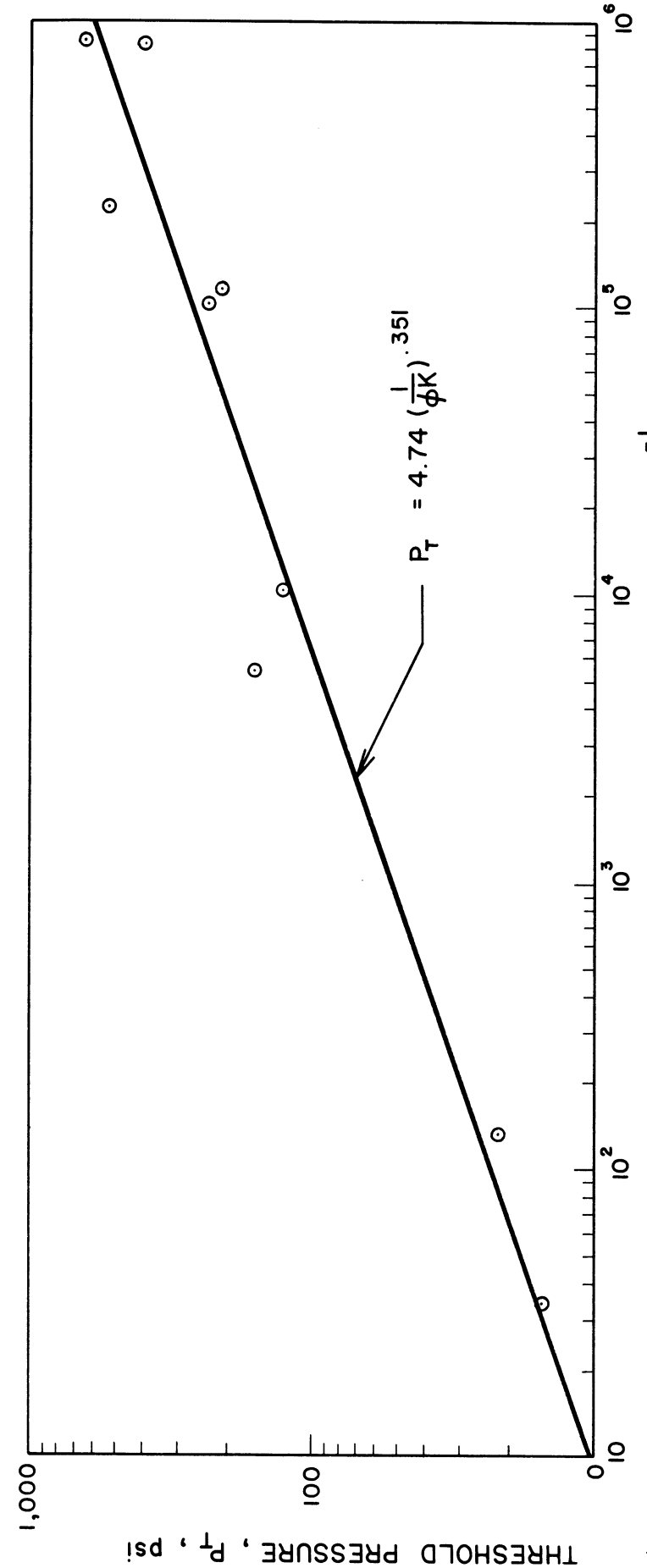

Figure 41. Threshold Pressure versus 1/(Porosity·Permeability).

was calculated for the data in Figures 39-41. The standard deviation of $\ln.P_t$ in Figures 39-41 was .153, .347, .314, respectively.

The exponent in Equation (46) or .497 agrees very closely with the exponent predicted by Leverett,[33,34] Equation (8). Equation (45), represents the best fit of the data and the exponent 0.43 is not greatly different from the exponent of 0.5 predicted by either Equation (8) or (35).

Equations (45), (46), and (47) represent suitable correlations for threshold pressures. In particular Equation (45) offers a good quantitative description of the data presented.

B. Correlation of Threshold Pressure Measured with Air-Water and Mercury

In 1949, Purcell[45] presented a technique for determining drainage capillary pressure curves by mercury injection. Purcell assumed that the contact angle for mercury and the rock surfaces was 0°.

By considering a capillary tube a relationship between mercury and air-water capillary pressure can be obtained. The capillary pressure in a tube of radius r partially immersed in mercury is

$$P_c(Hg) = \frac{2\sigma_{Hg} \cos 140°}{r}, \qquad (49)$$

while the capillary pressure in a tube partially immersed in water is

$$P_c(\text{air-water}) = \frac{2\sigma_{H_2O} \cos 0°}{r} \qquad (50)$$

Dividing Equation (49) by Equation (50) gives a relationship between mercury and air-water capillary pressure curves.

$$\frac{P_c(Hg)}{P_c(\text{air-water})} = \frac{\sigma_{Hg} \cos 140°}{\sigma_{H_2O} \cos 0°} \tag{51}$$

$$\frac{P_c(Hg)}{P_c(\text{air-water})} = \frac{-480 \cos 140°}{72 \cos 0°} = 5.0 \tag{52}$$

Purcell measured capillary pressure curves for several samples using mercury injection and also using the air-water diaphragm method. He presented his data for each core on a single plot by labeling the left hand ordinate for air-water capillary pressure and the right hand ordinate for mercury injection capillary pressure. The capillary pressure curves were plotted on scales having a ratio of 5 to 1 as indicated by Equation (52). Relatively close agreement was obtained between the mercury and air-water capillary pressure curves presented by Purcell.

According to Amyx, Bass, and Whiting[1] there is some question of the validity of incorporating the contact angle into the ratio of the capillary pressured in Equation (51). "The geometry of the pores of a rock is complex, and the relationship between the curvature of the interface and the radius of the pore is not necessarily a function of the cosine of the contact angle. It appears that an equally valid assumption is that the mean curvature of an interface in rock is a unique function of fluid saturation. This assumption permits the ratio of pressure to be defined as follows:"

$$\frac{P_c(Hg)}{P_c(\text{air-water})} = \frac{\sigma_{Hg}}{\sigma_{H_2O}} = 6.67 \tag{53}$$

A superior correlation for four out of six of the samples presented by Purcell is obtained by using a factor of 6.67 rather than 5.0 in the ratio of capillary pressures.

Purcell's work suggests a possible means of correlating threshold pressures of porous media. By measuring air-water threshold pressures and by obtaining the mercury threshold pressures by extrapolating the mercury capillary pressure curves it should be possible to obtain a correlation using either Equation (52) or (53).

Mercury capillary pressure curves for each of the samples used in this research work are presented in Figures 42-49. The mercury capillary pressures are read from the right hand ordinate. The left hand ordinate represent air-water capillary pressure curves. A factor of 5. between the two ordinates has been used.

Duplicate runs for samples G and P were made. The precision of these measurements for the threshold pressure obtained by extrapolating the mercury injection curves was less than 3%. No attempt was made to extrapolate the mercury injection curves for samples Q , R , and S since large inaccuracies would have resulted. The threshold pressure for each of these samples is near or above the upper pressure limits of the porosimeter used. Furthermore, for low porosity samples such as samples R and S inaccuracies arise due to the limited sample size of the porosimeter used and consequently the small amount of mercury penetrating the sample even at the upper limit of the porosimeter. Ideally, a porosimeter for obtaining threshold pressures should be designed with a larger sample holder and an upper pressure operating limit of 5,000 - 10,000 psi.

Threshold pressures obtained by extrapolating the mercury injection curves shown in Figures 42-49 are listed in Table X along with their air-water threshold pressures. These extrapolotions were based on the judgement of the author. For general on extrapolation using data points between 70-90% water saturations should give meaningful results. In addition to this data, Table X includes data for higher permeability

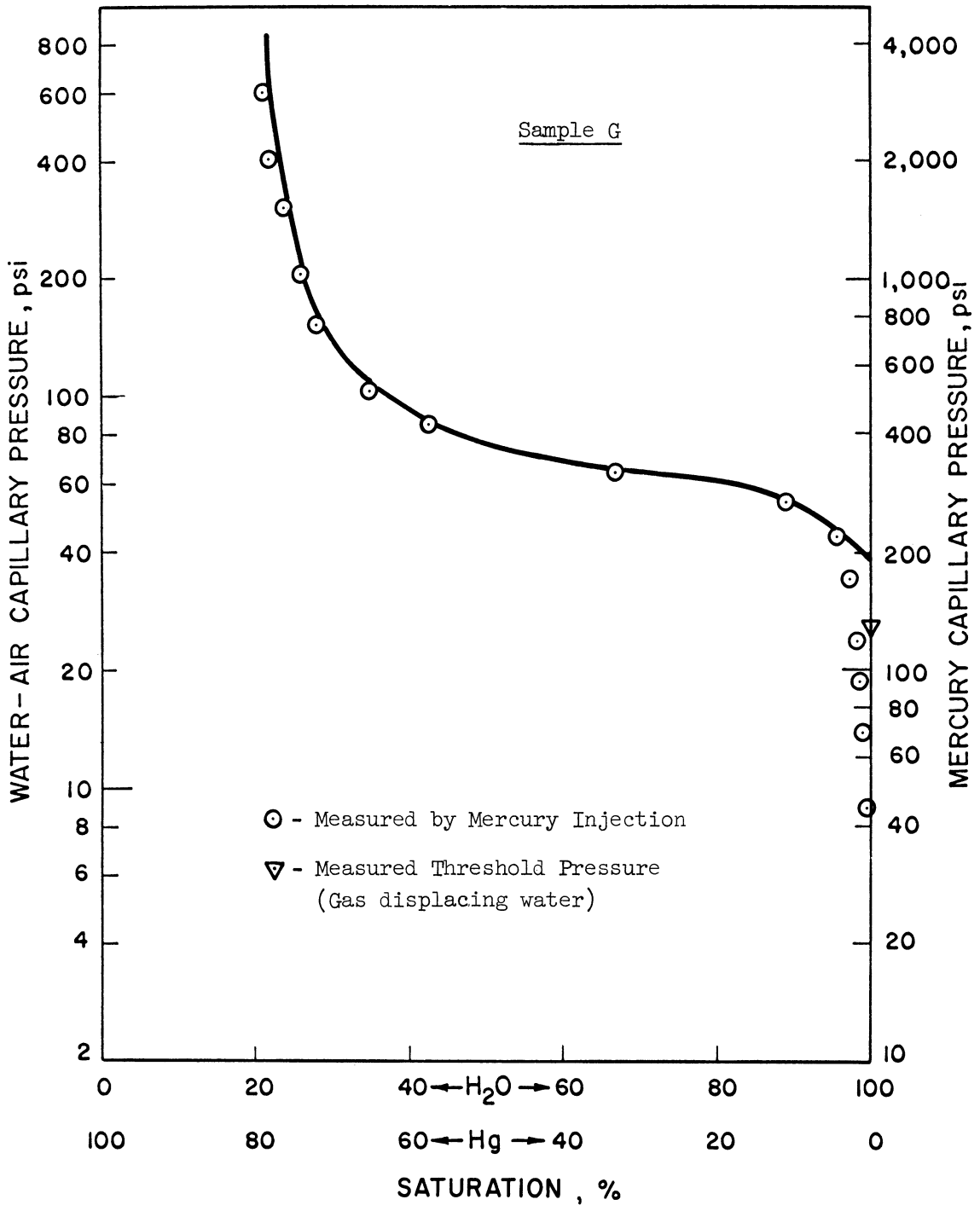

Figure 42. Capillary Pressure Curve for Sample G.

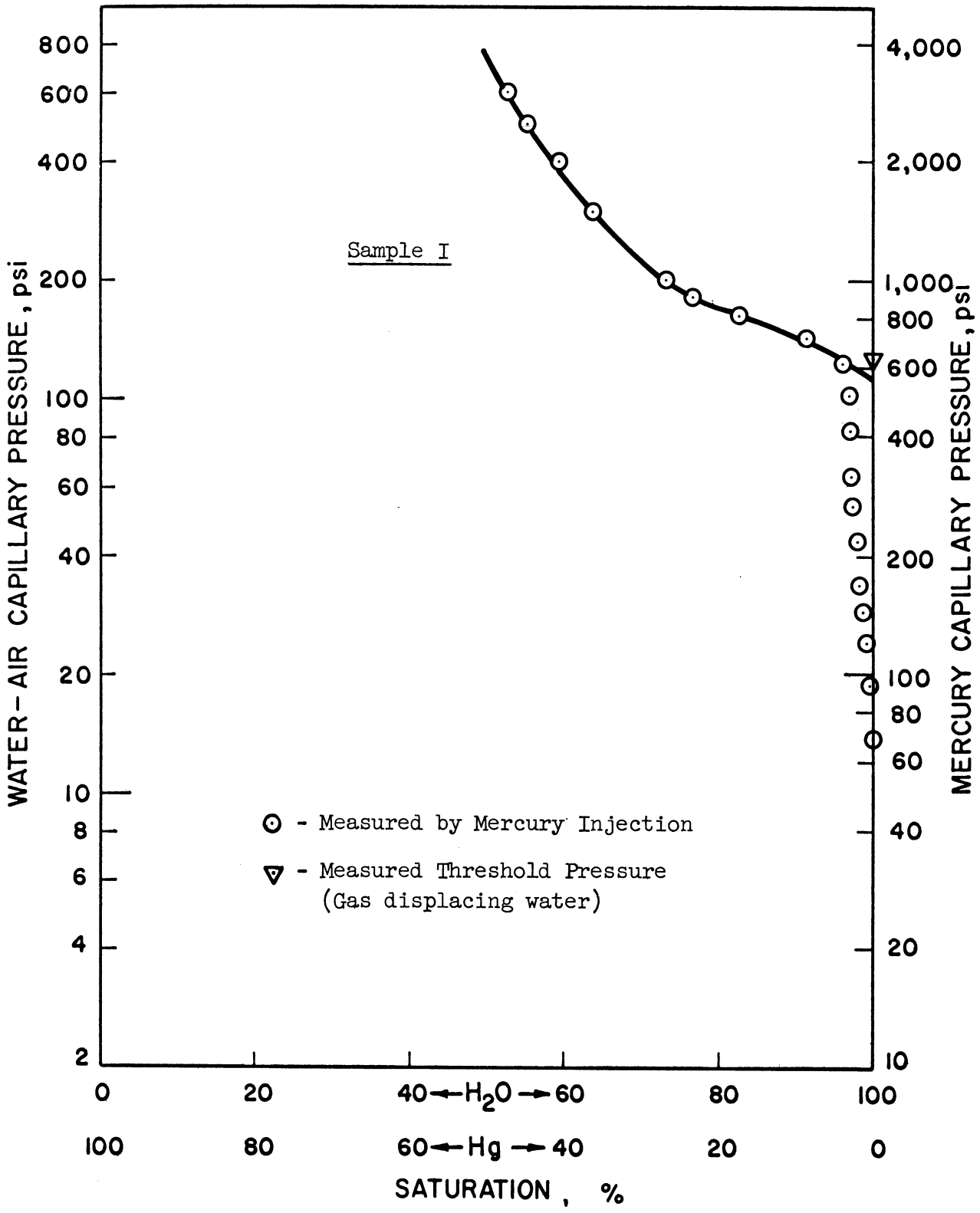

Figure 43. Capillary Pressure Curve for Sample I.

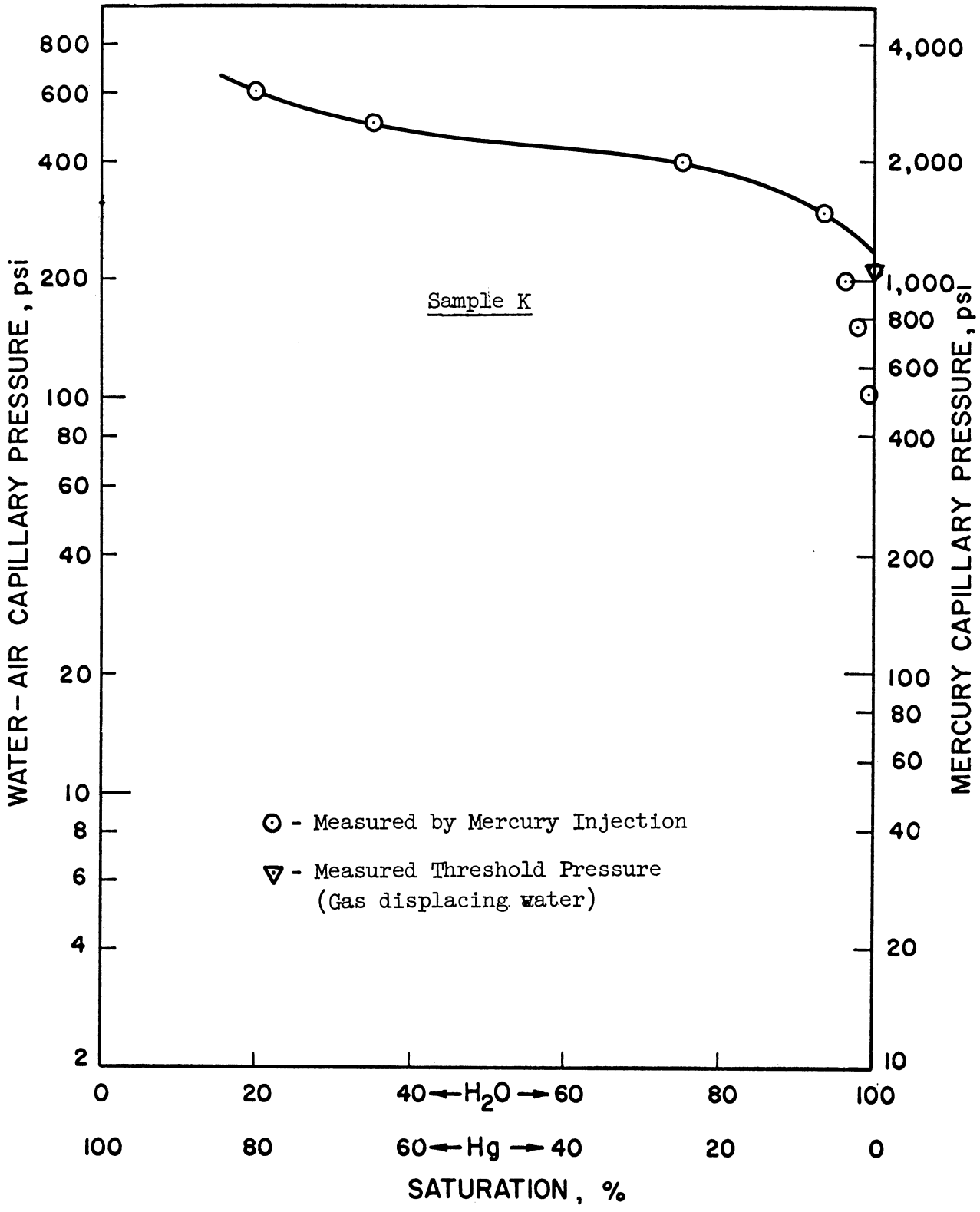

Figure 44. Capillary Pressure Curve for Sample K.

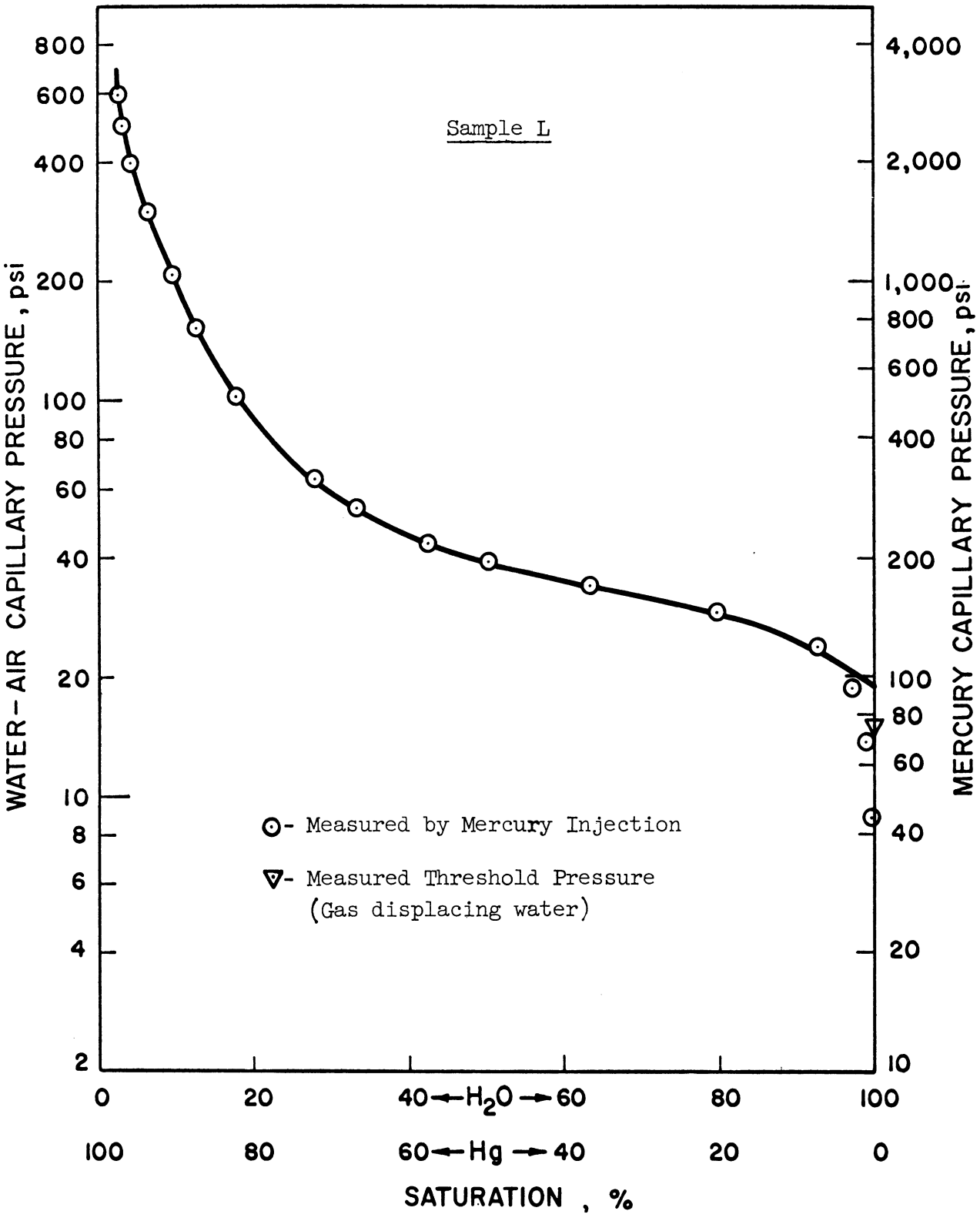

Figure 45. Capillary Pressure Curve for Sample L.

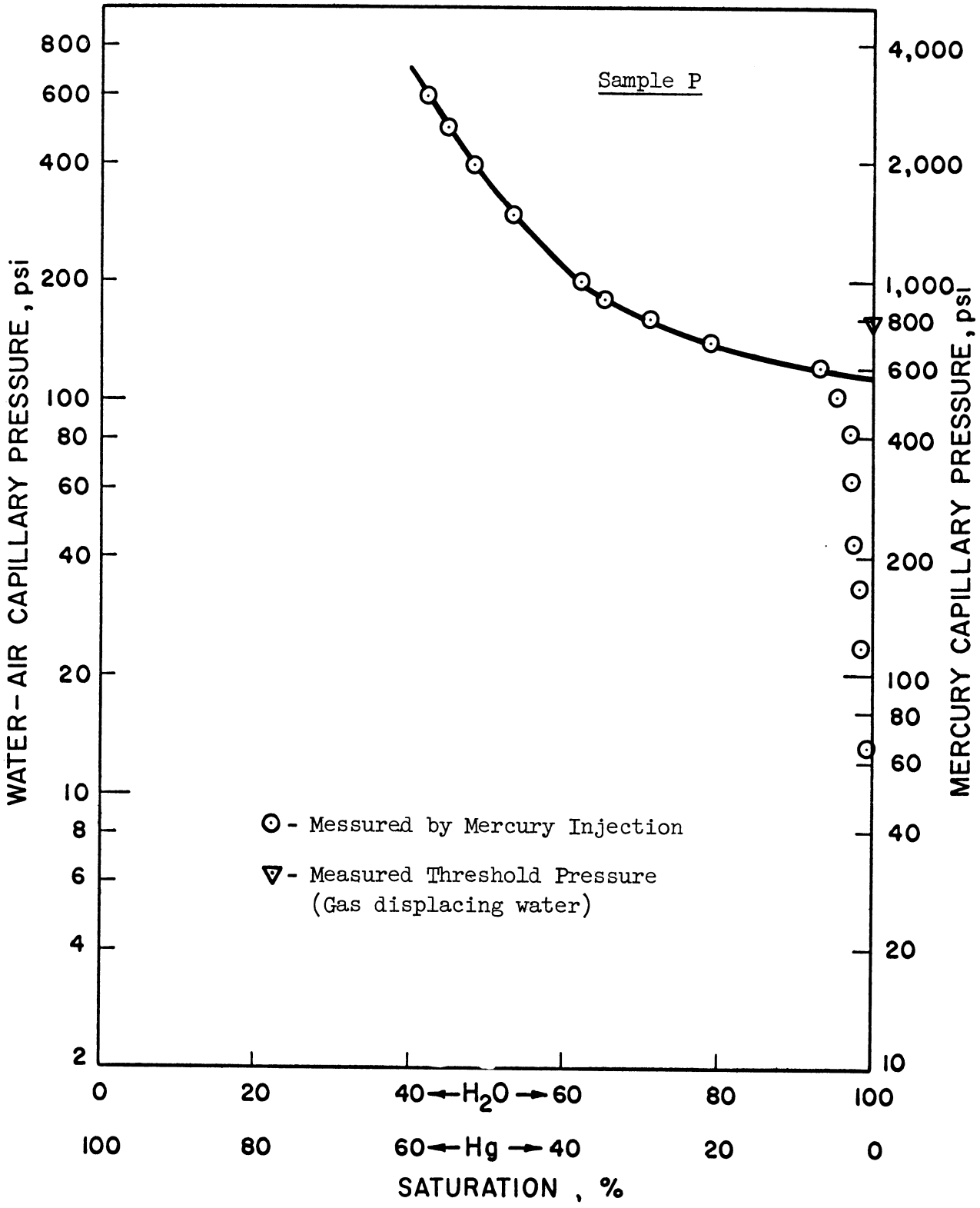

Figure 46. Capillary Pressure Curve for Sample P.

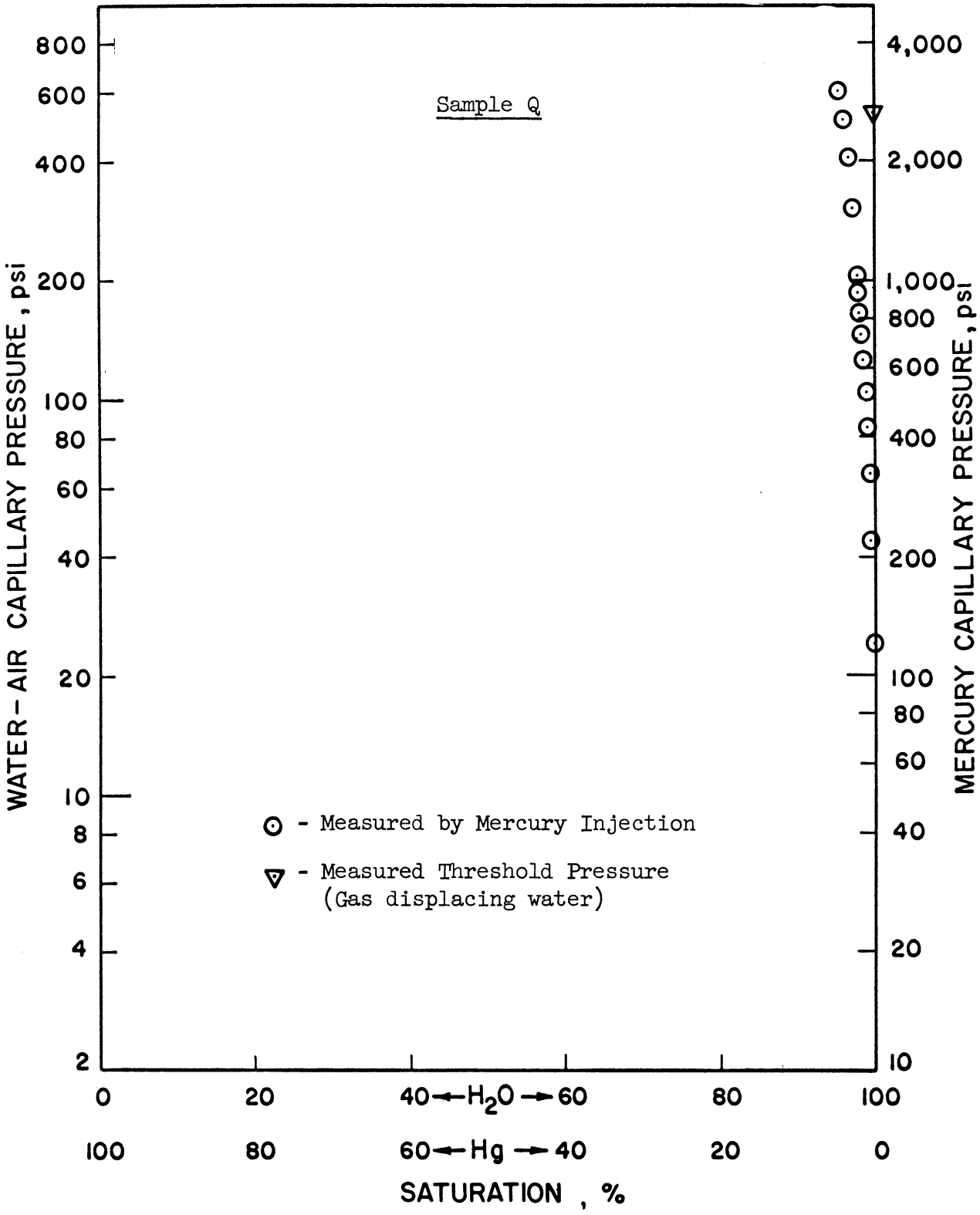

Figure 47. Capillary Pressure Curve for Sample Q.

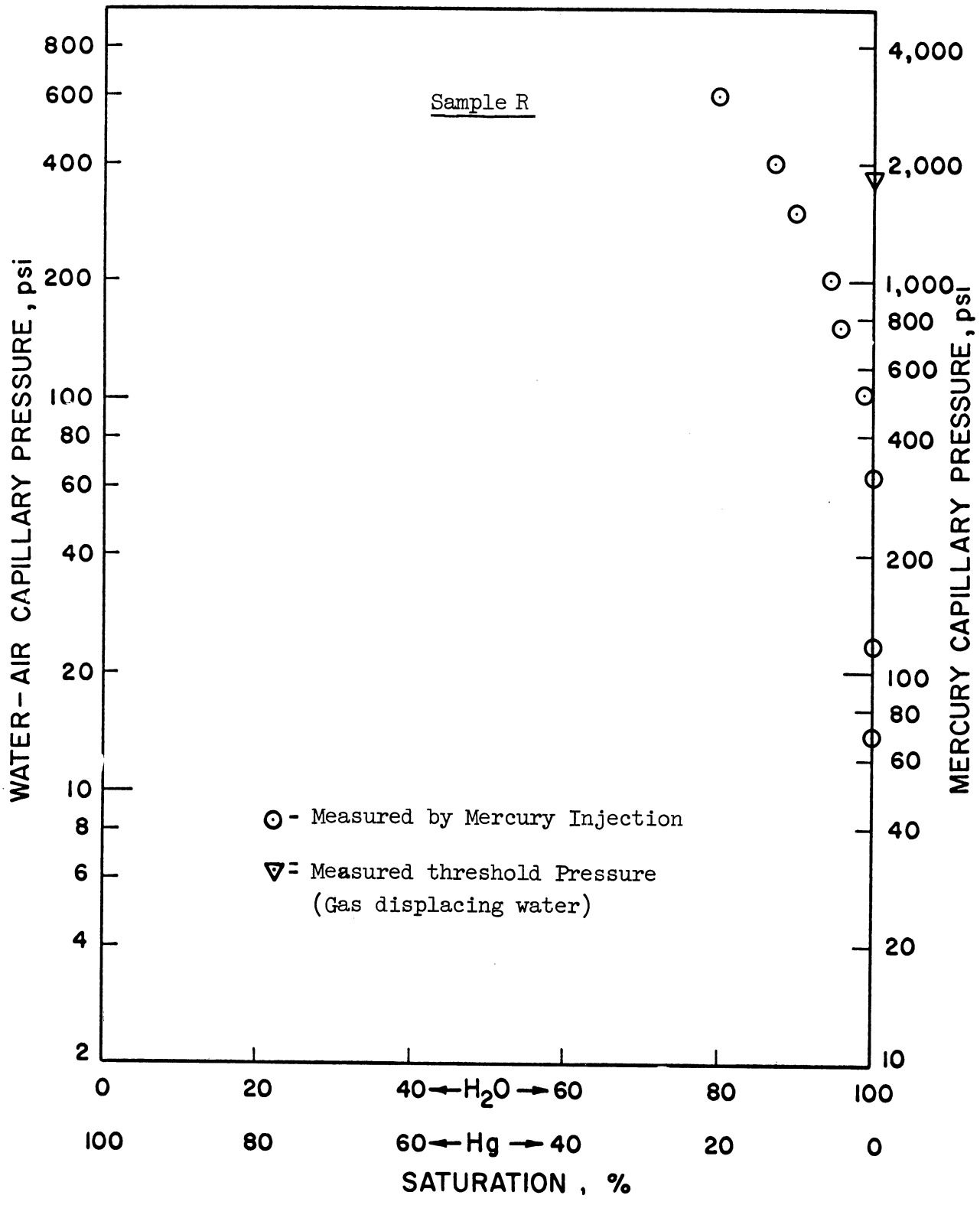

Figure 48. Capillary Pressure Curve for Sample R.

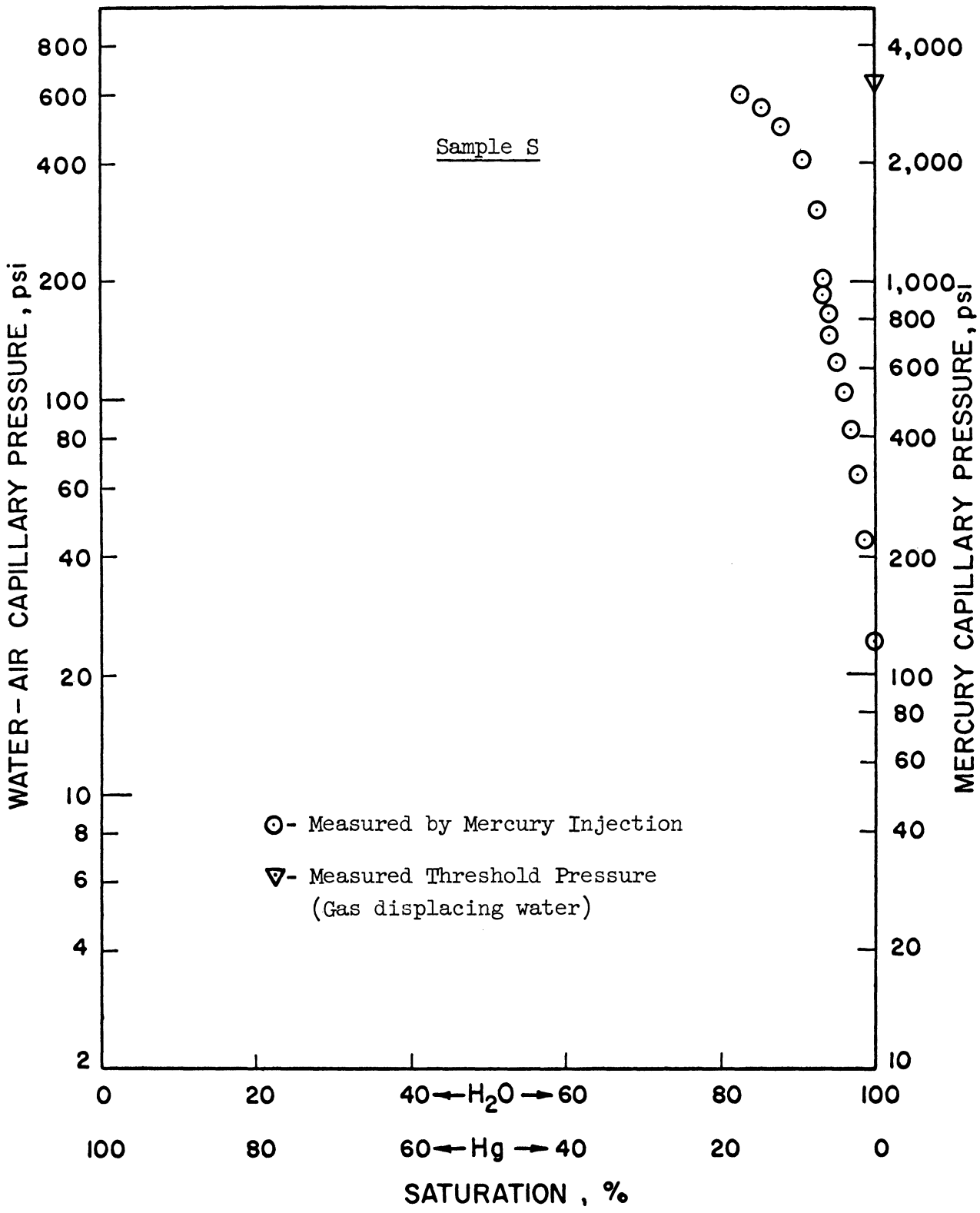

Figure 49. Capillary Pressure Curve for Sample S.

TABLE X

TABULATED COMPARISON OF AIR-WATER AND MERCURY THRESHOLD PRESSURES

Core Sample	Air-Water Threshold Pressure P_D(air-water), psi.	(Hg Threshold Pressure)/Factor, P_D(Hg)/Factor	
		Factor=5.0	Factor=6.67
Sample G	22.5	37.	28.
Sample I	125.	112.	84.
Sample K	212.	240.	180.
Sample L	15.5	18.5	13.9
Sample P	162.	116.	87.
	W.R. Purcell's Data		
San Andres Limestone	2.2	3.4	2.6
Frio Sandstone	1.6	2.8	2.1
Frio Sandstone	0.59	0.77	0.58
Paluxy Sanstone	0.94	1.4	1.0
Upper Wilcox Sandstone	0.71	1.5	1.2
San Andres Limestone	2.3	3.5	2.7

includes data for higher permeability samples presented by Purcell.[45] Purcell's paper presented the entire mercury and air-water capillary pressure curves. The data appearing in Table X was obtained by extrapolating Purcell's data in a manner similar to that in Figures 42-49.

A plot of the air-water threshold pressure versus the mercury threshold pressure adjusted by a factor of 5., Equation (52), appears in Figure 50, while a similar plot with the mercury threshold pressure adjusted by a factor of 6.67, Equation (53), appears in Figure 51. Both sets of data were fitted with an equation of the form

$$y = c_1 x^{c_2} \tag{54}$$

by the method of least squares. The resulting equation is a straight line on a log.-log. plot. The equation obtained in Figure 50 was

$$P_T(\text{air-water}) = .571 \left[\frac{P_T(\text{Hg})}{5.0}\right]^{1.117} \tag{55}$$

while that for Figure 51 was

$$P_T(\text{air-water}) = .779 \left[\frac{P_T(\text{Hg})}{6.67}\right]^{1.119} \tag{56}$$

The least squares fit minimized the sum of the squares of the deviations of the values along the abscissa. The standard deviation of the points about the regression line in Figure 50 was .209, while that for Figure 51 was 0.225.

Equation (55) or (56) provides an excellent quantitative description of air-water threshold pressure in terms of the mercury threshold pressure. This correlation also offers a great savings in time since a mercury threshold pressure can be obtained in less than an hour compared to several days for some low permeability samples of porous media.

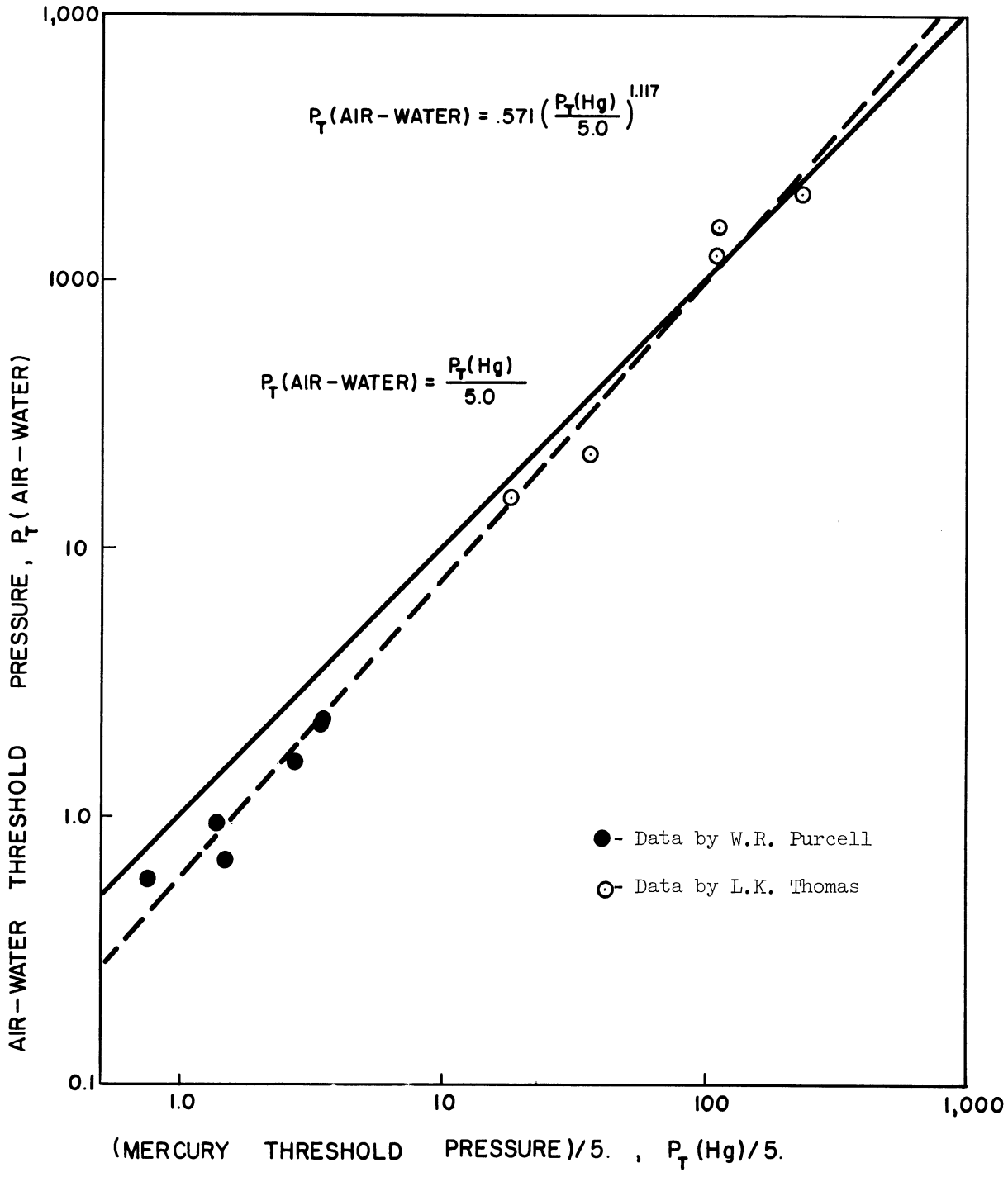

Figure 50. Air-Water and Mercury Threshold Pressure Correlation, P_T (air-water) = $P_T(Hg)/5.0$.

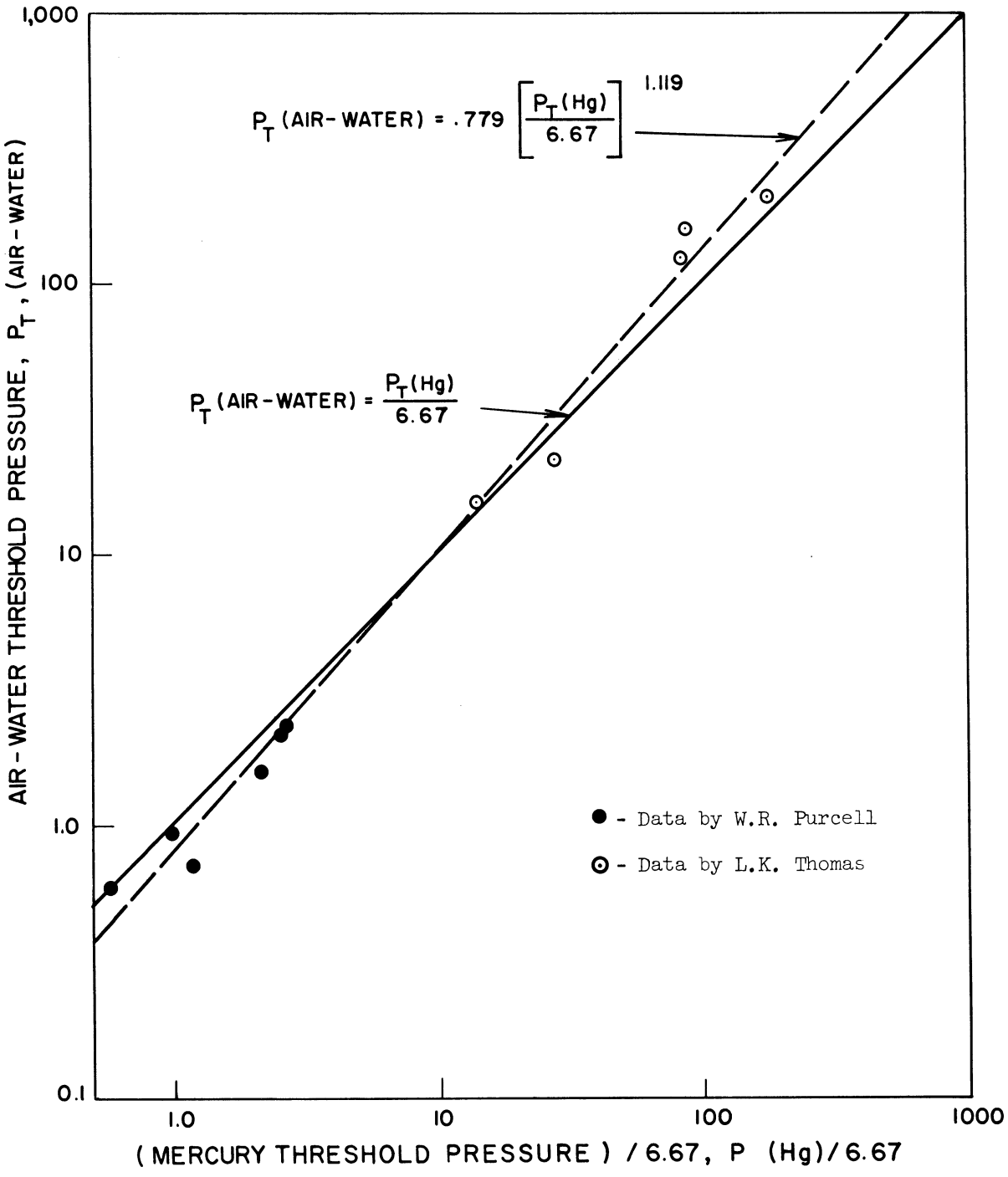

Figure 51. Air-Water and Mercury Displacement Pressure Correlation, P_T(air-water) = P_T(Hg)/6.67.

C. Effect of Time on Threshold Pressure

The question arises as to whether or not threshold pressures of porous media are functions of time. Two different samples, sample K and P, were allowed to stand 3-10 days under gas pressures below their threshold pressure. No movement of water resulted from these cores over this period of time. This is illustrated for sample K in Figure 42.

Further evidence concerning whether or not threshold pressures are a function of time is furnished by considering oil and gas reservoirs. The caprocks of these reservoirs have demonstrated their ability to retain oil and gas over periods of geologic time. The existence of oil and gas reservoirs having abnormally high discovery pressures such as those along the Gulf Coast[11,19] suggest still further evidence that the threshold pressures of caprocks are not a function of time.

Although the threshold pressure of porous medium is not a function of time, the small diminishing flow resulting from a sample of porous medium after each pressure increment prior to the threshold pressures is a function of time. Sufficient time must be allowed after each pressure increment to determine whether or not the threshold pressure has been reached. A discussion of the water movement from a caprock prior to reaching the threshold pressure is presented in the next section.

D. Movement of the Gas-Water Interface Prior to Reaching the Threshold Pressure

During the air-water threshold pressure measurements a small diminishing flow of water usually occurred from the outlet end of a core after each pressure increment preceding the threshold pressure. A typical example of this flow for sample K is presented in Figure 53. It

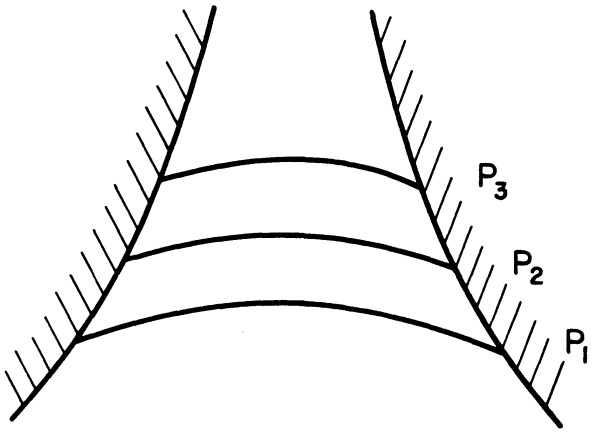

Figure 52. Position of the Gas-Water Interface in a Pore at Various Pressure Levels.
$P_1 < P_2 < P_3$

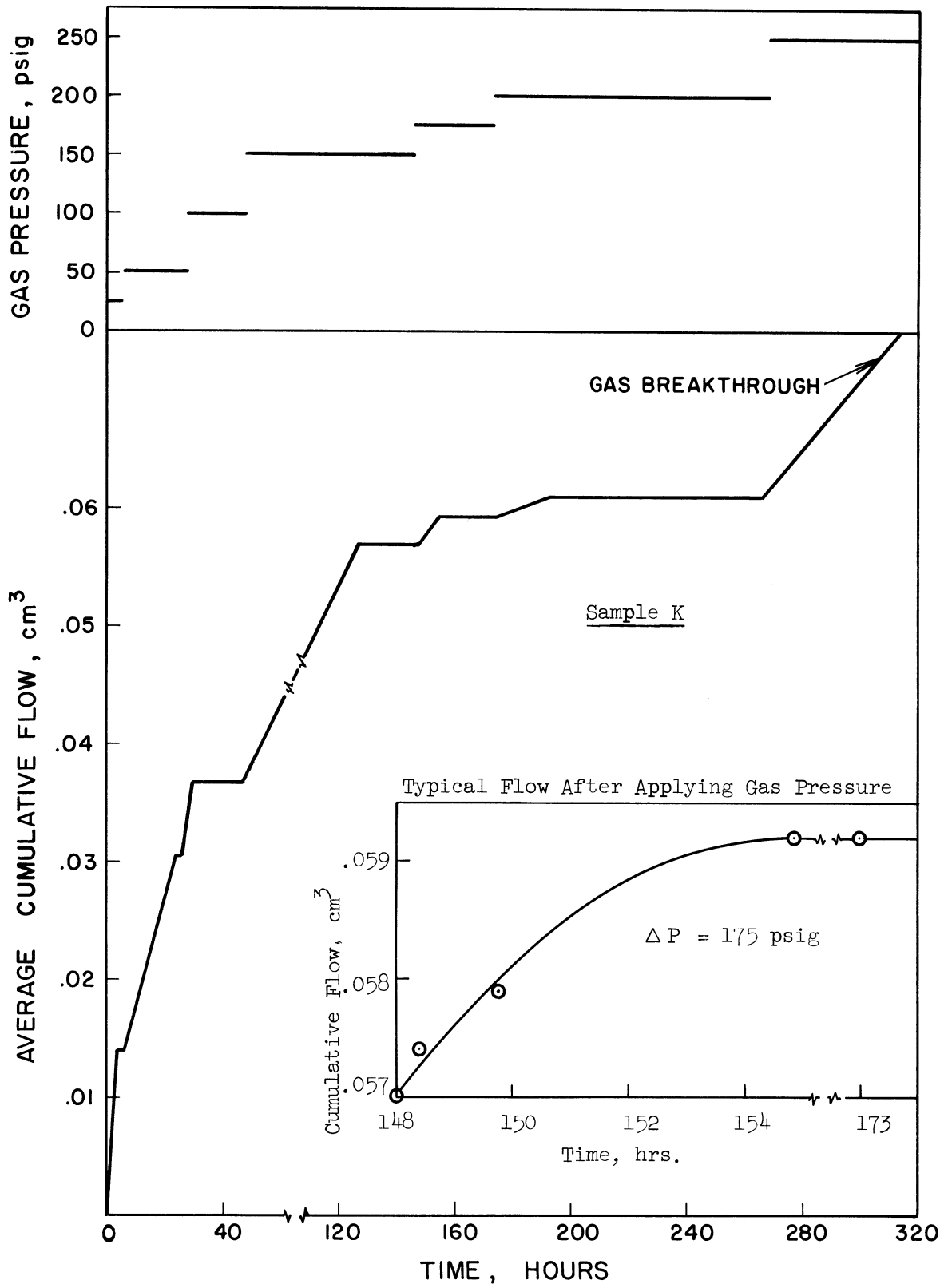

Figure 53. Cumulative Flow from Sample K during Threshold Pressure Measurement.

appears that after each pressure increment the gas-water interface at the base of a core sample moves through the larger pores until it reaches some constriction where the capillary forces are greater than the pressure forces. Thus, after each pressure rise a small diminishing movement of the gas-water interface would occur, Figure 52. When the threshold pressure is reached the gas-water interface would have reached the smallest constrictions in the largest pores in the caprock and a continuous motion of gas would occur from the caprock.

In order to verify the hypothesis stated above concerning the movement of the gas-water interface prior to reaching the threshold pressure, let us consider the flow of liquid from a simplified model of a pore. The model consists of a converging tube, Figure 54. The pressure at the inlet of the tube is equal to P_1, gauge pressure plus atmospheric pressure. The pressure at the outlet end of the tube is atmospheric. The variable x_1, corresponds to the position of the interface at any instance. x_{max} corresponds to the point in the tube where the smallest radius is reached. This is the point where the threshold pressure of the tube would be reached. The driving force for flow is given by

$$\Delta P = P_1 - P_c - P_a = P_G - P_c \quad . \tag{57}$$

If the radius of the tube in Figure 54 is given by

$$r = a + bx \quad , \tag{58}$$

$$\Delta P = P_G - \frac{26}{a+bx_1} \tag{59}$$

The resisting force is the result of friction, which occurs from x_1 to some length L. In reference to a pore in a porous medium the distance L would correspond to the distance from the gas-water interface to the outlet

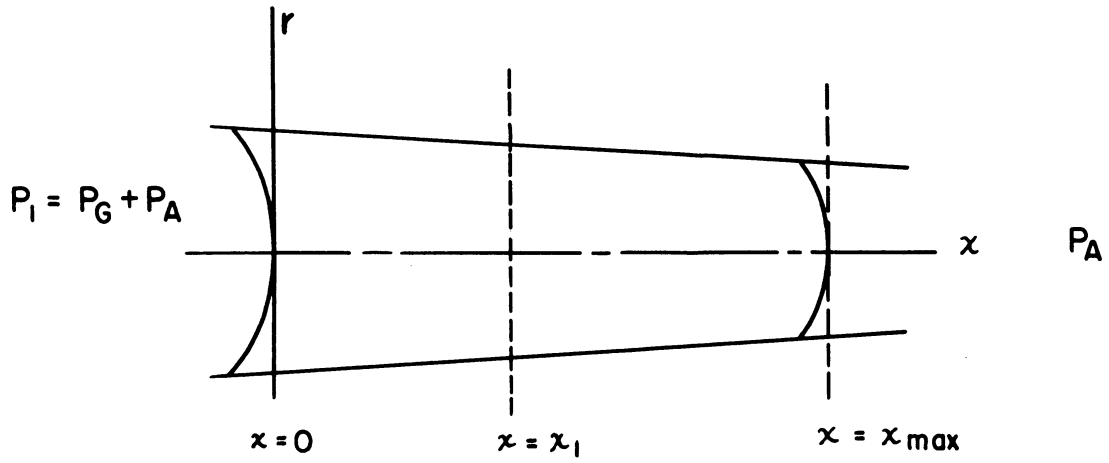

Figure 54. Movement of a Gas-Water Interface through a Converging Tube.

end of the sample. The resisting force at a given radius, r, is assumed to be equivalent to the resisting force in a tube of radius r and is given by[21]

$$\sum F = \frac{8\mu v_a L}{\rho r^2} \tag{60}$$

where

μ = viscosity of water

L = length of pore

ρ = density of water

r = radius of tube

v_a = average flow velocity

Making a momentum balance (neglecting acceleration terms) we have

$$\frac{1}{\rho}\int_{P_a}^{P_1-P_c} dP = \int d\sum F = \frac{8\mu}{\rho}\left[\frac{L}{x_{max}}\int_0^{x_{max}} \frac{v_a dx}{(a+bx)^2} - \int_0^{x} \frac{v_a dx}{(a+bx)^2}\right] \tag{61}$$

Equation(61) can be integrated if the average velocity is written in terms of the distance.

$$v_a = \frac{q(t)}{A} \qquad \frac{q(t)}{\pi(a+bx)^2} \tag{62}$$

Where $q(t)$ is equal to the volumetric flow rate. Substituting Equation (62) into Equation (61) and neglecting the second integral since $L/x_{max} \gg 1.0$ yields

$$P_G - \frac{2\sigma}{a+bx_1} = \frac{8\mu q(t)}{\pi}\frac{L}{x_{max}}\int_0^{x_{max}} \frac{dx}{(a+bx)^4} \tag{63}$$

Integrating and rearranging Equation (63) yields

$$q(t) = \frac{\frac{3\pi\, b\quad x_{max}}{8\mu L}\left(P_G - \frac{2\sigma}{a+bx_1}\right)}{\left[\frac{1}{(a)^3} - \frac{1}{(a+bx_{max})^3}\right]} \tag{64}$$

In order to get an equation for the position of the interface, x_1 , as a function of time we now eliminate $q(t)$ between Equation (64) and Equation (65).

$$q(t) = \frac{dx_1}{dt}\,\pi(a+bx_1)^2 \tag{65}$$

Eliminating $q(t)$ yields

$$(a+bx_1)^2\,\frac{dx_1}{dt} = \frac{\frac{3b}{8\mu L}\,x_{max}\left(P_G - \frac{2\sigma}{a+bx_1}\right)}{\left[\frac{1}{(a)^3} - \frac{1}{(a+bx_{max})^3}\right]} \tag{66}$$

Integrating this equation from time zero to some time t yields

$$\theta = c_3 t = \left(\frac{1}{a^3} - \frac{1}{r_{max}^3}\right)\left\{\frac{1}{3}\left[r_1^3 - a^3\right] + \frac{\sigma}{P_G^3}\left[(P_G r_1 - 2\sigma)^2 - (P_G a - 2\sigma)^2\right]\right.$$

$$\left. + \frac{8\sigma^2 b(r_1-a)}{P_G^{\,2}} - \frac{8\sigma^3}{P_G^3 r_{max}^3} - \frac{(P_G r_1 - 2\sigma)}{(P_G a - 2\sigma)}\right\} \tag{67}$$

where

$$c_3 = \frac{3b^2\, x_{max}\, P_G}{8\mu L}\ , \tag{68}$$

$$r_1 = a + bx_1\ , \tag{69}$$

$$r_{max} = a + bx_{max}\ . \tag{70}$$

The cumulative flow which occurs from $x = 0$ to $x = x_1$ for a driving force such that the threshold pressure is not exceeded is given by

$$Q(t) = \frac{\pi x_1}{3} (a^2 + ar_1 + r_1^2) \tag{71}$$

Equation (71) can be expressed in dimensionless form by dividing it by the cumulative flow which will have resulted when the interface stops.

$$Q(t_\infty) = \frac{\pi x_{stop}}{3} (a^2 + ar_{stop} + r_{stop}^2) \tag{72}$$

The interface stops when

$$P_G - \frac{2\sigma}{a+bx_1} = 0 \tag{73}$$

Therefore

$$x_{stop} = \frac{1}{b} \left(\frac{2\sigma}{P_G} - a \right) \tag{74}$$

and

$$r_{stop} = \frac{2\sigma}{P_G} \tag{75}$$

A plot of Θ versus $Q/Q(t_\infty)$ is presented in Figure 55.

A quantitative test of the validity of our hypothesis for the movement of the gas-water interface at the base of a caprock prior to exceeding the threshold pressure is not possible. This is due to the fact that the percent of the pores in which the interface is moving is not known. Even if this were known, other parameters in Equation (67) would have to be assumed before an attempt to fit experimental data with Figure 55 could be made. The general shape of Figure 55 does, however, agree with the flow observed from cores prior to exceeding the threshold pressure, see insert in Figure 53.

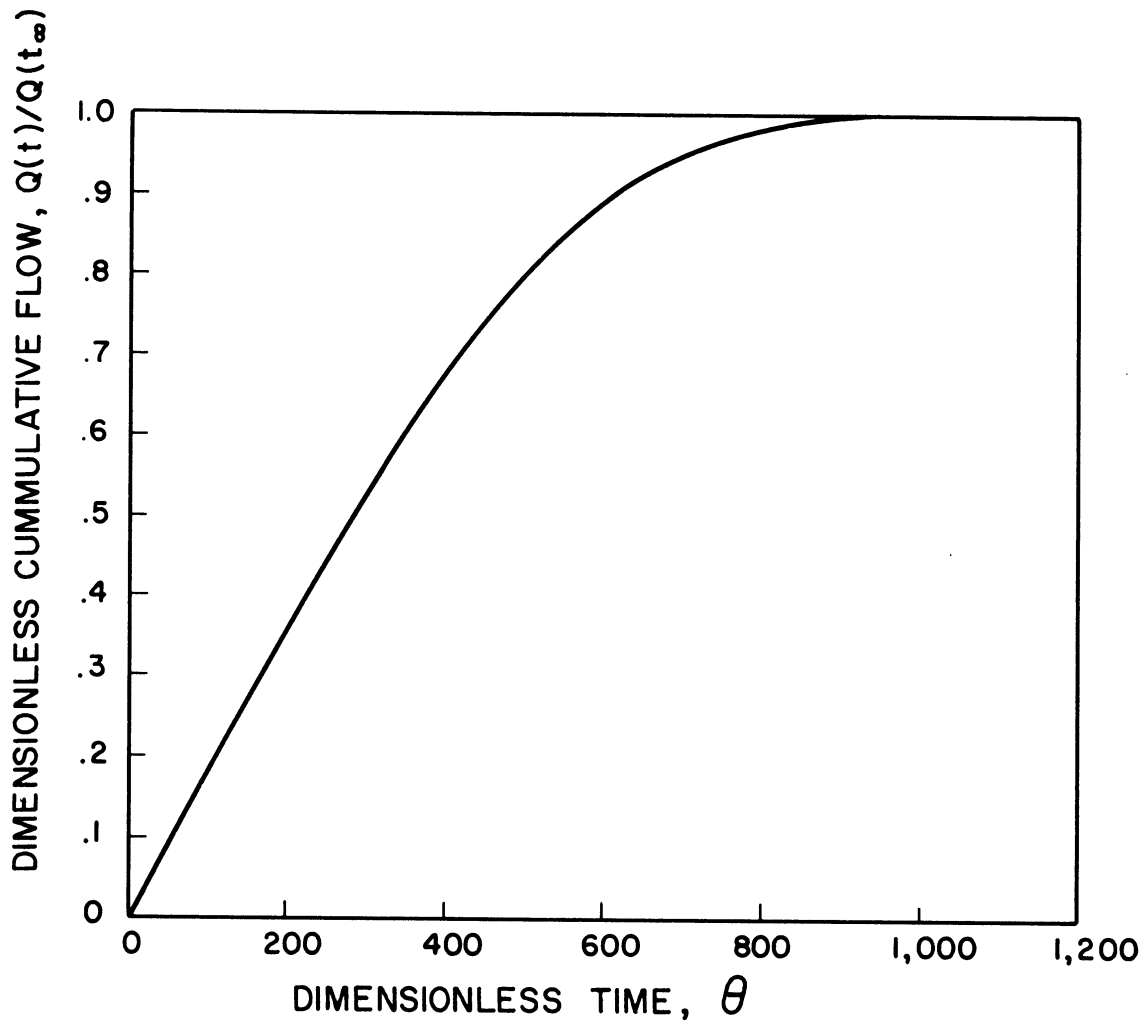

Figure 55. Flow Resulting from Gas Displacing Water from a Converging Tube.

E. Nature of the Gas Flow after Reaching the Threshold Pressure

It is of interest to determine the areal distribution of the gas flow prior to and just after exceeding the threshold pressure. Of particular interest is the question of whether or not channeling takes place during this time. Before investigating this problem a discussion of relative permeability is needed.

When two phases are present in a porous medium the flow which results in either of the phases is less than the single phase flow of one of these phases. The amount of flow in each phase is a function of its saturation and is expressed in terms of relative permeability. The relative permeability of a fluid in a two phase system is equal to the permeability of that fluid calculated from Darcy's equation divided by the single phase permeability of the porous medium. For the two phase flow of gas and water through a porous medium we have

$$v_g = - K \frac{k_{rg}}{\mu_g} \frac{dP_g}{dL} \tag{76}$$

and

$$v_w = - K \frac{k_{rw}}{\mu_w} \frac{dP_w}{dL} \tag{77}$$

where

v_g = superficial gas velocity

v_w = superficial water velocity

k_{rg} = relative permeability to gas

k_{rw} = relative permeability to water

μ_g = viscosity of the gas phase, cps

μ_w = viscosity of the water phase, cps

Figure 56 is a typical example of the relative permeability curves of a gas-water system in a porous medium.

Visual observations of gas emerging from the outlet ends of cores after their threshold pressures were reached indicate that a fairly uniform penetration of gas has occured across the faces of the cores. In addition to visual observations a photograph of the gas phase distribution for a core is presented in Figure 57. This photograph was taken after the core was removed from the core holder, but with the rubber sleeve still around the core. A layer of water was left on top of the core so that the gas bubbles would not escape. These observations indicate that for pressure levels at or slightly higher than the threshold pressure a rather uniform displacement takes place rather than channeling.

These observations are in accordance with the mobility ratio test for channeling. The mobility ratio[9] is defined by

$$\text{mobility ratio} = \frac{k_{rw}\,\mu_g}{k_{rg}\,\mu_w} \tag{78}$$

Channeling usually occurs when the mobility ratio is less than one. For gas and water this ratio is greatly affected by their viscosities at intermediate saturations and channeling occurs. At high water saturations, however, the low value of gas permeability yields a mobility ratio larger than one. Thus, it does not appear that channeling takes place prior to or just after exceeding the threshold pressure. Channel flow will develop, however, when a caprock has been desaturated to a point where an increased gas phase permeability occurs.

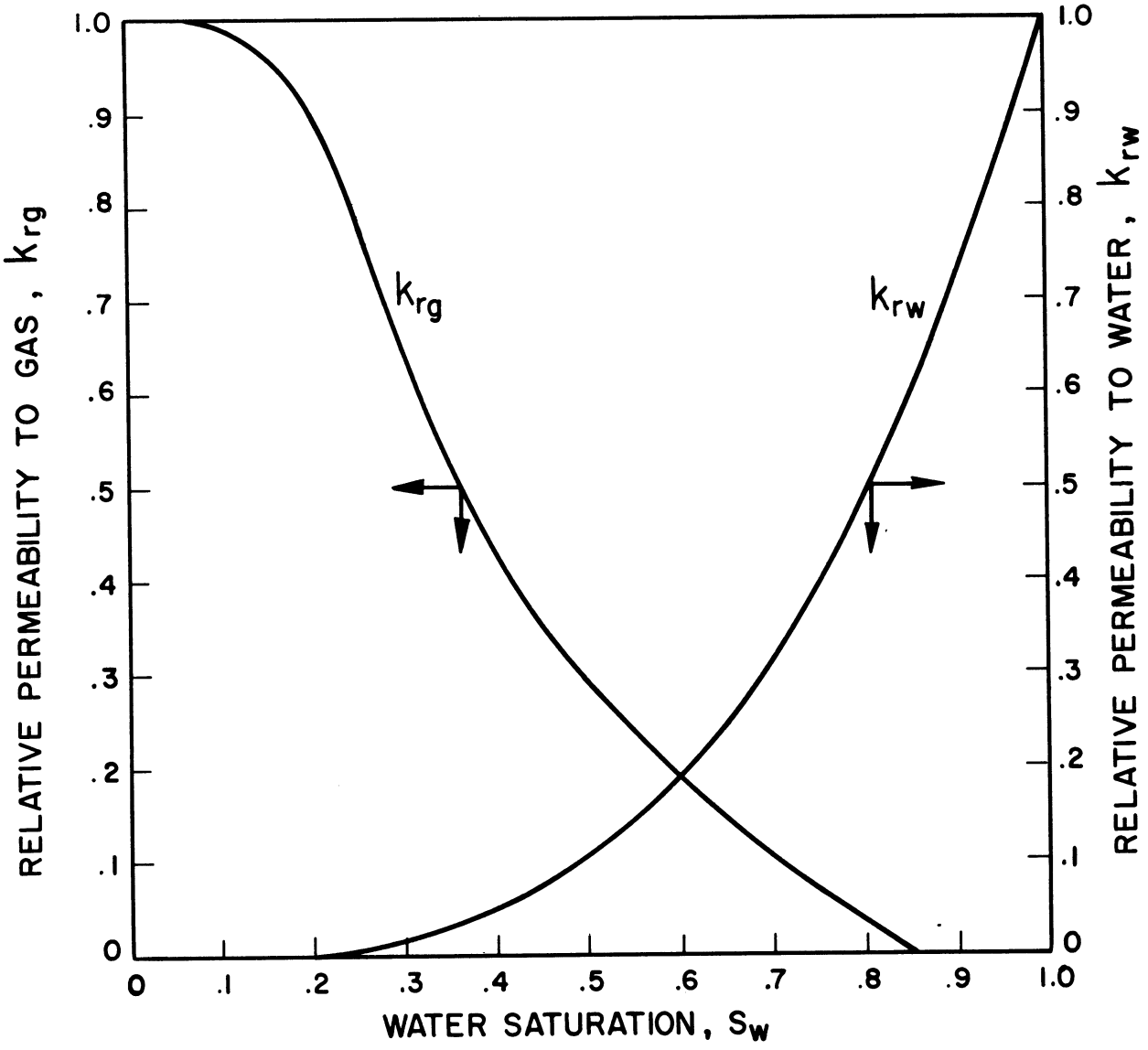

Figure 56. Typical Relative Permeability versus Saturation Plot.

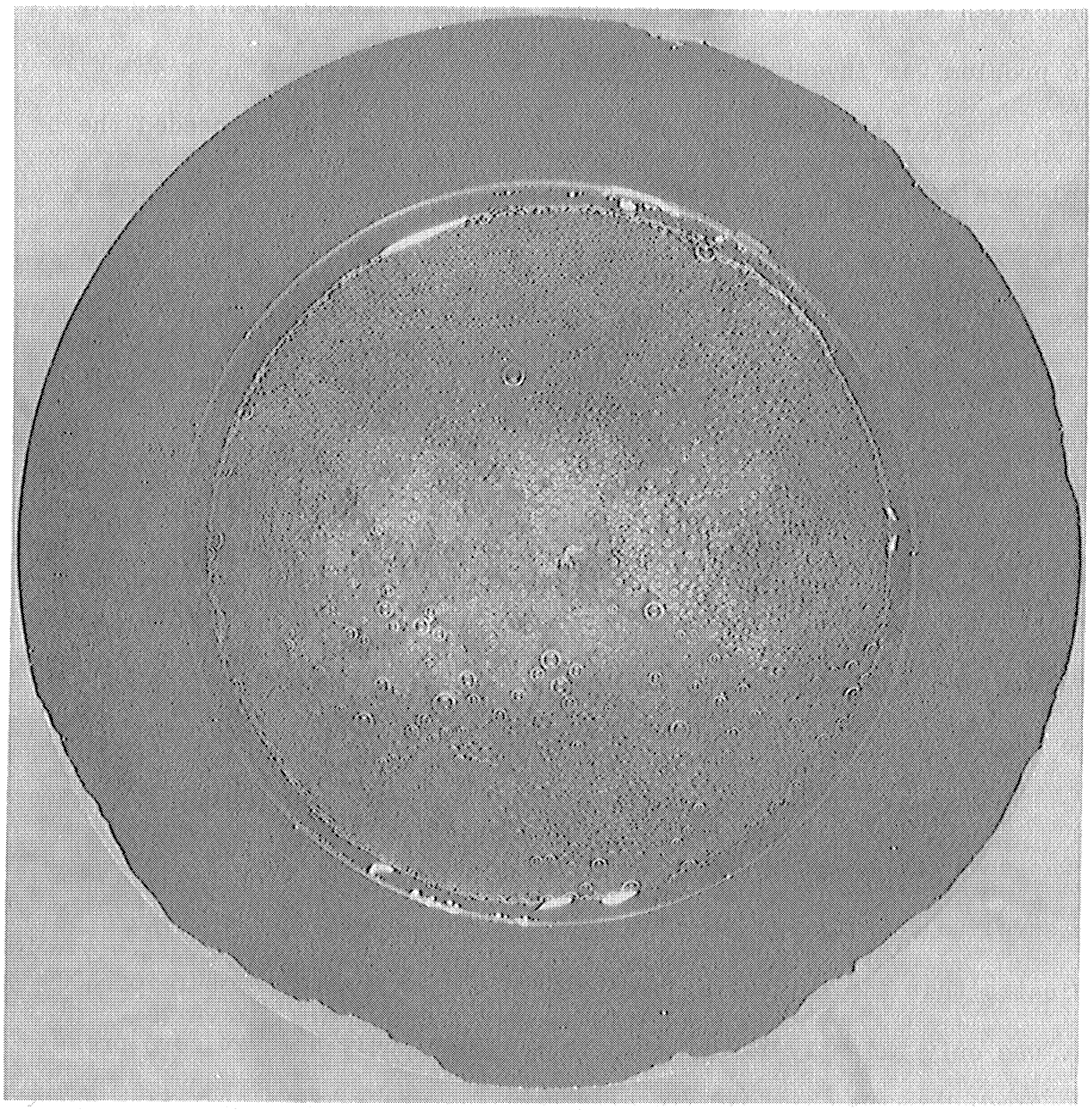

Figure 57 Gas Bubbles Penetrating Core after Exceeding Threshold Pressure.

F. Resaturation of a Caprock after Exceeding the Threshold Pressure

An important question arising in gas storage is whether or not a caprock can be resealed after the threshold pressure has been reached. This problem was investigated for samples G and Q .

After the threshold pressure for sample Q was exceeded the sample was subjected to increased gas pressures for a period of time. Average flow rates at each pressure level were measured. These measurements indicated that the flow rate from the outlet end of the core sample increased with time at a given pressure level and also with larger gas pressures, Figure 58.

A maximum pressure of 900 psi. was applied to sample Q . The gas pressure was then reduced to zero. The flow rate from the end of the core at zero pressure decreased continuously with time, Figure 58. This flow was the result of the expansion and expulsion of gas present in the core sample.

Sample Q was left with zero gas pressure for a period of time. It was then subjected to 400 psi. (over 100 psi. less than its threshold pressure) to see whether or not the sample could retain gas. Figure 58 indicates that the initial flow rate from the core at a pressure of 400 psi. was only slightly larger than it had prebiously been at zero pressure. This rate decreased with time and appeared to be approaching zero.

The results of tests to reseal sample G after its threshold displacement pressure was exceeded are shown in Figure 59. After the threshold pressure was exceeded the gas pressure at the base of sample G was reduced to zero. Water imbibed back into the sample for a period of time and then no further movement was noticed. The sample was then

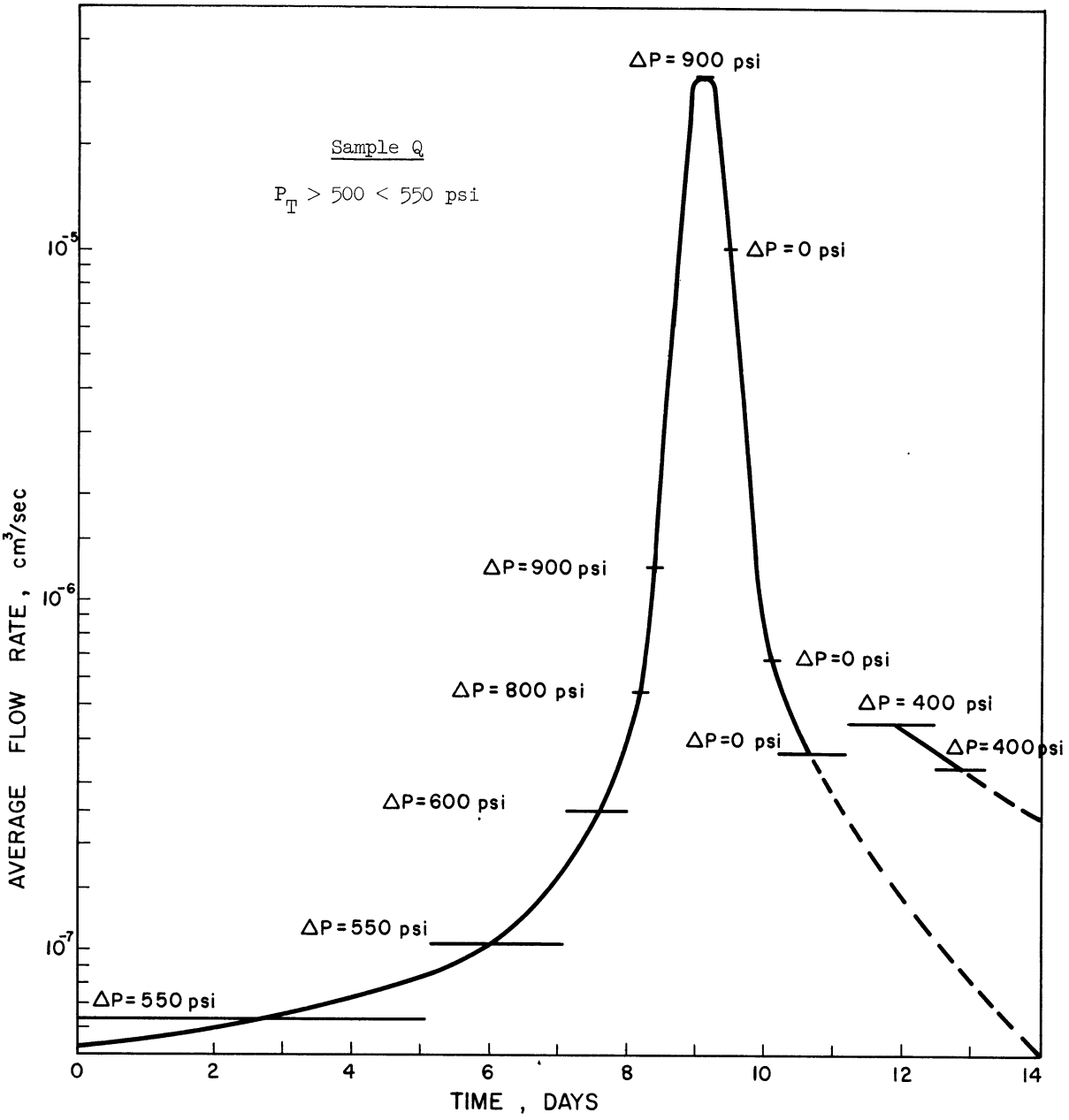

Figure 58. Resealing Sample Q after Exceeding its Threshold Displacement Pressure.

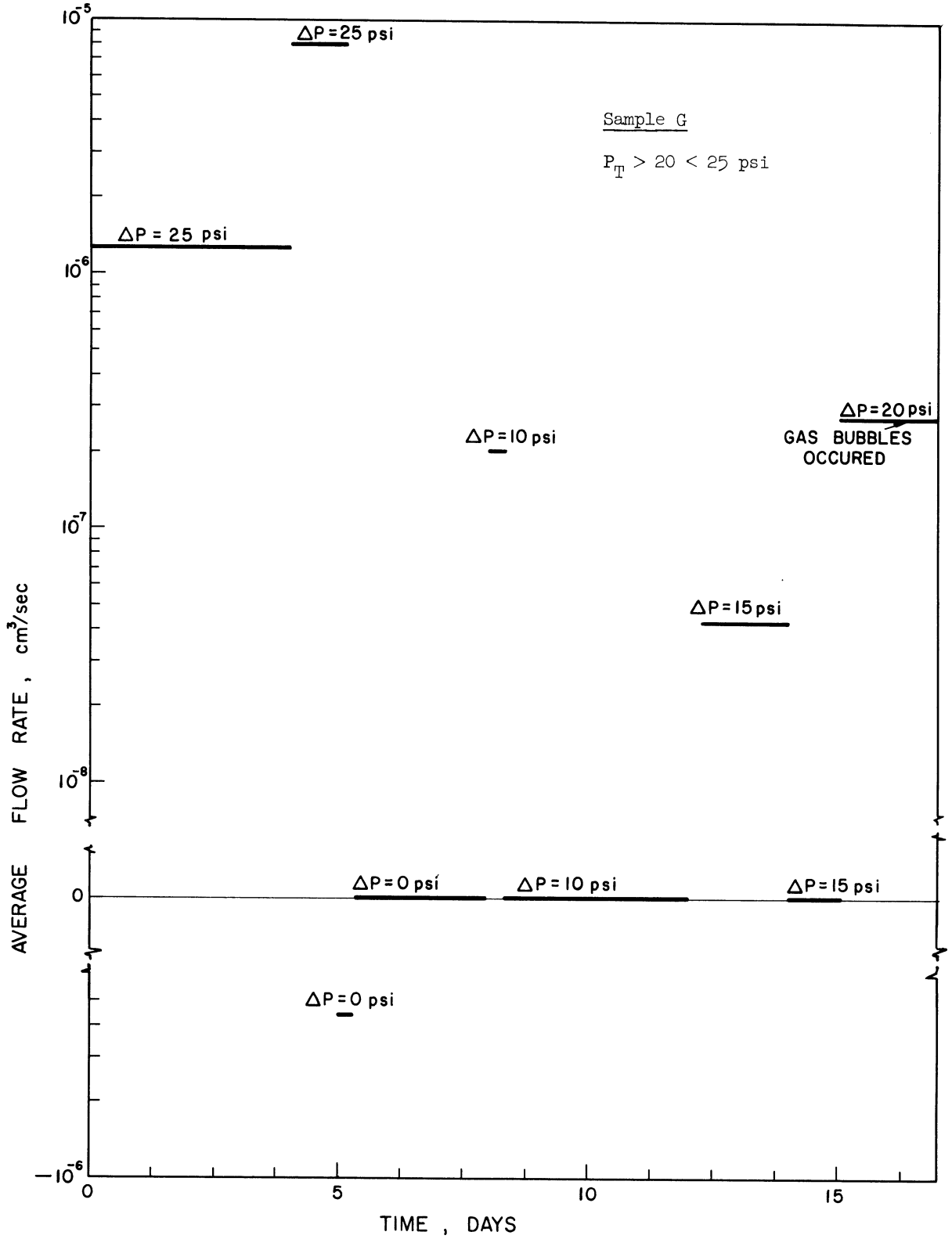

Figure 59. Resealing Sample G after Exceeding its Threshold Displacement Pressure.

subjected to 10 and 15 psi. pressure increments respectively. After each of these increments a diminishing flow which finally ceased took place. When a pressure increment of 20 psi. was applied to the sample a continuous flow resulted and gas bubbles emerged from the outlet end of the sample.

From the tests rung on samples G and Q it appears that a caprock can be resealed if the pressure in the gas reservoir is reduced to zero and water is allowed to imbibe back into the caprock.

A discussion pertaining to a safe operating pressure for a gas storage reservoir whose caprock has leaked and then has been resealed by allowing water to imbibe is presented in the next section.

G. Threshold Pressures of Partially Saturated Porous Media

Previous work on threshold pressure phenomena for high permeability core samples has been presented by Hassler, Brunner, and Deahl.[27] Their work included an investigation of the amount of gas pressure required to force gas through a partially saturated sample of porous medium. A discussion concerning threshold pressure has also been presented by Pirson.[44]

The measurements of threshold pressure versus saturation presented by Hassler, et al indicate that this data can be represented by a straight line, Figure 60. Gas saturations along this line are insular in nature, Figure 6. This line intersects the abscissa, threshold pressure equals zero, at the base of the gas phase permeability curve during drainage, Figure 61. This point is known as the highest critical saturation for gas, where critical saturation is defined as that saturated where a porous medium shows conductivity to gas independent of the applied

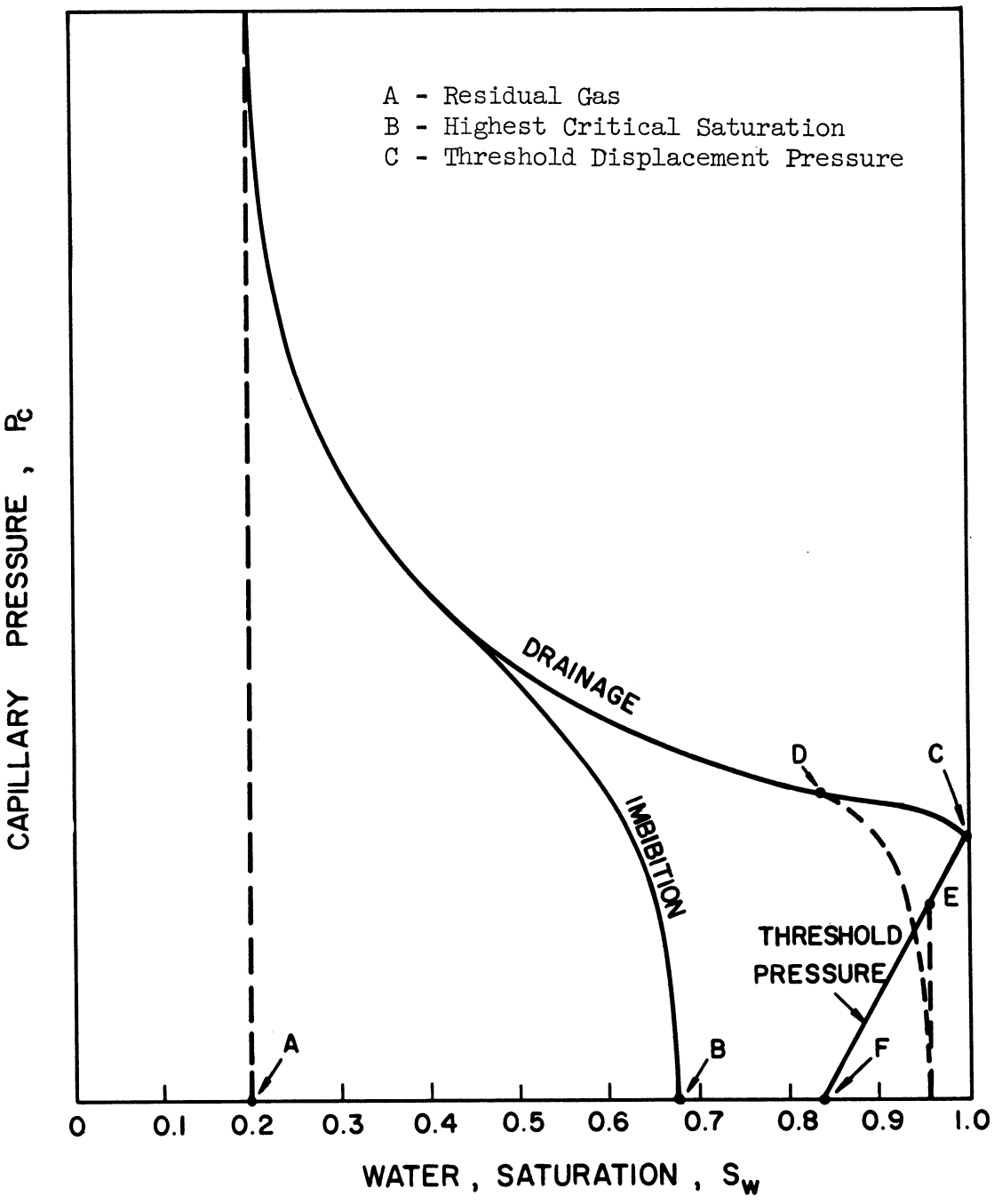

Figure 60. Threshold Pressures and their Relationship to Capillary Pressure.

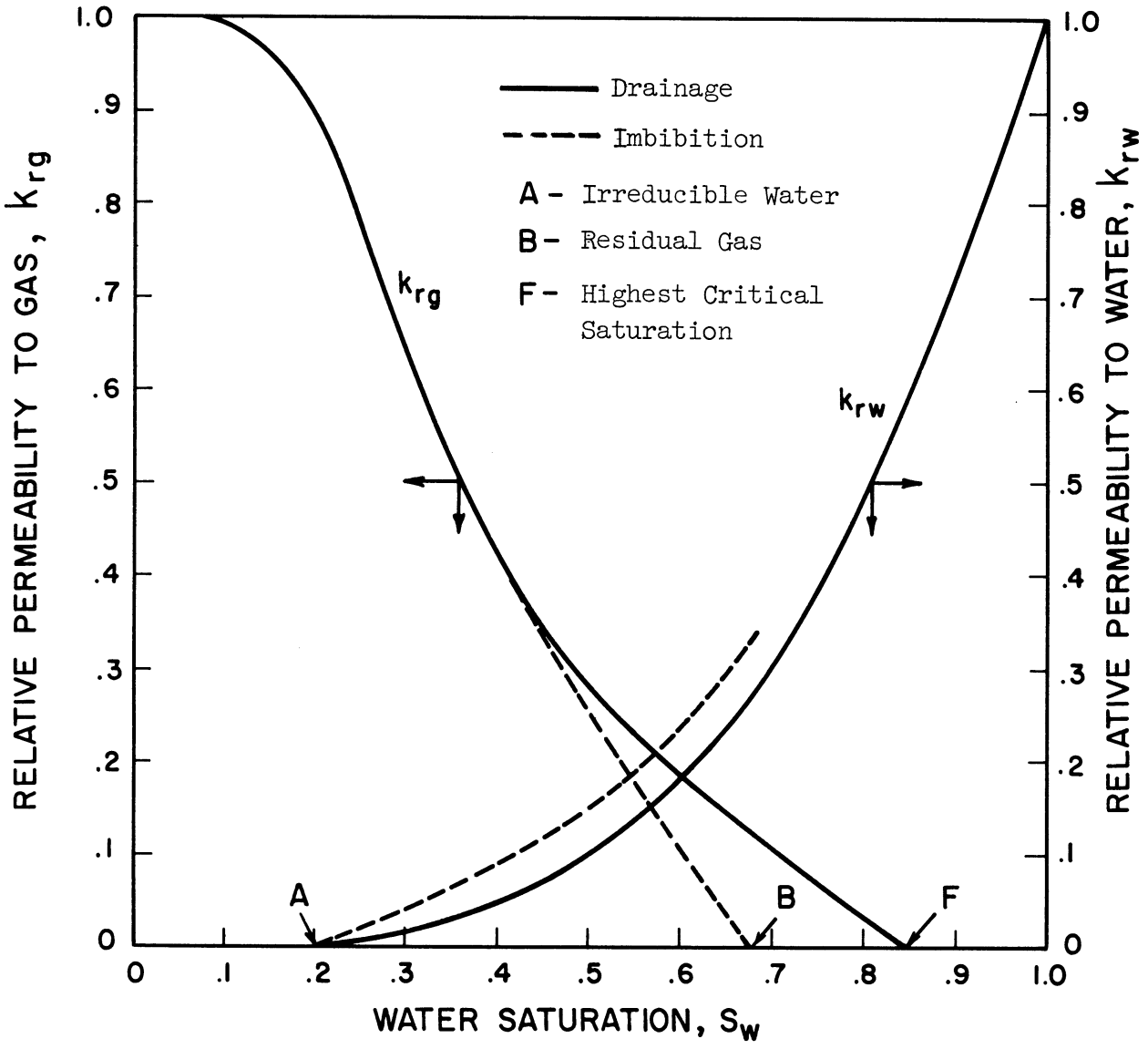

Figure 61. Drainage and Imbibition Relative Permeability Curves.

pressure gradient. The highest threshold pressure occurs at 100% water saturation, point C in Figure 60.

Before continuing our discussion about threshold pressures, the relationships which occur between the capillary pressure and relative permeability curves for a given porous medium should be pointed out. It has already been pointed out that the saturation where the threshold pressure becomes zero, point F in Figures 60-61, corresponds to the base of the gas phase permeability curve during drainage. The irreducible water saturation which was discussed in Chapter II corresponds to the point where the permeability to water both during drainage and imbibition goes to zero, point A in Figures 60-61. Point B in Figures 60-61 represents the residual gas saturation during imbibition. This point corresponds to the base of the gas permeability curve during imbibition.

Now let us examine the possibility of sealing a caprock overlying a gas reservoir after the threshold pressure has been exceeded. Assume that the gas pressure in the reservoir is such that the capillary pressure between the gas and the water in the caprock after capillary equilibrium has been reached corresponds to point D in Figure 60. If the gas pressure in the reservoir is now reduced to zero, water will imbibe back into the caprock following an intermediate imbibition curve, dotted curve, whose shape is similar to that of the imbibition curve. Thus, it appears that it is possible to reseal a caprock after exceeding the threshold displacement pressure, point C in Figure 60, provided that the caprock has not been desaturated to a point where the imbibition curve will fall to the left of the threshold pressure versus saturation line.

The safe operating pressure for a gas storage reservoir whose caprock has leaked and has then be resealed by imbibing water, is no longer determined by the threshold displacement pressure of the caprock. Rather, the safe operating pressure will be determined by the threshold pressure corresponding to point E in Figure 60.

VII. SUMMARY AND CONCLUSIONS

The objectives of this research work were to study the phenomena involved when a nonwetting phase, gas, displaces a wetting phase, water, from low permeability porous media such as caprocks overlying natural gas storage reservoirs. Specific items which were studied in this work include:

(1) the measurement of threshold pressures of low permeability porous media;

(2) the problem of predicting air-water threshold pressures of porous media from independent measurements;

(3) the effect of time on the threshold pressure of a porous medium;

(4) the movement of the gas-water interface at the base of a sample of porous medium saturated with water when subjected to pressures less than the threshold pressure;

(5) the nature of the gas flow through a porous medium after the threshold pressure is exceeded;

(6) and the problem of resealing a caprock after the threshold pressure has been exceeded.

Threshold displacement pressure measurements for eight samples of consolidated porous media were made. The reproducibility of these measurements was checked for two of the samples used, samples L and K . The threshold pressure of sample L was completely reproducible while the threshold pressure for sample K was reproducible to 7%. Other measurements taken in this research include: air permeability, turbulence factor, porosity, water permeability, formation resistivity factor, and mercury injection capillary pressure.

Theoretical developments relating threshold pressures to other properties of porous media were presented in Chapter III. Two equations were presented for correlating threshold pressures. Leverett's j-Function,

(References: 33, and 34), Equation (8)

$$P_T = \sigma\, j(S_w = 1.0)\sqrt{\frac{\phi}{K}} \tag{8}$$

and Equation (35)

$$P_T = \frac{\sigma}{\sqrt{k_o}\, F}\sqrt{\frac{1}{\phi K}} \tag{35}$$

A plot of Equation (35) using the data obtained in this research work plus data from the literature for higher permeability samples appears in Figure 38. Equation (35) represented most of the data presented in this work as well as data for higher permeability samples presented in the literature. Some of the threshold pressure data presented in this work, fell below the value predicted from Equation (35). Nonetheless, a quantitative agreement was obtained for the majority of the data used to test Equation (35) and certainly a qualitative description for all of the data was achieved.

Plots of threshold pressure versus reciprocal permeability, porosity divided by permeability, and reciprocal porosity times permeability for the data taken in this work appear in Figures 39-41, respectively. Equations representing the data in Figures 39-41 were obtained by the method of least squares. The resulting equations are:

$$P_T = 7.37\left(\frac{1}{K}\right)^{.43} \tag{45}$$

$$P_T = 19.1\left(\frac{\phi}{K}\right)^{.497} \tag{46}$$

and

$$P_T = 4.74\left(\frac{1}{\phi K}\right)^{.351} \tag{47}$$

The exponents in Equations (45) and (46) are in good agreement with the exponent of 0.5 predicted by Equations (8) and (35). Equations (45) - (47) represent suitable correlations for threshold pressure, with Equation (45) giving the best fit of the data. These equations are valuable for estimating threshold pressures from standard measurements usually performed on porous samples. For example, if the permeability of a given porous sample is known to be $5.(10^{-4})$ a threshold pressure of about 200 psi. is predicted by Equation (46). Equation (35) while of general utility contains a term, formation resistivity factor, which is not routinely measured.

Another correlation for threshold pressure was formulated by relating mercury and air-water threshold pressures, Chapter VI. Mercury threshold pressures were obtained by extrapolating mercury capillary pressure curves to values of zero mercury saturation. It was then possible to correlate this data with air-water threshold pressures by either Equation (55)

$$P_T(\text{air-water}) = .571 \left[P_T \frac{(\text{Hg})}{5.0} \right]^{1.117} \qquad (55)$$

or Equation (56).

$$P_T(\text{air-water}) = .779 \left[\frac{P_T (\text{Hg})}{6.67} \right]^{1.119} \qquad (56)$$

Either of these equations provide an excellent quantitative description of the data presented in this work plus data for higher permeability samples obtained from the literature.

The effect of time on the threshold pressure was studied. It was concluded from this study that threshold pressure is not a function of time.

The movement of the gas-water interface at the base of a sample of porous medium saturated with water when subjected to pressures less than the threshold pressure was analyzed. It was concluded that the diminishing movement of this interface after each rise in gas pressure is the result of the interface moving through the larger pores of a porous medium until constrictions are reached where the capillary forces are just in balance with the pressure forces.

The nature of the gas flow through a porous medium after the threshold pressure has been exceeded has been studied by visually observing the areal distribution of gas emerging from the outlet end of a core sample, Figure 57. It was concluded from these observations that the penetration of gas through the core is fairly uniform. These observations are also in agreement with the mobility ratio test for channeling.

$$\text{mobility ratio} = \frac{k_{rw}\,\mu_g}{k_{rg}\,\mu_w} \tag{78}$$

Channeling occurs when the mobility ratio is less than one, which is not the case prior to or just after exceeding the threshold pressure due to the low value of gas permeability. As more and more water is displaced from the porous sample, however, channeling will occur.

The problem of resealing a porous medium after exceeding its threshold pressure was investigated for samples G and Q . It was concluded from these measurements that it is possible to reseal a porous medium, which has not been desaturated below its highest critical saturation,[27] by letting water imbibe back into the caprock.

If a porous medium can be resealed, the safe operating pressure for the underlying gas reservoir will, however, no longer be determined by the threshold displacement pressure of the caprock. The safe operating

pressure will be determined by a threshold pressure whose value is less than the threshold displacement pressure of the caprock.

APPENDIX A

SAMPLE CALCULATIONS

1. Determination of Porosity

Core: Sample K,

Length: 5.21 cm = .171 ft

Cross-sectional Area: 11.59 cm^2 = .0125 ft^2

Temperature: 72F°

Dry weight: 164.216 gm

Bulk Volume: 5.21(11.59) = 60.4 cc

Weight of sample saturated with water: 166.169 gm

Weight of water in pores: 166.169
164.216
1.953 gm

Volume of water in pores: $\frac{1.953}{.997} = 1.96$ cc

Porosity: $\frac{1.96(100)}{5.21(11.59)} = 3.25\%$

2. Air Permeability

Core: Sample K,

Length: 6.95 cm. = .228 ft

Cross-sectional Area: 11.59 cm^2 = .0125 ft^2

Gas: Nitrogen

Integrated Flow Equation

$$\frac{MA(P_1^2 - P_2^2)}{2zRT\mu LW} = \frac{W}{A\mu}\beta + \frac{1}{K} \qquad (38)$$

where

M = molecular weight

P = pressure, psia

z = compressibility factor

R = gas constant, 10.73 $\frac{\text{psi ft}^3}{\text{16 mole °R}}$

T = absolute temperature, °R

μ = viscocity of nitrogen, lb_m/ft sec

L = length, ft

A = cross-sectional area, ft^2

W = mass flow rate, lb_m/sec

K = permeability, darcys

β = turbulence factor, ft^{-1}

Temperature: 76°F

Pressure and Flow Rate:

Inlet Pressure, psia	Outlet pressure, psia	Flow rate, ft^3/sec
319	14.5	$7.67(10^{-7})$
369	14.5	$9.82(10^{-7})$
421	14.5	$1.188(10^{-7})$
470	14.5	$1.342(10^{-7})$
511	14.5	$1.592(10^{-7})$

The quantity $\frac{MA(P_1^2-P_2^2)}{2zRT\mu LW}$ is plotted versus $\frac{W}{A\mu}$ in Figure 24

Sample calculation for first point in Figure 24:

$$W = \rho q = \frac{.07 \text{ lbm}}{ft^3} (7.67(10^{-7})ft^3/sec = 5.36(10^{-8})lbm/sec$$

$$\frac{W}{A\mu} = 5.37(10^{-8})\text{lbm/sec}\left(\frac{1}{.0125\text{ft}^2}\right)\left(\frac{\text{ft/sec}}{1.189(10^{-5})\text{lbm}}\right) = .360\text{ft}^{-1}$$

$$\frac{MA(P_1^2-P_1^2)}{2zRT\mu LW} = \frac{28(.0125)(101,700)\frac{32.2\ \text{lb}_m\,\text{ft}}{\text{lb}_f\ \text{sec}^2}\left(\frac{144\ \text{in}^2}{\text{ft}^2}\right)}{2(1)(10.73)(536)1.189(10^{-5}).228(5.37)10^{-8}} = 9.89(10^{16})\text{ft}^{-2}$$

Intercept:

$$\frac{1}{K} = 7.61(10^{16})\text{ft}^{-2}$$

$$K = \frac{1}{7.61(10^{16})\text{ft}^{-2}}\ \frac{\text{darcy}}{1.062(10^{-11})\text{ft}^2}$$

$$K = 1.24(10^{-6})\text{darcy} = 1.24(10^{-3})\text{md.}$$

Turbulence factor:

$$\beta = \text{slope} = \left(\frac{11.89-7.61}{.7}\right)^{10^{16}} = 6.1(10^{16})\text{ft}^{-1}$$

Note: The length of sample K quoted for this calculation is slightly longer than for the other calculation. This is because the core was shortened after the air permeability test (run in the Hassler holder) so that the water permeability and threshold pressure could be run in the high pressure core holder.

3. Water Permeability

Core: Sample K ,

Length: 5.21 cm = .171 ft

Cross-Sectional Area: 11.59 cm^2 = .0125 ft^2

Darcy's Law for Liquids:

$$q = -\frac{KA}{\mu}\frac{\Delta P}{L} \qquad (40)$$

where

q = flow rate, cc/sec

A = cross-sectional area, cm^2

P = pressure, atm

μ = viscosity, cps

L = length, cm

K = permeability, darcys

T = Temperature: 73°F

ΔP = Pressure drop: -404 psi

q = Flow Rate: $1.71(10^{-5})$cc/sec

μ = Viscosity of water: .934 cps

Water Permeability:

$$K = -\frac{q\mu L}{A\Delta P} = \frac{1.71(10^{-5})(.934)(5.21)(14.73)}{11.59(404)}$$

$$K = 2.62(10^{-7}) \text{ darcys} = 2.62(10^{-4}) \text{ md.}$$

4. Formation Resistivity Factor:

Core: Sample K

Length 5.21 cm = .171 ft

Cross-Sectional Area: 11.59 cm^2 = .0125 ft^2

Electrolyte: 5 wt% NaCl

Temperature: 75°F

Resistance: 1510 ohms

Resistivity of electrolyte: 12.88 ohm-cm

Formation Resistivity Factor:

$$F = \frac{\text{Resistance (A)}}{\text{L (Resistivity)}}$$

$$F = \frac{1510(11.59)}{5.21(12.88)} = 261.$$

Electrolyte: 10 wt % NaCl

Temperature: 78°F

Resistance: 951 ohms

Resistivity of electrolyte: 7.46 ohm-cm

Formation Resistivity Factor:

$$F = \frac{951(11.59)}{5.21(7.46)} = 283.$$

The true formation factor is obtained by plotting the reciprocal apparent formation factor versus the resistivity of the water, Figure 62 The intercept at zero resistivity indicates the true formation factor.

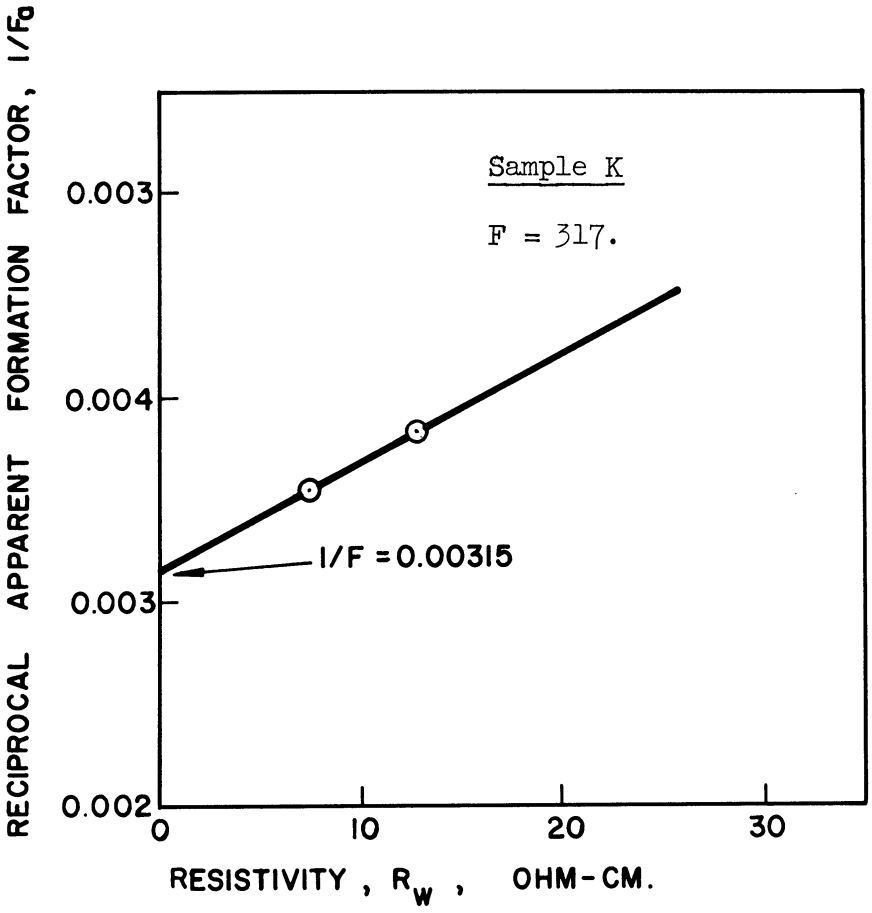

Figure 62. Determination of true Formation Factor for Sample K

APPENDIX B

THE VALIDITY OF KELVIN'S EQUATION WHEN APPLIED TO POROUS MEDIA

The vapor pressure of a vapor in equilibrium with a liquid exhibiting a curved surface differs from the vapor pressure of the same vapor over a flat surface of liquid. When a liquid is in droplet form its vapor pressure is increased, while the vapor pressure of a liquid in a capillary tube is decreased.

Kelvin's equation[4, 48] which can theoretically be derived from either energy or free energy balances relates the vapor pressure over a curved liquid surface to the vapor pressure of the same vapor over a flat surface as follows:

$$\ell n \frac{p}{p_o} = \frac{V}{RT}\left[\frac{2\sigma}{r}\right] \qquad (79)$$

where

p = vapor pressure over a curved vapor-liquid surface

p_o = vapor pressure over a flat surface

V = specific volume of the liquid

R = gas constant

T = absolute temperature

σ = surface tension of the liquid

r = radius of curvature of the curved vapor-liquid interface taken as positive when the interface is convex, towards the vapor phase.

For small pressure differences, $(p - p_o)$, $\ell n\ p/p_o$ may be approximated by $(p - p_o)/p_o$.

An expression for capillary pressure can now be obtained in terms of vapor pressures. The equation for the capillary pressure in a capillary tube is

$$P_c = \frac{2\ \gamma \cos \theta}{r} \quad . \tag{5}$$

Combining Equations (79) and (5) and assuming the contact angle is zero (a derivation presented in the Petroleum Transactions, AIME, 1949,[10] does not need this assumption) yields

$$P_c = \frac{RT}{V} \ell n \frac{p}{p_o} \tag{80}$$

or

$$P_c = \frac{RT}{V} \frac{(p-p_o)}{p_o} \tag{81}$$

A recent review of the literature places the validity of Equation (79) in doubt for small radii concave surfaces. First of all little direct data have been taken since the pressure differences indicated by Equation (79) are small. To make direct measurements of these pressure differences, extremely accurate control of temperature is needed since a variation of the vapor pressure of water by 1% may be achieved by varying the temperature by 0.1°C.

For convex surfaces Equation (79) has been verified for radii of curvature of several microns, for water droplets by Goodris and Kulikova (Reference 22), for droplets of dibutyl phthalate by Shereshefsky and Steckler,[52] for mercury droplets by Lyalikov,[35] and dioctyl phthalate and oleic acid by LaMer and Gruen.[32]

For concave surfaces the data which have been presented differ considerably from Equation (79) for values of r corresponding to those which might be found in porous materials. Shereshefsky[50] working with capillaries of 4.05 micron radius obtained a twenty-three fold lowering of vapor pressure compared to the values given by Equation (79) Shereshefsky and Carter[51] obtained lowerings in the vapor pressure of water 30 to 80 times that calculated for capillaries 3 to 10 microns in radius. Folman and Shereshefsky[20] also obtained similar lowerings of vapor pressure compared to calculated values for non-aqueous systems.

The general method used to measure the vapor pressure in the above mentioned cases (for both the convex and concave measurements) was quite unique. In each case a non-volatile solute was added to the liquid exhibiting the flat surface.

In the study of concave surfaces conical capillary tubes (or tubes of some other known geometry) were used. The capillary tubes filled with liquid were placed in a container along side a dish containing the dilute solution of liquid and the non-volatile solute. The system was then allowed to reach equilibrium. At equilibrium the levels of the liquid in the capillary tubes were noted, thus establishing the radius of curvature. The vapor pressure of the system was calculated from Raoult's law and then this value was compared with the value obtained by substituting r into Equation (79). The validity of Raoult's law was stated to give adequate accuracy for the solutions involved in these experiments, and the validity of Equation (79) for convex surfaces based on the same type of experiment, verifies this technique.

Folman and Shereshefsky[20] have discussed the possible reason for the observed lowering of vapor pressures in capillaries. They

conclude that the abnormal pressure lowering is induced by the capillary walls. This explanation seems quite reasonable for small capillaries and factors supporting this explanation are included in their article. On the other hand, the wall effects should be neglegible for large capillary tubes, and Thoma[55] working with capillaries of tenths of a millimeter radius has obtained results in agreement with Kelvin's relation.

Several articles appear in the literature in which Kelvin's relation is used to relate the vapor pressure of the wetting phase in a porous media to its capillary pressure. None of these articles presented capillary data measured by conventional methods to support their data. Calhoun, Lewis, and Newman[10] took data from zero to ten percent water saturations by the vapor pressure method to supplement their conventional capillary data at higher water saturations. Saito[48] took vapor pressure measurements on low permeability formations in an attempt to establish the threshold pressure by extrapolating the capillary pressure curve to 100 percent saturation. Messer[36] employed an evaporation method for measuring the capillary pressure curve. In this work the equation for diffusion through a porous material was combined with Kelvin's equation to give a qualitative relationship from which the capillary pressure curve could be predicted.

APPENDIX C

EVAPORATION OF WATER FROM A CAPILLARY TUBE

To determine whether or not losses of water from the micropipette used in the threshold pressure measurements were appreciable, diffusion calculations were made. The equation for diffusion through a stagnant film is given by

$$N_{Az} = \frac{PD_{AB}}{RT} \frac{1}{(z_2 - z_1)} \ell n \frac{P_{B2}}{P_{B1}} \qquad (82)$$

where

N_{Az} = Molar flux relative to stationary coordinates

P = Total pressure

T = Temperature

D_{AB} = Mass diffusivity in a binary system

R = Gas constant

z = Distance in direction of diffusion

P_{A1} = Partial pressure of gas A at z_1, (liquid interface)

P_{A2} = Partial pressure of gas A at z_2, (end of capillary tube)

P_{B1} = Partial pressure of gas B at z_1

P_{B2} = Partial pressure of gas B at z_2

The conditions used to calculate the amount of evaporation from the micropipet are considered to be the worst conditions which might have existed. These conditions are

$$D_{AB} = .256 \text{ cm}^2/\text{sec}$$

$P = 1 \text{ atm} = 760 \text{ mm Hg}$

$T = 25°C = 298°K$

$R = 62.36(10^3) \frac{\text{mm.Hg.cm}^3.}{\text{gm.mole°K}}$

$z_2 - z_1 = 10 \text{ cm}$

$P_{A1} = 23.6 \text{ mm.Hg.}$ (Vapor pressure of water)

$P_{A2} = 4.72 \text{ mm.Hg.}$ (Partial pressure corresponding to 10% relative humidity)

$P_{B1} = 736.4 \text{ mm.Hg.}$

$P_{B2} = 757.6 \text{ mm.Hg.}$

Making these substitutions in Equation (82) yields

$$N_{Az} = \frac{760(.256)}{10(298)62.4(10^3)} \ell n \frac{757.6}{736.4}$$

$$= 3.09(10^{-8}) \frac{\text{gm.mole}}{\text{cm}^2\text{sec}}$$

$$= 5.56(10^{-7}) \frac{\text{gm}}{\text{cm}^2\text{sec}}$$

$\therefore$ Total evaporation in one day

$$= 5.56(10^{-7}) \frac{\text{gm}}{\text{cm}^2 \text{ sec}} \left(\frac{\text{cm}^3}{\text{gm}}\right) \quad 3600(24) \frac{\text{sec}}{\text{day}} \left(\frac{10\text{mm}}{\text{cm.}}\right)$$

$$= 0.48 \text{ mm/day}$$

Data for water evaporating from a .1cm^3 micropipette was taken. One end of the pipette was sealed by inserting the tube into a short piece of tygon tubing and then pinching off the tube with a clamp. The bore radius of the pipette was 0.5 mm and the average distance from the water interface to the end of the pipette was 19.2 cm. Table XI lists the position of the interface as a function of time. The average evaporation rate was .00087 cm^3/day which corresponds to 1.03 mm/day.

In addition to the fact that this evaporation rate is small, most of the threshold pressure experiments were run with a globule of water between the water interface in the micropipette and the end of the pipette. This eliminates evaporation of water from the interface.

TABLE XI

EVAPORATION OF WATER FROM A CAPILLARY TUBE

Time, days	Pipette Reading, cm^3	Amount Evaporated, cm^3/day
0	.0124	
		.0009
1	.0115	
		.0006
2	.0109	
		.0008
3	.0101	
		.0008
4	.0093	
		.0010
5	.0083	
6	---	
		.0010
7	---	
8	.0053	
9	---	
		.0008
10	---	
11	.0028	
12	---	
13	---	
		.0009
14	---	
15	---	
16	-.0015	

APPENDIX D

EMPIRICAL CORRELATION OF THRESHOLD PRESSURE VERSUS POROSITY/PERMEABILITY

During the author's first year of graduate work, 1962, a purely empirical correlation for threshold pressure was attempted. This correlation was in part based on Leverett's J-Function correlation

$$P_T = j(S_w = 1.0)\sigma\left(\frac{\phi}{K}\right)^{\frac{1}{2}} \qquad (8)$$

A correlation of the following form was attempted.

$$P_T = A\left(\frac{\phi}{K}\right)^B$$

The above equation represents a straight line on a log.-log. plot with a slope of B and an intercept equal to the logarithm of A.

Most of the data used in this correlation were supplied by Northern Illinois Gas Compnay and were taken by Core Laboratories in Dallas, Texas. Data was also taken by the author on concrete core samples. (Reference 56) These samples were mounted in schedule 40 pipe with epoxy resin.

Data supplied by the Northern Illinois Gas Company is presented in Table XII. Tabulated values of threshold pressure versus the ratio of porosity/permeability for data taken in this research work appear in Table XIII. All of the data appearing in Tables XII and XIII are plotted in Figure 63. A least squares fit of the data was obtained by minimizing the deviations along the ordinate. Equation (83) represents the least squares fit of the data.

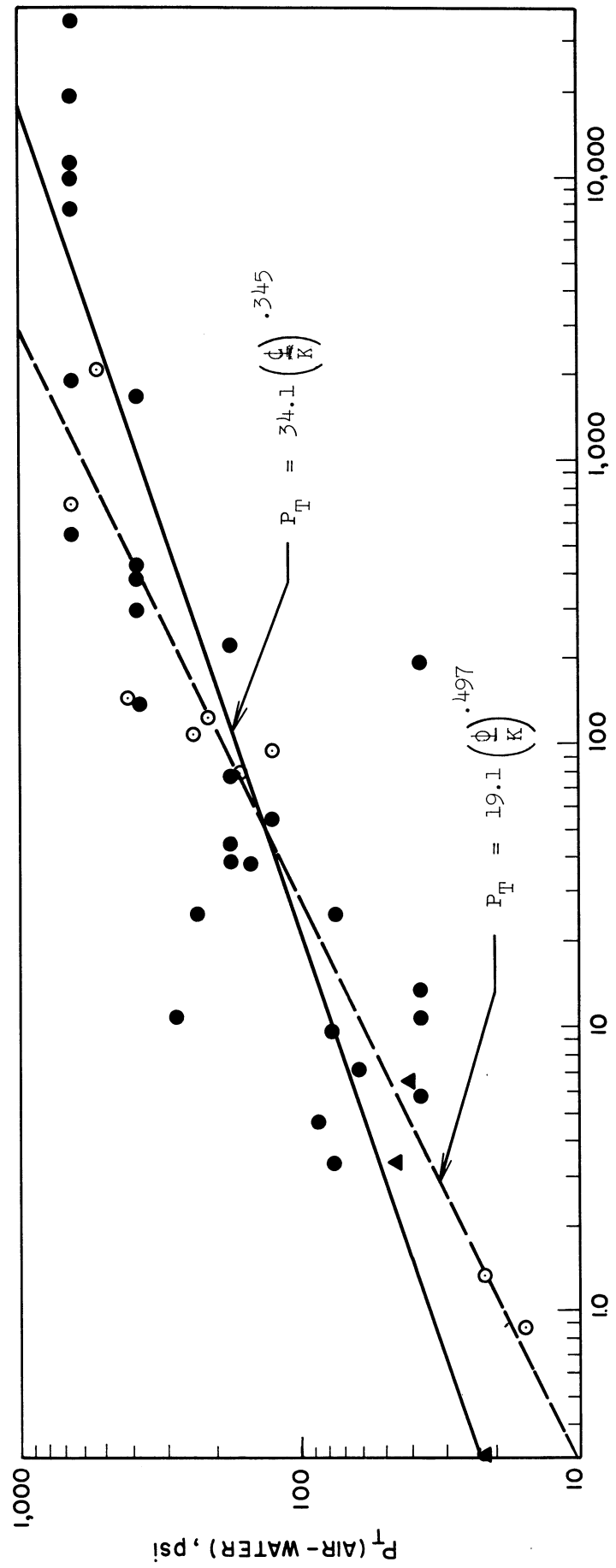

Figure 63. Empirical Correlation of Threshold Pressure versus Porosity/Permeability.

TABLE XII

THRESHOLD PRESSURE DATA FROM NORTHERN ILLINOIS GAS COMPANY

ϕ, %	K(10^6), md.	ϕ/K, frac./md.	P_T, psi
.7	1,500	4.66	> 80 < 90
13.2	17	7,760.	> 500 < 800
1.6	411	39.	> 100 < 250
1.3	43	302.	> 250 < 500
.8	58	138.	> 250 < 500
.8	1,370	5.84	> 25 < 50
.9	349	24.8	> 50 < 100
.4	1,200	3.33	> 50 < 100
1.5	1,400	10.7	> 25 < 50
1.3	58	224.	> 100 < 250
8.8	3	29,300.	> 500 < 800
5.7	4,170	13.7	> 25 < 50
5.4	278	194.	> 25 < 50
18.0	16	11,250.	> 500 < 800
2.0	2	10,000.	> 500 < 800
11.0	3	36,600.	> 500 < 800
5.2	134	388.	> 250 < 500
1.0	1,400	7.15	> 50 < 75
2.2	580	37.9	> 125 < 175
1.5	590	25.4	> 216 < 250
2.8	2,500	11.2	> 250 < 300
2.6	2,700	9.63	> 50 < 100
1.8	400	45.	> 150 < 200
3.9	710	55.	> 100 < 150
1.8	230	78.2	> 150 < 200
10.6	62	1,710.	> 250 < 500
2.1	11	1,910.	> 500 < 800
1.7	41	415.	> 250 < 500
.6	11	545.	> 500 < 800

TABLE XIII

TABULATED THRESHOLD PRESSURES VERSUS POROSITY/PERMEABILITY

Core Label	ϕ, %	K, md.	$\frac{\phi}{K}$, $\frac{frac}{md}$	P_T, psi
Sample G	10.	.0742	1.35	> 20 < 25
Sample I	9.48	$1.0(10^{-3})$	94.8	> 100 < 150
Sample K	3.26	$2.62(10^{-4})$	124.	> 200 < 225
Sample K	3.26	$2.97(10^{-4})$	109.	> 225 < 250
Sample L	15.9	.178	.88	> 15 < 16
Sample P	11.9	$1.52(10^{-3})$	78.3	> 150 < 175
Sample Q	9.64	$4.61(10^{-5})$	2,090.	> 500 < 550
Sample R	1.31	$9.15(10^{-5})$	143.	> 350 < 450
Sample S	2.89	$4.07(10^{-5})$	710.	> 600 < 700
Concrete Sample(56)	19.0	$2.92(10^{-2})$	6.51	40
Concrete Sample(56)	14.0	$4.58(10^{-1})$	.31	22
Concrete Sample(56)	19.8	$5.81(10^{-2})$	3.41	44

$$P_T = 34.1\left(\frac{\Phi}{K}\right)^{.345} \qquad (83)$$

The standard deviation of the points about the regression line in Figure 63 was 0.565.

The dotted line in Figure 63, Equation (46), represents the least squares fit of the author's data.

$$P_T = 19.1\left(\frac{\Phi}{K}\right)^{.497} \qquad (46)$$

This correlation was presented in Chapter VI.

BIBLIOGRAPHY

1. Amyx, J. W., Bass, D. M., and Whiting, R. L., Petroleum Reservoir Engineering, McGraw-Hill Book Co., Inc., New York, 1960.

2. Archie, G. E., "The Electrical Resistivity Log as an Aid in Determining Some Reservoir Characteristics," AIME, Petroleum Trans., 146, (1942), 54.

3. Bethel, F. T., and Calhoun, J. C., "Capillary Desaturation in Unconsolidated Beads," AIME, Petr. Trans., 198, (1953), 197.

4. Bikerman, J. J., Surface Chemistry, Academic Press Inc., 1958.

5. Bird, R. B., Stewart, W. E., and Lightfoot, E. N., Transport Phenomena, John Wiley and Sons, Inc., New York, 1960.

6. Botset, H. G., "Flow of Gas-Liquid Mixtures through Consolidated Sand," AIME, Petr. Trans., 136, (1940), 91.

7. Briggs, J. E., "Countercurrent Gravity Segregation in Porous Media," Ph. D. Thesis, Univ. of Michigan, 1963.

8. Buckley, S. E., and Leverett, M. C., "Mechanism of Fluid Displacement in Sands," AIME, Petr. Trans., 146, (1942), 107.

9. Calhoun, J. C., Jr., Fundamentals of Reservoir Engineering, University of Oklahoma Press, Norman, Okla., 1960.

10. Calhoun, J. C., Lewis, M., and Newman, R. C., "Experiments on the Capillary Properties of Porous Solids, AIME, Petr. Trans., 181, (1949), 189.

11. Cannon, G. E., and Crase, R. E., "Excessive Pressures and Pressure Variation of Depth of Petroleum Reservoirs in the Gulf Coast Region of Texas and Louisiana," AIME, Petr. Trans., 127, (1938), 31.

12. Carman, P. C., "Capillary Rise and Capillary Movement of Moisture in Fine Sands," Soil Science, 52, (1941), 1.

13. Carslaw, H. S., and Jaeger, J. C., Conduction of Heat in Solids, Oxford University Press, 2nd Edition, 1959.

14. Churchill, R. V., Operational Mathematics, McGraw-Hill Book Company, Inc., New York, 1958.

15. Coats, K. H., Rapoport, L. A., McCord, J. R., and Drews, W. P., "Determination of Aquifer Influence Functions from Field Data," Society of Petroleum Engineers, Paper Number SPE-897.

16. Cornell, D., "Flow of Gases Through Consolidated Porous Media," Ph. D. Thesis, University of Michigan, 1952.

17. Cornell, D., and Katz, D. L., "Flow of Gases through Consolidated Porous Media," Industrial and Engineering Chemistry, 45, (1953), 2145.

18. de Witte, A. J., "Saturation and Porosity from Electric Logs in Shaly Sands," Oil and Gas Journal, March 4, 1957.

19. Dickinson, G., "Geological Aspects of Abnormal Reservoir Pressures in Gulf Coast Louisiana, Bulletin of the Amer. Assoc. of Petro. Geologists, 37, 410.

20. Folman, M., and Shereshefsky, J. L., "Liquid-Vapor Equilibrium in Microscopic Capillaries," Journal of Physical Chemistry, 59, (1955), 607.

21. Foust, et al., Principles of Unit Operations, John Wiley and Sons, Inc., New York, 1960.

22. Geodrič, R., and Kulikov, L., Journal Russ. Phys. Chem. Soc., 56, (1924), 167.

23. Gorring, R. L., "Multiphase Flow of Immiscible Fluids in Porous Media," Ph. D. Thesis, University of Michigan, 1962.

24. Handbook of Physics and Chemistry, Chemical Rubber Publishing Co., Cleveland, Ohio, 1956-1957.

25. Handy, L. L., "Determination of Effective Capillary Pressures for Porous Media from Imbibition Data," AIME, Petr. Trans., 219, (1960), 75.

26. Harmsen, G. I., "The Concept 'Hydraulic Radius' in Porous Media," AIME, Petr. Trans., 204, (1955), 274.

27. Hassler, G. L., Brunner, E., and Deahol, T. J., "The Role of Capillarity in Oil Production," Petr. Tech., Sept., 1943, T. P. 1623.

28. Hewitt, C. H., "Analytical Techniques for Recognizing Watersensitive Reservoir Rocks," Journal of Petroleum Technology, August, (1963), 813.

29. Hill, H. J., Milburn, J. D., "Effect of Clay and Water Salinity on Electrochemical Behavior of Reservoir Rocks," AIME, Petr. Trans., 207, (1956), 65.

30. Katz, D. L., et. al., Handbook of Natural Gas Engr., McGraw-Hill Book Co., Inc., New York, 1959.

31. Katz, et. al., Movement of Underground Water in Contact with Natural Gas, The American Gas Association, New York, 1963.

32. LaMer, V. L., and Gruen, R., Trans. Faraday Soc., 48, (1952), 410.

33. Leverett, M. C., "Capillary Behavior in Porous Solids," AIME, Petr. Trans., 142, (1941), 152.

34. Leverett, M. C., Lewis, N. B., and True, M. E., "Dimensional Model Studies of Oil-Field Behavior," AIME, Petr. Trans., 146, (1942), 175.

35. Lyalikov, K. S., Acta Physicochim, U.R.S.S. 12, (1940), 42.

36. Messer, E. S., "Interstitial Water Determination by an Evaporated Method," AIME, Petr. Trans., 192, (1951), 269.

37. Morrow, N. R., and Harris, C. C., "Capillary Equilibrium in Porous Materials," AIME, Petr. Trans., 234, (1965), 15.

38. Muskat, M., Wyckoff, R. D., Botset, H. G., and Meres, M. W., "Flow of Gas-Liquid Mixtures through Sands," AIME, Petr. Trans., 123, (1937), 69.

39. Naar, J., Wygal, R. J., and Henderson, J. H., "Imbibition Relative Permeability in Unconsolidated Porous Media," AIME, Petr. Trans., 225, (1962), 13.

40. Nielsen, R. L., "On the Flow of Two Immiscible Incompressible Fluids in Porous Media," Ph. D. Thesis, University of Michigan, 1962.

41. Osoba, J. S., Richardson, J. G., Kerver, J. K., Hafford, J. A., and Blair, P. M., "Laboratory Measurements of Relative Permeability," AIME, Petr. Trans., 192, (1951), 47.

42. Pathnode, H. W., and Wylie, M. R. J., "The Presence of Conductive Solids in Reservoir Rocks as a Factor in Electric Log. Interpretation," AIME, Petr. Trans., 189, (1950), 47.

43. Perry, J. H., Chemical Engineers' Handbook, McGraw-Hill Book Co., New York, 1950.

46. Rose, W., "Theoretical Generalizations Leading to the Evaluation of Relative Permeability," AIME, Petr. Trans., 189, (1949), 111.

47. Rose, W., and Bruce, W. A., "Evaluation of Capillary Character in Petroleum Reservoir Rock," AIME, Petr. Trans., 186, (1949), 127.

48. Saito, H., "Capillary Measurements of Porous Medium by Vapor Pressure Method," Sixth WPC in Frankfort, June, 1963.

49. Scheidegger, A. E., The Physics of Flow Through Porous Media, University of Toronto Press, Toronto, Canada, 1957.

50. Shereshefsky, J. L., J. Am. Chem. Soc., 50, (1928), 2966.

51. Shereshefsky, J. L., and Carter, C. P., "Liquid-Vapor Equilibrium in Microscopic Capillaries," Journal of the American Chemical Society, 72, (1950), 3682.

52. Shereshefsky, J. L., and Steckler, S., Journal Chem. Phys., 4, (1936), 108.

53. Tek, M. R. and Wilkes, J. O., New Concepts in Underground Storage of Natural Gas, The American Gas Association, New York, 1966.

54. Templeton, C. C., "A Study of Displacements in Microscopic Capillaries," Journal of Petr. Tech., 6, (1954), 37.

55. Thoma, H., Z. Physik, 64, (1938), 224.

56. Thomas, L. K., Michigan Gas Association Fellowship Report, University of Michigan, Ann Arbor, Michigan, 1962-1963.

57. Thomas, L. K., Michigan Gas Association Fellowship Report, University of Michigan, Ann Arbor, Michigan, 1962-1963.

58. Thomas, L. K., Michigan Gas Association Fellowship Report, University of Michigan, Ann Arbor, Michigan, 1964-1965.

59. Thomas, L. K., Michigan Gas Association Fellowship Report, University of Michigan, Ann Arbor, Michigan, 1965-1966.

60. Trask, P. D., Applied Sedimentation, John Wiley and Sons, Inc., New York, 1950.

61. Winn, R. H., "The Fundamentals of Quantitative Analysis of Electric Logs," Symposium on Formation Evaluation, AIME, October, 1955.

62. Wyllie, M. R. J., and Gardner, G. H. F., "The Generalized Kozeny-Carman Equation," World Oil, March 1958, 123.

63. Wyllie, M. R. J., and Rose, W., "Some Theoretical Considerations Related to the Quantitative Evaluation of the Physical Characteristics of Reservoir Rock from Electrical Log Data," AIME, Petr. Trans., 189, (1950), 105.

64. Wyllie, M. R. J., and Spangler, M. B., "Application of Electrical Resistivity Measurements to Problems of Fluid Flow in Porous Media," Bull. Am. Assoc. Petrol. Geologists, Feb. 1952, 359.